INDC(AUL)-033/G

NOT FOR PUBLICATION

AAEC/AP-PR1985

INIS-XA-N--169

AUSTRALIAN ATOMIC ENERGY COMMISSION

LUCAS HEIGHTS RESEARCH LABORATORIES

PROGRESS REPORT OF APPLIED PHYSICS DIVISION

JULY 1984 - JUNE 1985

NOT FOR PUBLICATION

CONTENTS

FOREWORD

The activities of the Division during 1984/85 were again directed towards the general program objectives of the past two years. A shift in emphasis resulted in some organisation changes. The increased importance of nuclear safeguards research in the Government's support for the International Atomic Energy Agency program has prompted a re-arrangement of the nuclear physics and science activities. Dr J.R. Bird holds the responsibility for the Nuclear Science Section comprising the Nuclear Applications Group, Biomedical and Reactor Applications Group and the Neutron Scattering Group. The newly formed Safeguards and Nuclear Physics Section is headed by Dr J.W. Boldeman and includes the Safeguards Group and Nuclear Physics Group. The organisation of the remainder of the Division is unchanged.

The work on the electronic properties of hydrogen in silicon has been particularly rewarding and the plasma physics studies received recognition with an IAEA sponsored workshop on Compact Torus Research held in Sydney in March 1985.

1. NUCLEAR SCIENCE

The 3 MeV accelerator at Lucas Heights was used in the 1960s for pioneering work on ion beam techniques for determining sample composition, crystal structure and for microbeam scans of material surfaces. This work was initiated in collaboration with the Department of Physics, University of New South Wales, and, together with work using the Moata reactor, established experience which was the basis for the formation of a Nuclear Applications and Energy Studies Section in 1980.

The work of the section involved the physics of neutron and ion beam interactions and the development of new uses of such beams. The latter ranged widely over fields such as nuclear safeguards, geoscience, advanced materials, bio-medicine, industrial applications, archaeology and art.

The Government's support for the IAEA's programs prompted the formation, in mid-1985, of a separate section devoted to Safeguards and Nuclear Physics. The Nuclear Science Section has been structured to encompass groups involved with nuclear applications, bio-medical and reactor application and neutron scattering.

1.1 Neutron Beam Applications

1.1.1 Neutron moisture meters

(D.J. Wilson)

Neutron moisture meters have been in use for many years to determine the moisture content of a matrix such as soil, concrete, grain, timber, etc. The standard technique used is to calibrate the moisture meter in a chosen medium containing known quantities of water. This method limits the application to simple homogenous systems.

In order to extend the use of these instruments into more complex systems in which the materials and density of the matrix varies from point to point, a detailed investigation of the physics of neutron behaviour in such matrix-water mixtures is in progress. Results so far obtained are currently being applied to two problems:

(1) Two of the more important parameters affecting the interpretation of moisture meter data are the macroscopic absorption and scattering cross-sections of the matrix. A joint project with the CSIRO Division of Soils, Adelaide, has

recently commenced and aims to provide a rapid and cheap determination of these parameters. The building of a suitable 1 m cube of graphite is making slow progress due to staff shortages and difficulty in obtaining cadmium sheet for neutron shielding. Eventually the system is expected to become a service to moisture meter users.

(2) A collaborative project with the Environmental Science Division aims to determine the varying water concentration profiles in a complex system (White's overburden dump at Rum Jungle). The absorption cross-section of the dump material varies between about 4 x 10^{-3} cm^2g^{-1} and about 12 x 10^{-3} cm^2g^{-1} which at a density of 1 gcm^{-3}, and the same count rate could mean a water content between 0.16 grams of moisture per gram of dry soil (gg^{-1}) (at 4 x 10^{-3} cm^2g^{-1}) and 0.23 gg^{-1} (at 12 x 10^{-3} cm^2g^{-1}). This illustrates the need to measure this cross-section by a technique such as that described in paragraph (1) above.

Any attempt to determine the absolute water content in the overburden heap must take into account the soil parameters. Relative changes in water content are not so sensitive to soil parameters, however the relationships between parameters and count rate are non-linear and the use of these techniques considerably improves the accuracy of the results. This is an essential part of the studies being undertaken to resolve and control some of the environmental hazards associated with mining.

Other problems under investigation are the contribution to the total error due to inaccuracies in the measured values of the soil parameters, the effect of moisture concentration gradients either side of the measuring point, the problem of duplex soils in which the soil parameters change more or less abruptly at a plane and the bore hole geometry, liner thickness and material.

1.1.2 Moata reactor

(D.J. Wilson, T. Wall)

The Moata reactor is used on demand for development work, some routine applications and to a limited extent during HIFAR shutdowns. Moata was shutdown from 10.7.84 to 11.9.84 to enable modifications to be made to the thermal column. A large

irradiation cavity was installed for the Neutron Capture Therapy project and an additional ionisation chamber was positioned in the North Cavity to enable testing of alternative start-up and operational instrumentation. Usage has averaged approximately one day per week with occasional periods of increased use; particularly during the HIFAR shutdown which commenced in April 1985, HIFAR operators were trained to operate Moata specifically to enable gold isotope supplies to be maintained by the CPU. This exercise continued throughout the extended HIFAR shutdown and involved a minimum of 1 day per week of Moata operation. Other additional user demands caused by the HIFAR shutdown included irradiation of fission track dating packages for the Department of Geology, University of Melbourne and the supply of radioisotopes for ASNT courses.

During this period the reactor was operated for 70 separate start ups, of which 13 were for the NCT project. Other projects which required significant operational effort included neutron activation analysis, both for divisional research and for the CSIRO's Division of Energy Chemistry and fission track analysis.

The Moata supervisor Mr D.J. Wilson joined a 3 man IAEA expert group assembled at the request of the government of Sri Lanka, to take part in a Research Reactor Feasibility Study at the Radioisotope Centre, Colombo from 28.8.84 to 13.9.84. The electricity demand in Sri Lanka is doubling every seven years and the whole of its hydro resources will be utilised within 10 years. There is no fossil fuel available and the country appears to be committed to nuclear power. In order to provide training in nuclear technology with the added advantages of short lived isotope production, academic and industrial research, it is proposed to build a research reactor. The expert group was required to examine the following areas of interest:

(a) the current experience in nuclear science and technology;

(b) the potential users of a research reactor;

(c) the role of such a reactor in the country's nuclear development;

(d) the effective utilisation by universities, industry and government institutions, and

(e) the importance of a research reactor in the technical and industrial development of the country.

Finally the group advised the Sri Lankan Government on the type and availability of the assistance available through the IAEA for training and development and the most satisfactory size of reactor to suit the requirement and the availability of expertise.

1.1.3 Uranium assay

(T. Wall)

This commercial analysis service commenced operation in 1974 using Applied Physics Division's reactor facilities and staff. By 1982, 30,000 samples had been processed at a unit price between 2 and 4 dollars per sample. Over 14,000 other analyses were carried out for the former Uranium Exploration Division. A combination of decreasing demand from mining companies and increasing difficulties with providing staff to run and maintain the service has led to a large decrease in commercial activity since 1982. Concurrent with the external demand, APD also acted as service support for ongoing AAEC projects and this has resulted in over 10,000 separate analyses being provided for uranium ore processing research and for Environmental Science Division projects. In anticipation of making the commercial and internal operation of the service more reliable, an assay rig on HIFAR has been brought into operation and this can be operated by HIFAR staff.

1.1.4 Fission track studies

(T. Wall, D.J. Wilson)

This reactor technique for measurement of very low levels of uranium in geological and biological materials began its development in APD in the early 1970s. Initially, the technique was confined to the measurement of low neutron flux levels and fission rates by combining the fission track detector with a low mass standard uranium foil. Development has now reached the stage where exposure to low levels of contamination of uranium mining and milling workers is routinely monitored, research into uptake of uranium in the vicinity of ore bodies by biota is far advanced and trace particulate contamination at

sites such as Maralinga is detected by activities based on standard irradiations carried out using Moata. Much of this work has been done in collaboration with the Office of the Supervising Scientist and the School of Public Health and Tropical Medicine at the University of Sydney.

Ongoing research into the geochemistry of the migration of uranium and other actinides from primary ore deposits is also supported by fission track studies. The method has also been used to quantify trace element uranium concentrations in granite formations for more fundamental geological research. Lately, collaboration has commenced with Geology Departments at the Universities of New England and Melbourne which are involved with track dating of rocks and minerals.

1.1.5 Fission track dating

(T. Wall)

Glass dosimeters have been commonly used to measure neutron flux levels of an irradiation of a fission track dating package. The fission track density, ρ_d, of a mica solid state nuclear track detector placed adjacent to the glass is normalised to the flux ϕ by

$$\phi = B\rho_d$$

where B is a constant, determined by activation detectors placed close to the glass/mica assembly.

Calibration of the glass dosimeter has proved difficult (Hurford and Green [1]) and an alternative approach using vacuum evaporated uranium sources to measure fission rates in a fission track dating irradiation has been developed in Applied Physics Division.

Natural uranium sources, between 4 and 20 μgcm^{-2} were made by vacuum evaporation (Applied Physics Division Progress Report 1983-84). Several analytical techniques (NAA, DNA, alpha spectrometry and fission track analysis) were used to quantify the uranium concentration (Table 1.1).

These sources were then used to:

1. Measure the fission rate at the Moata irradiation position of a fission track dating package.
2. Measure the fine structure of fission rate within a fission track dating package.

3. Show that similar mineral ages may be obtained by using these sources to those obtained using dosimeter glasses.

This work will be presented at the 13th International Conference on Solid State Nuclear Track Detectors in Rome (September 1985).

Table 1.1
Analytical data of evaporated uranium sources

All concentrations are in μg U cm^{-2}

	ANALYTICAL METHOD				
Source	Alpha Spectrometry	NAA	DNA	SSNTD	Tracks Counted
A3	-	22.2 ± 0.5	22.5 ± 0.7	21.9 ± 0.6	10696
A4	-	21.1 ± 0.5	22.9 ± 0.7	21.9 ± 0.6	11389
A5	-	23.6 ± 0.5	22.5 ± 0.7	21.5 ± 0.6	10478
A6	22.1 ± 0.7	22.2 ± 0.5	22.4 ± 0.7	21.9 ± 0.6	10193

1.1.6 Neutron activation analysis of granite rock

(T. Wall)

Work was completed on the use of Moata for NAA of large batch rock samples for rare earth element (REE) analysis. It was found that NAA could be used successfully to measure REE concentrations of hornblende, plagioclase, orthoclase, biotite and sphene, all separated minerals from the granite complex at Walcha Road, New England, NSW. The REE were measured (Table 1.2) together with other trace elements and Fe. This work showed that the mineral sphene accounted for a large fraction of the total REE concentration in the rock.

1.2 Ion Beam Applications

1.2.1 Monitoring of occupational exposure to heavy metals

(E. Clayton, K. Wooller*)

(*Dept of Industrial Relations)

Over the past five years the Section has developed a program for the use of the PIXE technique for analysis of biological samples. The area of application we have chosen is a collaborative study with the Division of Occupational Health (New South Wales Government) into monitoring exposure to heavy metals in the work place.

Table 1.2
Mineral separates analyses FS962 (Pluton rim) Walcha Road

	Whole Rock	Sphene	Hornblende	Biotite	Orthoclase	Plagioclase/ Albite
La	42	2099	42	7.6	6.1	7.2
Ce	89	6988	147	nd	8.4	8.2
Nd	nd	3576	107	nd	nd	nd
Sm	7.3	682	24	1.3	0.39	0.4
Eu	1.5	136	2.2	0.1	0.6	0.55
Tb	0.94	nd	2.8	0.08	nd	0.07
Yb	2.3	256	7.4	nd	nd	nd
Lu	0.36	30	1.1	nd	0.03	0.03
Fe_2O_3*	4.42	3.4	15.2	18.0	0.09	0.06
Hf	6.3	nd	3.9	0.88	0.13	0.41
Th	37	3974	7.3	5.5	2.2	3.3
Sc	15	8.6	118	11.8	0.08	0.10
Ta	2.1	nd	nd	nd	nd	nd
U	6.9	752	4.2	3.6	nd	nd
Rb	214	nd	nd	992	364	315

Fe_2O_3 expressed as weight per cent.

All other concentrations in $\mu g g^{-1}$.

* Total Fe expressed as Fe_2O_3.

nd not determined.

The standard method used in New South Wales to monitor exposure to elements such as lead is to analyse blood or urine samples for their element concentration and take action if this level is above limits set by legislation. We have investigated the use of hair analysis as we believe it offers some advantages. Its collection is non-invasive and the samples can be easily transported and stored without refrigeration. Its analysis for trace elements is reasonably easy and furthermore the concentration for many elements is much higher in hair than in either blood or urine. In addition a multielement technique

such as PIXE allows the interaction between various elements to be studied. For example, lead-workers may also be exposed to tin, zinc, copper, cadmium, arsenic or chromium.

We have already completed a survey of the trace element content of scalp hair from male workers in New South Wales. That survey had two aims; firstly, to establish a database of concentration data from control groups not occupationally exposed and secondly, to see whether hair concentrations could be correlated with the appropriate blood or urine levels, particularly for the group of workers exposed to a variety of heavy metals. This was successful as we found significant correlation between hair lead and blood lead and in another group working in a tanning factory there was significant correlation between hair arsenic and urine arsenic levels.

Having established that there is a correlation between hair levels and other measurements we are now building upon this study by attempting to see whether hair levels can follow the short term variation in levels that one sees when monitoring occupational exposure. Twenty workers exposed to lead oxides and arsenical lead in a lead acid battery manufacturing plant have been sampled every six weeks for the past fifteen months. During that period their blood lead values have fluctuated according to their exposure, which in some cases was so extreme as to warrant their removal from that exposure.

Sample collection has concluded and we are now commencing the PIXE analysis of their hair samples, to see whether this exposure will also be reflected in their hair levels. Essentially we will analyse the hair results in comparison with blood results to see whether they have the same pattern of high and low levels depending upon their exposure.

We are participating in an IAEA Coordinated Research Program on Nuclear Techniques in Occupational Health and Eric Clayton attended the second meeting of this program at Ispra (Italy) in September 1984. For this study we decided to wash our samples in a mild detergent. This does not have a drastic effect upon hair and is practicable for the worker to apply. We supply him with shampoo sample and he washes his hair the night before collection. So far there has been excellent compliance with this procedure. This protocol differs from

that of the IAEA, which we have found removes a large proportion of some elements and leaves an unrepresentative sample for analysis. This was discussed at Ispra, but there was no agreed protocol decided upon by the meeting as everyone had had some problems with this question.

To summarise our work in biological monitoring, we have found that trace element analysis of scalp hair offers the possibility of accurate monitoring of exposure to heavy metals in the workplace. We are now attempting to see whether the time variation in hair levels is sufficiently sensitive that they can be applied routinely.

1.2.2 Surface studies

(J.R. Bird, P. Duerden, D.D. Cohen, G.B. Smith*)
(*NSWIT)

A major project, which arose from Lucas Heights work on ion beam techniques, concerned the use of ion implantation for the production of solar cells. When this project was transferred to CSIRO jurisdiction, an Ion Implantation Research Group was established by the AAEC Applied Physics Division, CSIRO Chemical Physics Division and RMIT Microelectronics Centre. This group organises meetings for the discussion of topics of mutual interest. Since that time AAEC work on semiconductor and other material surfaces has been concentrated on the development of methods of analysis with emphasis on the effects of surface roughness and topography on ion beam measurements. This work has been carried out in collaboration with the NSWIT and during 1984 was the subject of an AAEC contract for the development of spectrum simulation methods.

A special vacuum chamber has been installed on the 3 MV accelerator for non-destructive measurements of surface layer composition and the depth dependence of specific isotope concentrations (to depths of the order of 1 μm). This chamber has precision controls of sample position and angular orientation as well as of the angular position of two ion detectors. This is necessary to permit ion irradiations at glancing angles to the surface. Glancing angle measurements have been shown to give a dramatic improvement in the depth resolution which can be achieved in oxygen analysis (10 $\mu g cm^{-2}$). The same chamber can be used for backscattering measurements of many

elements and the depth profiling of hydrogen by the forward scattering technique.

Applications of the new chamber include studies of: solar absorbers which have considerable surface roughness; semiconductor materials which have regular patterns of surface topography; ^{18}O assay in metabolism studies (see 1.2.6) and hydration dating of obsidian.

1.2.3 Archaeometry

(J.R. Bird, P. Duerden, C. Clayton)

There are two main reasons for the growth in contributions by the Nuclear Applications Group to the field of Archaeometry (scientific techniques for art and archaeology).

(1) Ion beam techniques have proved to be particularly useful for rapid non-destructive sample analysis;

(2) The archaeologists involved since the first enquiries in 1973 have been particularly patient during the development of equipment and techniques. The first reason has now effectively negated the second and a flood of new enquiries is being received.

The most dramatic development has been in the organisation of the "Lapita Homelands Project" in which "twenty scientists, mostly leaders in their particular fields of Pacific prehistory, from Australia, the USA, New Zealand, PNG, Holland and Britain" will seek "to determine whether the Bismarck Archipelago of Papua New Guinea was a 'long term staging post' from which the initial migration of people across the Pacific Islands began" (ANU Reporter).

The first reason given above, has also led to the publication of a review article in 1983. This review appeared at a crucial time in the preparation of a proposal for the installation of a small accelerator at the Louvre (Laboratoire de Recherche des Musees de France) to be devoted to studies in Art and Archaeology. Dr J.R. Bird was invited to attend an International workshop on Ion Beam Techniques in Art and Archaeology held at Pont-a-Mousson, France in February 1985. The workshop was attended by approximately 40 persons, including representatives of the Ministere de la Culture and LRMF (France), NATO and the Council of Europe. It undertook a detailed evaluation of the problems facing museum scientists and of the use of ion

beams to solve those problems. The results are to be published in Nuclear Instruments and Methods.

Recent work at Lucas Heights which was summarised for the workshop at Pont-a-Mousson, includes the following projects:

Obsidian catalogue

A final catalogue of the results of the elemental analysis on obsidian source material from the SW Pacific is nearing completion. Three hundred and fifty samples from approximately 150 geologically distinct sources are included to provide information on element variability within samples from a particular source, and also between repeat measurements made on individual samples.

Obsidian artefacts

Measurements on several thousand artefacts are also being prepared for publication but the results have already been used in numerous papers which have detailed the movement of obsidian through the Melanesian island chain and led to the proposed Lapita homelands project described above.

Australian obsidian

A series of PIXE-PIGME measurements have been made on twelve artefacts from collections at the Australian Museum, Sydney. They were originally from the Seelands, New South Wales, rock shelter and have been described in the literature as obsidian. Obsidian, and other glassy material, from the adjacent Mt. Warning region of northern New South Wales were also analysed. The measured elemental compositions were used as a data base for statistical assessment.

The main conclusions of this work can be summarised as follows:

- Obsidian from the Nightcap Range in northern New South Wales and some of the obsidian from the Border Range further north, form a reasonably well defined compositional group which differs from other known sources in the South-west Pacific.
- Twelve artefacts from the Seelands rock shelter which have been described as possibly obsidian are completely different in composition to the above source group.

- The artefact lithology is probably black chert, with possible pyrite inclusions. Such cherts are known to occur within the New England region and a new search is needed to locate a specific source for this material.
- The knowledge of the prehistoric transfer of materials between people resident in various parts of the Northern Rivers area of New South Wales is neither enhanced nor diminished by these results until a definitive source of the black chert is identified.

Motupore Island (PNG) pottery

The same measuring techniques have been proved useful for relating sherds from a prehistoric site to clay and filler materials from neighbouring localities. Sherds from up to 200 km distance can be linked to this known pottery manufacturing area.

Buka Island (PNG) pottery

Similar work has shown two major pottery groups can be identified in this area.

Admiralty Islands (PNG) pottery

Measurements on extracted mineral fractions show clustering of compositional groups, in agreement with XRF measurements made at the University of Auckland on the elements identified in the clays.

Torone (Greece) pottery

Measurements have been carried out and data analysis is underway.

Pottery variability

Measurements on 23 samples from the Middle East have refuted a published hypothesis that variability can be used to establish the economic importance of various sites.

1.2.4 Nuclide migration

(P. Duerden, E. Clayton, D. Garton, P. Airey, B. Davey*, D. Gray*) (*University of Sydney)

Groundwater migrates principally through major fracture patterns. However, the effectiveness with which rocks such as granites can retard the transport of radionuclides depends not only on the adsorption properties of fracture surfaces, but

also on the extent to which solutes diffuse into the bulk rock through microfissures. Experimental techniques are being developed to study the distribution of uranium, uranium daughter products and other elements surrounding pre-existing fractures in NT uranium ore bodies. The aim of the project is to correlate the uranium daughter product indicator element ratios with the mineralogy near pre-existing fractures, and to correlate the data with the predictions of matrix-diffusion theory. We have used the PIXE-PIGME facility to analyse samples of schists from the vicinity of major fractures in drill cores from the Ranger (NT) ore body.

A large suite of elements was measured with the technique and element concentrations were derived from the simultaneous X- and gamma-ray analyses for elements having atomic numbers (Z) of 3, 5, 9 and in the range 11 to 92. This includes all the elements whose oxides are the major components of the minerals. Results from an unweathered rock sample are included in Figure 1.1, where a selection of the major and minor element analyses are plotted in the form of a histogram. The horizontal axis represents a series of 1 mm diameter beam spot analyses made at 1 mm intervals across the sample.

The sample, S3/114 comes from a depth of 27.2 metres at Ranger and is mildly weathered quartz-mica-chlorite schist from the upper mine sequence. The partially weathered character of the rock and the strong pleochroic colours of the veins suggests that the uranium is present as a secondary U (VI) mineral.

From Figure 1.1 we can see that position 3 on the sample is low in Si, high in Al, Mg and Fe and from an area rich in a magnesium chlorite. Position 6 is high in Si, low in K, Fe and intermediate in Mg and from a zone which carries a higher than normal amount of quartz. The high uranium site (spot 4) is particularly interesting because it can be clearly distinguished from the other spots and is high in K, Th and Rb and low in Mg, Li, F, Cu, Ni, Ti and Ca.

The results of a regression analysis suggests that this mineral is unlikely to be any of the secondary minerals sklodowskite, kasolite, renardite, curite or metatorbernite, but the possibility of saleeite, a very common secondary

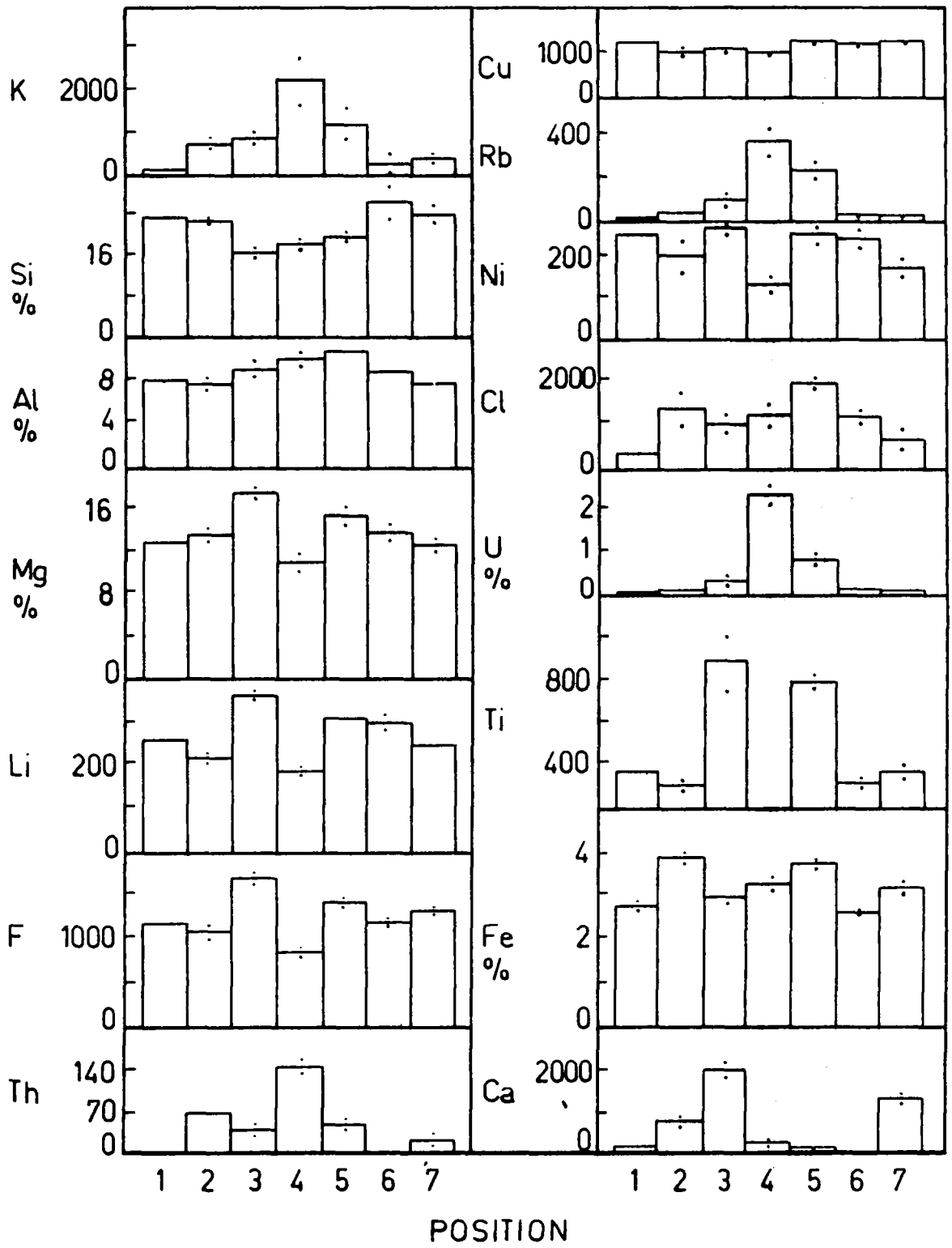

Fig. 1.1 Major and minor element analyses of sample S3/114. The histograms represent a series of analyses made at 1 mm intervals across the sample.

mineral at Ranger, cannot be excluded in the absence of analyses for P.

It is therefore concluded that the uranium-bearing vein is located near the centre of this traverse and likely to be in primary form, perhaps as pitchblende which is the most common primary mineral at Ranger.

The PIXE-PIGME techniques are being refined by the construction of a new analysis chamber, so that it will be possible to produce a 2-dimensional map of a wide range of elements on a petrological slide and thus enable the distributions to be correlated with the detailed petrology. The new chamber will include collimation of the incident beam so that a resolution of 50 μm on the sample will be possible. An optical system will be included with both transmission and reflected sample illumination and X-Y positioning of the sample will be provided so that an area 25 by 50 mm can be analysed with a positional precision of ± 10 μm.

Complementary experiments, which use a combination of fission track and alpha track techniques on petrological slides, are already under way to determine the distributions of uranium and uranium daughter products. Correlation of the uranium/uranium daughter product (principally radium) ratio and the multi-element distributions with the mineralogy will allow the impact of specific minerals on transport to be assessed.

1.2.5 Desert varnish

(P. Duerden, D.D. Cohen (AINSE), D. Garton, D. Dragovich*) (*University of Sydney)

'Desert (rock) varnish' is a naturally occurring, frequently shiny, often continuous, dark-coloured, thin (generally between 5 and 200 micrometers) layer which is well developed on many stable rock surfaces in arid areas (Ziegler et al. [2]). The varnish is usually composed of silicate clay minerals, bonded to each other by manganese and iron oxides and hydroxides and to the underlying rock. Other elements, including Ca, Ti, K, P, S and Na, are also present in minor amounts. Although the best varnish examples appear on fine-grained iron-bearing rocks, discontinuous varnish covers develop on quartz veins and limestone, indicating that the varnish is not necessarily derived from the rock on which it was formed.

At a site near Broken Hill, continuous to patchy layers of varnish cover siltstones, conglomerates and fine-grained sandstone. Varnished and partly varnished Aboriginal rock engravings are present on many of these surfaces. Permission was obtained to remove small samples (between 15 to 30 mm^2) of varnished rock from surfaces near engravings, in a field situation which suggested that varnishes were of differing ages. Recent work in the United States of America by R.I. Dorn [3], indicates that younger varnish has a higher ratio of (Ca + K): Ti than older varnish. If the cation ratios of samples from apparently different varnishes can be measured, the results may be able to indicate their relative ages. Because the sample sizes were small and the varnish layers thin, we used non-destructive ion beam analysis techniques to measure the element concentration in these layers and to obtain, if possible, some indication of their thickness.

The experiment was carried out in two parts,

(1) The elemental composition was measured by particle induced X-ray emission (PIXE) and proton induced gamma-ray emission (PIGME), using protons and alpha particles over a range of incident ion energies so that any variation in measured element composition could be understood as a function of sampled depth.

(2) Rutherford backscattering (RBS) spectra were measured using both incident alpha particles and protons with a range of incident energies to establish whether a varnish/rock interface can be detected. The results from these measurements were compared with calculations made using the RBS code formulated by Ziegler et al. [2] and a typical RBS spectrum from the varnish layer on rock 5 is shown in Figure 1.2. It can be seen that the calculated spectrum for a simple homogeneous system, (O, Si, Ca, Fe and Ba with concentrations of 51.0, 28.0, 4.7, 14.6 and 1.5% by weight respectively) provides a good representation of the measured spectra. The techniques have proved to be most satisfactory for analysing variable thicknesses of desert varnish. As was expected, the PIXE measurements provide the best guarantee that only the varnish layer is being sampled. However, the relatively

low X-ray production cross-sections and the absence of Li, F, Na and possibly Mg and Al concentrations, make a low energy (1.5-2.0 MeV) PIXE-PIGME analysis a more suitable alternative. Confirmation of sample composition for a range of depths provides a unique method for instilling confidence in the results. The use of RBS to confirm sample uniformity also appears to provide information about the sample that cannot be easily replicated by other methods.

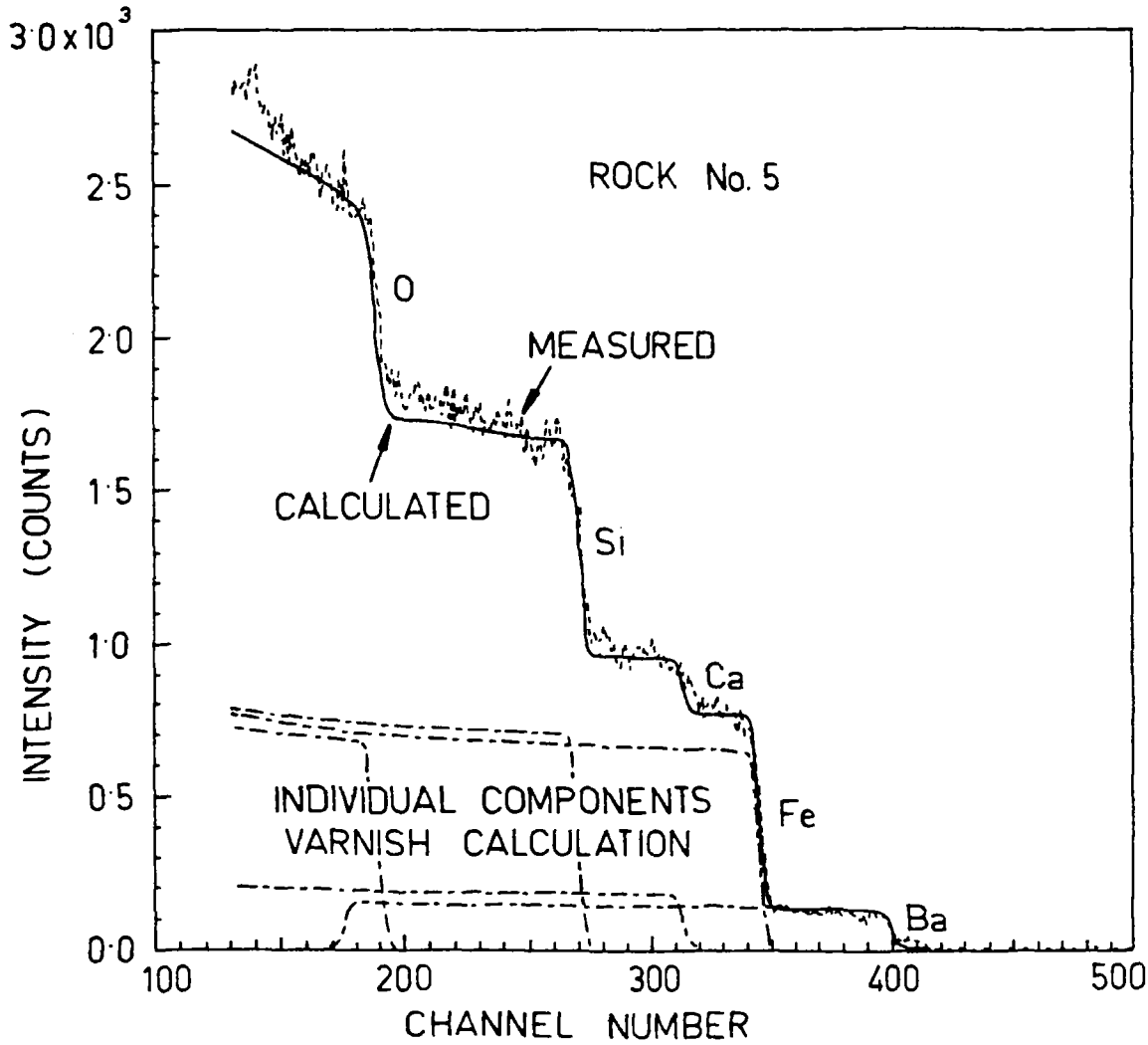

Fig. 1.2 Calculated and measured Rutherford backscattering spectra for 2.35 MeV alpha particles incident on rock 5.

1.2.6 Water analysis in small biological samples

(D. Cohen (AINSE), A. Katsaros (AINSE), S.D. Bradshaw*)
(*Uni. of Western Australia)

The $^{18}O(p,\alpha)^{15}N$ reaction for analysis of ^{18}O enriched water in small biological samples has been developed in collaboration with the University of Western Australia (Zoology Dept).

The discovery that the oxygen of respiratory CO_2 is in isotopic equilibrium with the oxygen of body water in animals paved the way for studies on the material and energy balance of free-ranging animals. Oxygen in the body is turned over as a result of exchange of both CO_2 and H_2O with the environment and, if the hydrogen turnover is known independently, then CO_2 production can be estimated. The advantage of this approach is that energy metabolism can be measured in unrestrained animals living normally in their natural habitat and it is evident that many of the accepted data on energy metabolism in animals, derived from laboratory experiments, are seriously in error.

Currently animals are injected with $^{3}H_2{}^{18}O$ (ca. 3ml/kg of 97% enriched ^{18}O). ^{3}H turnover is then assessed by liquid scintillation counting and ^{18}O concentrations are analysed by the $^{18}O(p,n)^{18}F$ nuclear reaction at the UCLA Laboratory of Nuclear Medicine and Radiation Biology, using 22.1 MeV protons produced by a medical cyclotron. The disadvantages of this method are the high costs involved (US$ 550/30 samples) and the inevitable delays associated with sending samples overseas for analysis and these constraints have motivated our development of an alternative method of analysis which utilises the $^{18}O(p,\alpha)^{15}N$ nuclear reaction in the 3 MeV Van de Graaff accelerator at Lucas Heights.

At Lucas Heights we have used the 846 keV proton resonance in this reaction to analyse Ta_2O_5 samples prepared from both natural (0.2% ^{18}O) and 98% enriched ^{18}O water samples. Samples of Ta_2O_5 can be prepared from less than 0.2 ml of water and ultimate ^{18}O sensitivities are 0.05% for 5 minute run times, well below the natural background of 0.2%.

1.2.7 F in Queensland coals

(E. Tiller (Darling Downs CAE), D.D. Cohen (AINSE))

In collaboration with the Darling Downs CAE, Toowoomba,

the UHV PIGME facility is being used for a series of measurements of the F concentration of Queensland coals.

1.2.8 Study of ohmic contacts on GaAs

(D.D. Cohen, G. Sutherland*, A. Nassibian*)
(*University of Western Australia)

Rutherford backscattering techniques have been employed to investigate the compositional nature of various Au/Ge/Ni ohmic contacts to GaAs.

An ohmic contact is non-injecting and has a linear I-V characteristic in both forward and reverse directions. For III-V compound semiconductors, the quality of ohmic contact is a significant factor affecting device performance and reliability. Yet while GaAs semiconductor devices such as MESFETS, Gunn oscillators, injection lasers and hetero-junction FETS are finding ever-increasing applications, the art of producing low resistance, reproducible, stable and reliable ohmic contacts is far from satisfactory.

The best ohmic contacts to GaAs to date have been annealed Au/Ge/Ni contacts in approximately 5%/11%/84% proportions by weight. After deposition, this multi-component system is heated by any one of a variety of means to induce the growth of a thin, highly doped, n-type region at the metal-semiconductor interface. (The n-type dopant is the Ge(Gp IV) displacing the Ga(Gp III) atoms in the GaAs lattice). It is this thin (~0.2μm) highly doped layer that causes tunnelling to be the dominant mechanism of conduction across the contact, thus resulting in its ohmic behaviour.

The metallurgical interactions at the metal-semiconductor interface during the annealing process are far from well understood. It was in efforts to increase this understanding that the depth resolution (5 nm) of Rutherford backscattering was used to examine the composition of the alloyed region.

By varying the initial Au/Ge/Ni deposition and examining the resultant composition after alloying, much insight into the metallurgical reactions taking place and the role of each of the constituent species in ohmic contact formation was gained. The effect of the annealing process on the active structure of the device was also measured. In Figure 1.3 we show the measured RBS spectrum for a typical GaAs ohmic contact before

and after alloying under various conditions. Clearly the Au depth distributions are quite different for the different alloying techniques.

1.2.9 Impurities in niobium crystals

(D. Cohen (AINSE), J. Osborn (Monash Uni.))

Several niobium single crystals samples have been analysed

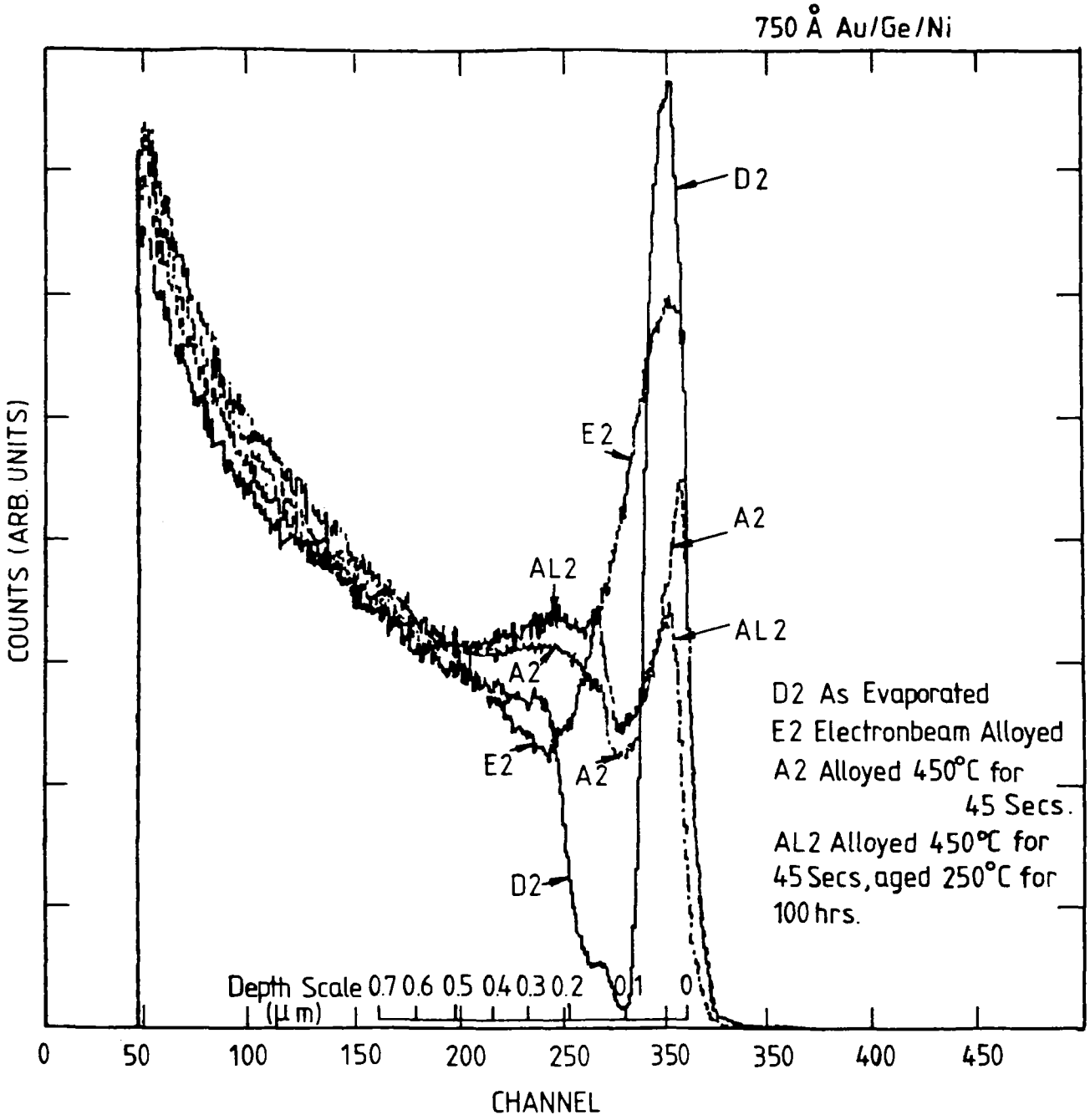

Fig. 1.3 RBS spectrum from GaAs ohmic contact

by PIXE to determine impurities present. The crystals are to be used in a study of hydrogen in niobium and some impurities are likely to act as trapping centres for hydrogen.

The following impurities were detected: chromium, iron, copper, zinc and tantalum, at levels of the order of 0.1%; and tungsten, at levels of 3% to 5%. These levels were unexpectedly high, considering that the crystals were grown by zone refinement and other workers who have analysed crystals from the same source by spark source mass spectrometry have found impurity levels below 100 $\mu g g^{-1}$ for these elements, except for tantalum. It is possible that additional tungsten and copper impurities were introduced into the surface layer while planing the crystals in a spark machine with a copper-tungsten cathode.

To test the possibility that the tungsten is concentrated in the surface layers, several samples were examined by Rutherford backscattering. This confirmed that the high tungsten concentrations were near the surface. The results were consistent with the hypothesis of a gradual decrease in tungsten concentration with increasing depth within about 1 μm from the surface.

A typical PIXE spectrum is shown in Fig. 1.4. 0.526 mm of perspex was used as a filter to reduce the low energy bremsstrahlung background. The tungsten impurities are clearly seen as the L series lines for tungsten.

1.2.10 L-subshell ionisation calculations

(D.D. Cohen (AINSE))

The experimentally measured X-ray yields, I_p, in a peak p originating from an initial L-subshell vacancy, are converted to subshell ionisation cross sections σ_i^I(i = 1, 2 or 3) by the use of fluorescence yields w_i, Coster-Kronig transitions f_{ij} and radiative transition rates S_{pi}. The final choice of experimental or theoretical values for w_i, f_{ij} or S_{pi} can vary the experimentally calculated ionisation cross sections by up to 50%.

For light-ion bombardment of targets above gadolinium, modern X-ray energy dispersive techniques are capable of resolving at least ten different L X-ray lines associated with a vacancy in the L_1, L_2 or L_3 subshells. We therefore have both a choice of atomic parameters and a choice of particular

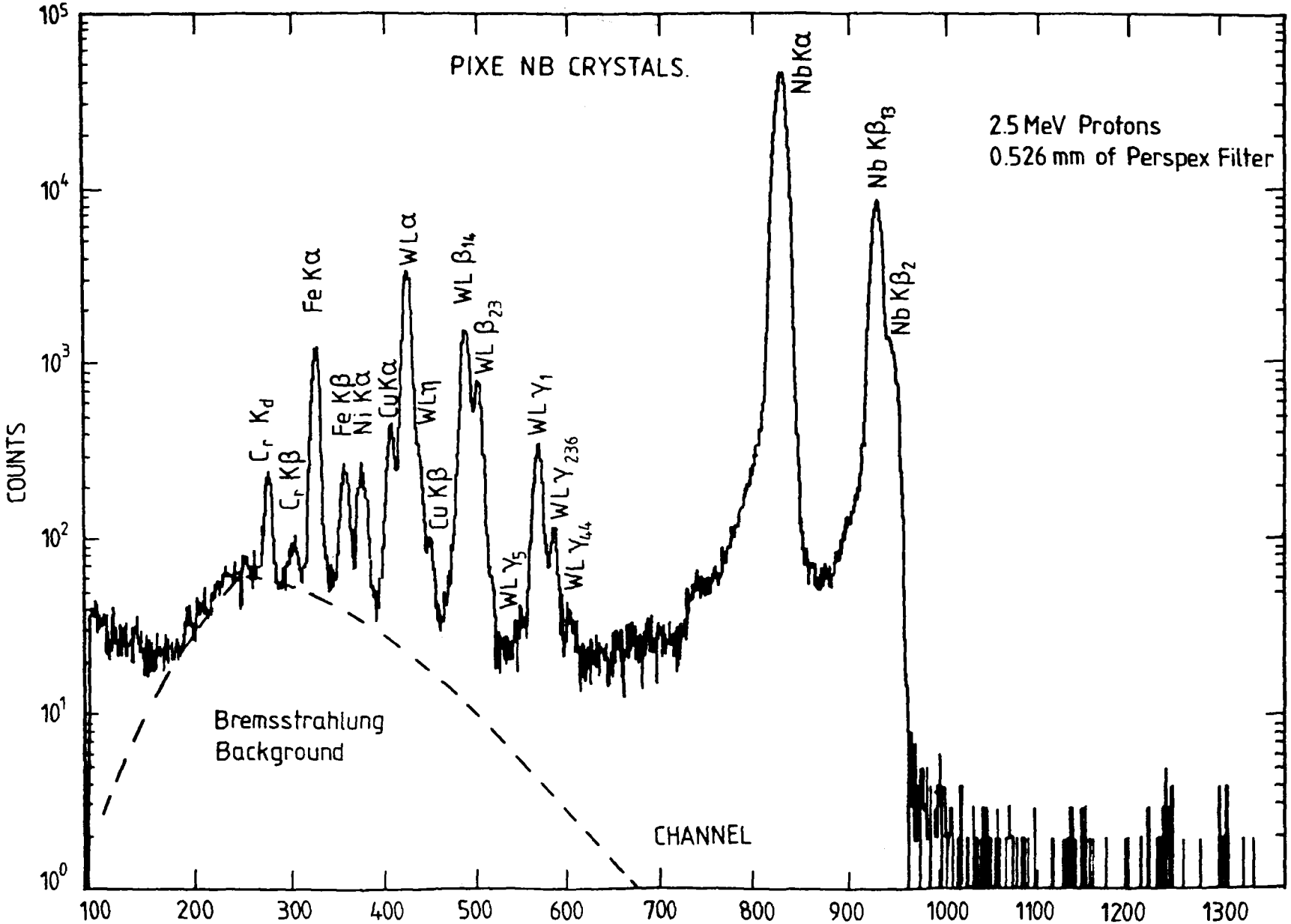

Fig. 1.4 PIXE spectrum from niobium single crystal

peaks p, which we may use to solve for the three ionisation cross sections σ_i^I(i = 1, 2 or 3). This can give rise to a large spread in the final result and may account for some of the discrepancies, which often amount to several times the quoted errors, which have been found in the published literature.

The X-ray production cross sections for a peak p and ion of energy E, $\sigma_p^x(E)$, are related to the yield/μC in that peak $I_p(E)$ in the following manner.

$$\sigma_p^x(E) = \frac{2.013 \times 10^{16} I_p(E)}{A\Omega x} \qquad (1)$$

for a thin target and

$$\sigma_p^x(E) = \frac{2.013 \times 10^{12} \rho}{A\Omega} \left[S(E) \frac{dI_p(E)}{dE} + \mu_p \frac{\cos \theta_i}{\cos \theta_o} I_p(E) \right] \qquad (2)$$

for a thick target where A is the number of target atoms per cm^3, x is the target thickness (in μm), Ω is the detector solid angle (in sr), ρ is the target density (in g cm^{-3}), S(E) is the ion stopping power (in MeV $cm^{-2}g^{-1}$), μ_p is the mass attenuation coefficient (in $cm^{-2}g^{-1}$) for X-ray peak p and ϕ_i and ϕ_o are the inward and outward going angles measured to the target surface normal.

The X-ray production cross sections for the most commonly resolved L_α, L_β and L_γ series peaks are then related to the three ionisation subshell cross sections σ_i^I(i = 1,2,3) in the standard way:

$$\sigma_1^x = [\sigma_1^1(f_{12}f_{23}+f_{13})+\sigma_2^1 f_{23}+\sigma_3^1]\omega_3 S_{13} \qquad (3)$$

$$\sigma_\alpha^x = [\sigma_1^1(f_{12}f_{23}+f_{13})+\sigma_2^1 f_{23}+\sigma_3^1]\omega_3 S_{\alpha 3} \qquad (4)$$

$$\sigma_\eta^x = (\sigma_1^1 f_{12}+\sigma_2^1)\omega_2 S_{\eta 2} \qquad (5)$$

$$\sigma_\beta^x = \sigma_1^1[\omega_1 S_{\beta 1}+\omega_2 f_{12} S_{\beta 2}+\omega_3(f_{13}+f_{12}f_{23})S_{\beta 3}]+ \sigma_2^1(\omega_2 S_{\beta 2}+\omega_3 f_{23} S_{\beta 3})+\sigma_3^1\omega_3 S_{\beta 3} \qquad (6)$$

$$\sigma_\gamma^x = \sigma_1^1(\omega_1 S_{\gamma 1}+\omega_2 f_{12} S_{\gamma 2})+\sigma_2^1\omega_2 S_{\gamma 2} \qquad (7)$$

$$\sigma^{x}_{\gamma 1} = \sigma^{1}_{1}\omega_2 f_{12} S_{\gamma 1,2} + \sigma^{1}_{2}\omega_2 S_{\gamma 1,2} \quad (8)$$

$$\sigma^{x}_{\gamma 5} = \sigma^{1}_{1}\omega_2 f_{12} S_{\gamma 5,2} + \sigma^{1}_{2}\omega_2 S_{\gamma 5,2} \quad (9)$$

$$\sigma^{x}_{\gamma 23} = \sigma^{1}_{1}\omega_1 S_{\gamma 23,1} \quad (10)$$

$$\sigma^{x}_{\gamma 44'} = \sigma^{1}_{1}\omega_1 S_{\gamma 44',1} \quad (11)$$

$$\sigma_{TOT} = \bar{\omega}_1 \sigma^{1}_{TOT} = \nu_1\sigma^{1}_{1} + \nu_2\sigma^{1}_{2} + \nu_3\sigma^{1}_{3} \quad (12)$$

where

$$\nu_1 = \omega_1 + f_{12}\omega_2 + (f_{13} + f_{12}f_{13})\omega_3 \quad (13a)$$

$$\nu_2 = \omega_2 + f_{23}\omega_3 \quad (13b)$$

$$\nu_3 = \omega_3 \quad (13c)$$

and S_{pi} is the fraction of the radiative transition to the ith subshell associated with the L_p peak. For example, $S_{\gamma 2}$ refers to the fractional radiative width of all L_γ transitions in the L_2 subshell ($l_{\gamma 1}$, $L_{\gamma 5}$, $L_{\gamma 6}$) while $S_{\gamma 23,1}$ refers to only the $L_{\gamma 23}$ transitions in the L_1 subshell.

Equations (1) to (12) link the experimentally measured $I_p(E)$ to the three unknowns σ^{1}_{i}(i=1,2,3). Several combinations of the ten equations (3) to (12) can and have been used to solve for the experimentally measured subshell ionisation cross sections.

We have tried four approaches to solving these equations for the three unknowns σ^{I}_{i} (i=1,2,3).

Namely 1) Equations 4, 6 and 7 called the $\alpha\beta\gamma$ technique or TRY1.

2) Equations 4, 8 and 12 called the $\alpha\gamma_1$TOT technique or TRY2.

3) Equations, 4, 8 and 10 called the $\alpha\gamma_1\gamma_{23}$ or Datz technique or TRY3.

4) The mean of the $\alpha\beta\gamma$ and $\alpha\gamma_1$TOT techniques with some fine tuning on the minor Ll, $L\eta$ and $L\gamma_1$ lines, called TRY4.

Large variations can exist in the experimentally calculated ionisation cross sections σ^{1}_{i} for the L shell, even though

the same L peak X-ray production cross sections σ_p^x are used as a starting point. These differences are produced by the different analysis techniques, as well as the different data bases used by many authors to convert their σ_p^x to σ_i^I values. The $\alpha\beta\gamma$(TRY1) and $\alpha\gamma_1$TOT(TRY2) techniques are not recommended on their own, since they are both sensitive to the data bases (ω_i, f_{ij}, S_{pj}) chosen. However the mean of these two techniques together with the fine tuning suggested by us (TRY4) compares well with the method of Datz (TRY3), the main differences being in the L_1 subshell for heavy target atoms. This is probably due to the uncertain $L\gamma_{23}$ branching ratios within the L_1 subshell.

1.2.11 L-subshell X-ray production by 100-250 keV/amu ions

(D.D. Cohen (AINSE), M.F. Harrigan (Melbourne Uni.))

Individual L-subshell ionisation cross sections have been measured for bombardment by 100-200 keV H^+ ions in 10 keV steps of a thick Gd(Z=64) target and for bombardment by 600-1000 keV He^+ ions in 100 keV steps of thick W(Z=74) and thick and thin Au (Z=79) targets. The He^+ bombardment was performed in the AAEC 3 MV Van de Graaff and H^+ bombardment using the Melbourne University KAMAN A1254 neutron generator with H_2 gas supply. The beam was mass analysed to remove H_2^+.

Experimental results for the individual L subshells are compared with the theoretical predictions of the ECPSSR theory, developed by Brandt and Lapicki [4], in Figure 1.5.

The ratios of $\sigma_{exp}/\sigma_{theory}$ obtained (see Fig. 1.5) exhibit a trend with ion energy consistent with data published previously taken at higher bombarding energies, indicating an increasing deviation between experiment and theory as the reduced velocity decreases (see Fig. 1.6).

The general underprediction of experiment by the ECPSSR theory may, in part, reflect the use of SCH wavefunction rather than more realistic Dirac-Hartree-Slater (DHS) wavefunctions as suggested by Chen et al. [5] and more recently used in a calculation for K-shell ionisation by Mukoyama and Sarkadi [6]. the use of DHS wavefunctions is expected, however, to produce only 10-40% differences in the theoretical predictions of ionisation cross sections and hence another mechanism must be sought to

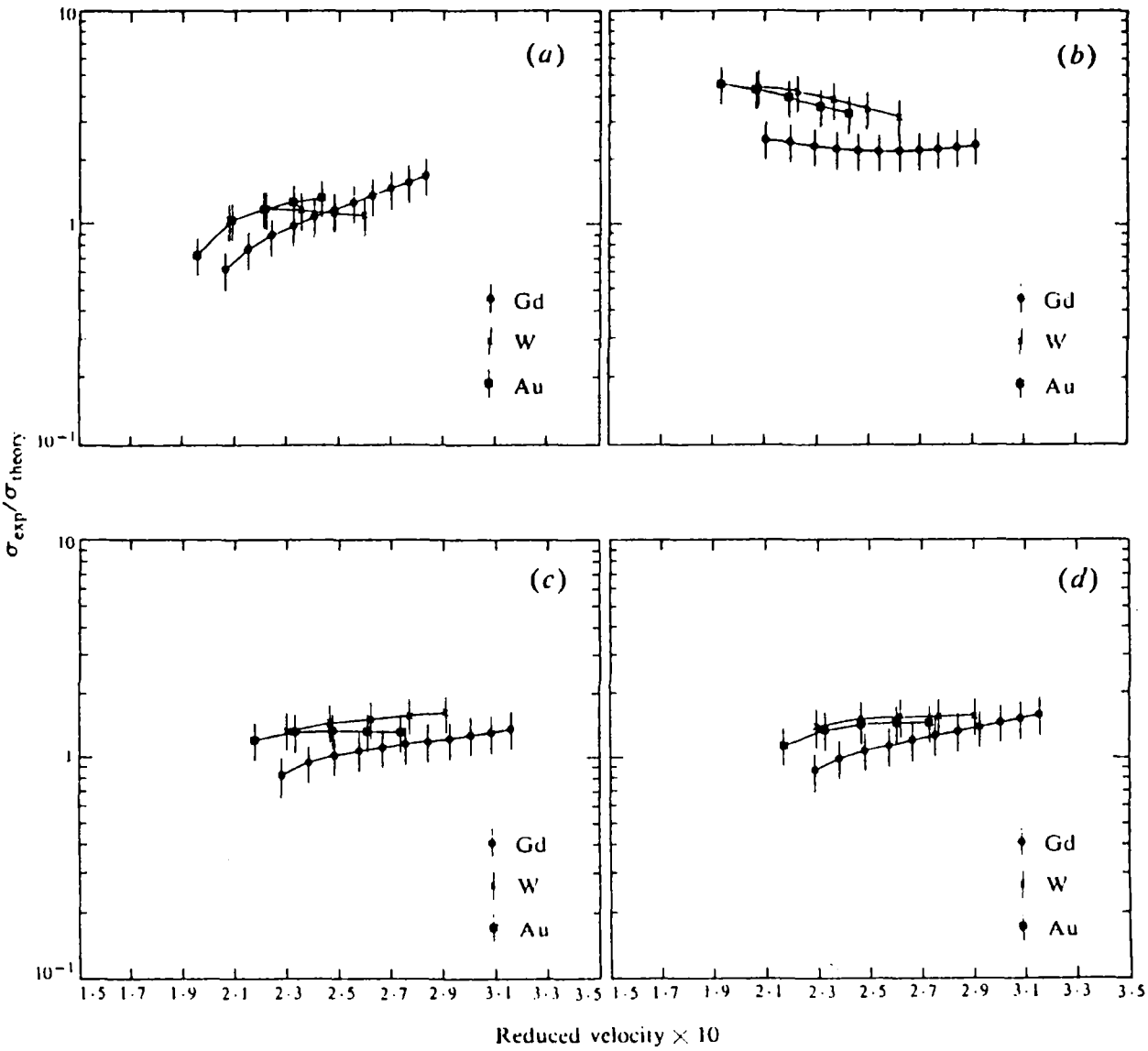

Fig. 1.5 Plot of the ratio $\sigma_{exp}/\sigma_{theory}$ against reduced ion velocity for Gd, W and Au for the (a) L_1 subshell, (b) L_2 subshell, (c) L_3 subshell, (d) L_{tot} shell. The solid curves are not least squares fits to the data but are inserted for clarity.

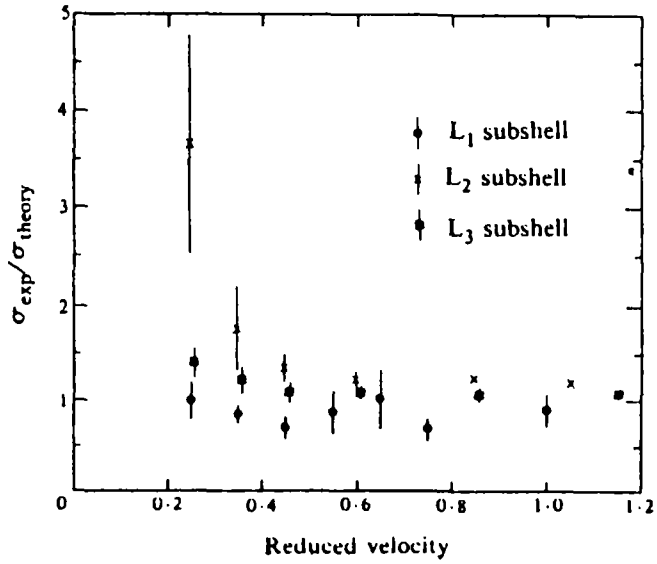

Fig. 1.6 Plot of the ratio $\sigma_{exp}/\sigma_{theory}$ against reduced ion velocity for current and previous experimental data. The data are plotted in corrected reduced ion velocity bins. There is an increasing deviation from unity for the L_2 subshell as the reduced ion velocity decreases.

explain the current discrepancy. Such a mechanism should possibly include ion effects as well as target effects.

One possible mechanism which could produce the effect is via a collision induced intra-shell transition. Here a primary vacancy initially produced in the L_1 subshell can transfer to the L_2 or L_3 subshell whilst the ionising projectile is still within the Coulomb field of the nucleus. Transfer to the L_2 subshell is more likely due to the comparatively small difference in binding energy. Such a mechanism is expected to be more significant when the ratio of target electron orbital time to collision time (i.e. the reduced ion velocity) is less than one. For the results reported here the reduced ion velocity ranges from ~0.19 to ~0.32. This mechanism would enhance the experimentally observed L_2 and L_3 subshell ionisation cross sections at the expense of the L_1 subshell.

1.2.12 Trace element analysis of fossil fuels

(E. Clayton and L. Dale - CSIRO Division of Energy Chemistry)

As a consequence of the increasing use of coal as an energy source there is a need for a detailed characterisation of coals and the by-products of combustion and processing. Environmental controls on industrial discharges are becoming stricter and the concentrations of a wide range of trace elements need to be known to assess their impact on the environment. To satisfy these demands multi element analytical techniques are required which can provide data with high precision and accuracy. PIXE is being used in conjunction with a number of instrumental techniques such as X-ray Fluorescence (XRF) and Neutron Activation Analysis (NAA) to provide a comprehensive data base on Australian coals.

Because of the potential environmental hazard of fluorine its determination is of great interest. PIGME has been applied in a number of studies on coal, fly ash and oil shale. As an instrumental method requiring minimal sample preparation PIGME has been an ideal technique for round robin studies where sample preparation methods have led to divergent results.

1.3 Neutron Scattering

(C.J. Howard, M.M. Elcombe, R.B. Knott, J.J. White)

Neutron scattering (making use of beams of thermal

neutrons from the reactor HIFAR) continued to find widespread application. Applied Physics Division staff again contributed to the development of techniques and facilities for neutron scattering, and engaged in selected applications.

1.3.1 Powder diffraction

The high resolution neutron powder diffractometer (HRPD) has performed well throughout the year. The HRPD has been used continually, mostly by visitors working either independently or with AAEC or AINSE staff. Its applications include examination of battery materials, determination of the structural stability of caesium substituted hollandites (relevant to SYNROC) and studies of the crystal structure of gamma-brass.

Members of the AAEC group work on checking and improving diffractometer performance, on developing improved methods for data analysis, and on some particular applications. For example, the analysis of powder diffraction patterns depends to a considerable degree on understanding the factors affecting the intensity distribution in these patterns, and studies have been made (in collaboration with Dr R.J. Hill, CSIRO Div. of Mineral Chemistry) of the factors affecting the shapes of the peaks in the diffraction patterns. In collaboration with Dr Hill and Prof. R.A. Young (Georgia Inst. Tech., Georgia, USA), computer programs are being developed for Rietveld analysis of powder diffraction patterns. Applications of current interest to AAEC staff include measurement of residual stresses in deformed steels (in collaboration with Monash Univ.), the detailed structure of $PbHPO_4$ (in collaboration with Edinburgh Univ.) and the determination of the crystal structure of a newly discovered low temperature phase of NaOD.

1.3.2 Inelastic scattering

The triple axis spectrometer (TAS) has continued to operate satisfactorily despite increased downtime caused by computer failure (replacement of the computer and interface is in progress). In collaboration with CSIRO and Monash University, a major effort has been made to observe the Kikuchi effect with neutrons. This effect is well known to workers in electron diffraction. While the theoretical prediction of this effect is straightforward, the experimental conditions necessary for its observation are complex. Results obtained with the TAS immediately prior to the long shutdown are encouraging.

1.3.3 Structural biology

The one-dimensional position sensitive detector recently installed on the structural biology diffractometer is now routinely producing high quality data. This detector, the first of a new generation of detector systems, represents a major improvement in the quantity and quality of neutron diffraction data. Experiments are currently in progress to investigate, in collaboration with the pharmaceutical company Sandoz Australia Pty Ltd the interaction of the immunosuppressant drug, cyclosporin A, with reconstituted cell membranes.

1.4 Data Processing

(S. Craig, E. Clayton, R.J. Cawley* (*Applied Maths and Computing Division))

Major computing facilities are as follows:

1. PDP11/23
   - 12 I/O ports
   - 2 VT125 graphic terminals
   - 1 VT100 VDU
   - LA120 dot matrix printer
   - LA 34 graphics printer
   - 2 RL02 10 Mbyte disks
   - 4 Data-way lines (site network)
2. PDP11/40
   - 9 I/O ports
   - 1 CIT 414 graphics terminal
   - 1 Decwriter IV hard copy terminal
   - 1 HP 7470 Plotter
   - 2 RL02 10 Mbyte disks
   - 2 RX02 Floppy drives
   - 1 VT11 graphics device
   - 1 Ortec CAMAC crate & controller
   - 2 Data-way lines (site network)
3. 2 LeCroy 3500 Programmable Multi-channel Analysers
   - 5 I/O ports
   - 1 Mini CAMAC crate (plus ADC's dead timers, etc.)
   - 1 Printer
   - 2 Floppy disk drives

4. 1 NEC APC Personal Computer (colour, graphics)
   2 I/O ports
   1 Bit pad
   2 Floppy disk drives
   1 SMUT line (site network)
5. 1 GT40 Graphics device
   2 Data-way lines (site network)
6. Other
   PDP11/10 (2 data way lines)
   Various micro computers
   Various VDU terminals

The section's facilities are, for the most part, currently directed towards three main areas.

1. Data acquisition
2. Data transfer
3. Site network access

Local analysis of data is currently kept to a minimum with emphasis placed on transferring data to the site's IBM 3481 where use is made of its superior 'number crunching' power and archiving capabilities. However, local analysis is performed on the PDP11/40 and some preliminary analysis capability is being developed for the PDP11/23.

LeCroy 3500

The two LeCroys are used as portable data acquisition stations. The 3500 is a programmable multichannel analyser which houses a mini CAMAC crate (8 stations). The acquisition modules are ADCs controlled by dead-timers. Output registers are used to drive experiments, allowing unattended automated sample change and data acquisition.

The acquired data can be stored on the LeCroy's floppy disk or transferred to the PDP11/23 and stored on hard disk from which it can be retrieved or transferred to the IBM for analysis and archiving. The data may also be analysed at the LeCroy either qualitatively or by using a peak search routine.

Since, on almost all occasions, data is transferred to the PDP11/23, much work and time is devoted towards streamlining this process and making it as fast and reliable as possible. This is necessary since time is critical during experiments, and the LeCroys are, like most systems of their type, incapable

of transferring data and controlling experiments simultaneously.

PDP11/23

The main task of the PDP11/23 is to act as a middle man in the transfer of data to and from the IBM. Data is received from the LeCroys or other data acquisition systems and stored on hard disk, edited if required, and transferred (either automatically or manually) to the IBM for analysis.

The PDP11/23 is running under RSX11M which is a multiuser operating system. This enables it, along with other tasks, to service several data acquisition systems at the same time. In addition, users are able to access the IBM (and other nodes) through the site network system allowing them to analyse and view data and obtain hard copy outputs locally.

Some preliminary analysis of data has been developed this year for the PDP11/23 and it is envisaged that this will be improved and expanded. However, there is no intention of replacing the analysis performed on the IBM since the PDP11/23 simply lacks the size and power to do the analysis effectively. In order to save disk space, it is now possible to analyse a PIGME spectrum and load the resulting data into the high channels of the corresponding PIXE spectrum.

Considerable effort has continued to be applied to the speed and reliability of data transfer. In addition the software has been expanded to allow data transfer from acquisition systems other than LeCroys. Facilities have been developed which allows the user to edit his data files prior to transfer to the IBM. In addition local plotting of data is now possible.

PDP11/40

The PDP11/40 is used by the Safeguards and Nuclear Physics section as a standalone data acquisition system capable of collecting data from multiple experiments simultaneously. Software development on this machine has been directed towards data collection, analysis, presentation and archiving for Pulse Height, Correlated Event and Multi Parameter experiments.

Experimental data is acquired from a CAMAC crate via an ORTEC unibus CAMAC controller. Device drivers have been written to access stations within the crate to which the data

is fed by an experiment using suitable electronics. The data is passed to an appropriate program which displays the data and supplies the user with the necessary tools for analysis. The user can then store the data on disk for further analysis, plotting or archiving.

1.5 Neutron Diagnosis and Therapy Project

1.5.1 Boron neutron capture therapy

(B.J. Allen, H. Linklater, D.J. Wilson)

(a) Moata Neutron Capture Therapy Facility - Neutron capture therapy experiments require a flux of approximately 10^9 neutrons $cm^{-2}s^{-1}$ and a much lower concomitant gamma dose. This has been achieved in a rig installed in the thermal column of the reactor Moata which uses boron carbide in epoxy for neutron shielding and lead and bismuth for gamma-ray shielding. Neutron and gamma dose measurements are made with gold foils and enriched ^6LiF and ^7LiF thermoluminescent detectors (TLD). Biological measurements have recently commenced to measure radiation damage to peripheral human blood, bone marrow and leukaemia cells in collaboration with St Vincent's and Westmead Hospitals and hamster and human melanoma cells in collaboration with Environmental Science Division.

(b) Malignant Melanoma - In collaborative experiments between Applied Physics Division and the Queensland Institute of Medical Research, the uptake and incorporation of chlorpromazine (CPZ) and thiouracil (TU) have been tested on a library of human melanoma (HM) cell cultures. Results showed that TU has enhanced incorporation for melanomas with high tyrosinase and melanin content.

Amelanotic and melanotic HM cell lines have been cultured for use in in vitro studies of neutron capture therapy for 10BPA, an enriched IOB compound obtained from Dr Y. Mishima, Kobe University School of Medicine, Japan, which shows enhanced incorporation for both melanotic and amelanotic melanoma.

The cultures are implanted in nude mice (NM) and grown as HM xenografts for benchmark testing of TU in the HM-NM model. A biohazard cabinet has been installed in Isotope Division for this purpose.

A boron analogue of TU is being synthesised in Isotope Division and the biodistribution of this compound will be

compared directly with the TU benchmark. B-TU will be an entirely new compound.

The Department of Pharmacy, Sydney University is conjugating a decaborane compound obtained by the AAEC to an intermediary protein which is then coupled to albumin. Boron analysis of the products of this synthesis has been carried out at the AAEC with an inductively coupled plasma spectrometer. Monoclonal antibodies (MCA) from the University of Newcastle have been supplied for the next stage, i.e. the loading of the MCA with the boron compound and subsequent testing of the MCA specificity. MCA for melanoma associated antigens have been obtained from the US for the final application.

(c) Bone Marrow Transplantation for Leukaemia - In recent years, bone marrow transplantation has led to improved survival rates for patients with chronic myeloid leukaemia or acute lymphoblastic and non-lymphoblastic leukaemia. However, only well matched sibling donors can be used and, even then, morbidity and mortality from graft versus host disease (GVHD) can arise (i.e. the donor marrow rejects the recipient).

In a collaborative project between Applied Physics Division and St Vincent's and Westmead Hospitals, NCT is being applied to the task of eliminating donor T-cells (which cause GVHD). Cobalt boride (Co_2B) particles would be coated with MCA against the T-cells, mixed with donor marrow and irradiated in the NCT rig in Moata. T-cells or leukaemia cells will be selectively culled relative to the stem cells which are needed for blood cell production.

Co_2B particles have been synthesised at the Australian Radiation Laboratory and examined with the AAEC transmission and scanning electron microscopes. The Co_2B particles were coated successfully with MCA from the University of Melbourne.

1.5.2 Total body nitrogen facility

(B.J. Allen, N. Blagojevic*, H. Linklater)

(*Isotope Division)

Following the successful operation of a prototype facility in Applied Physics Division last year, a mechanised table has been constructed with preset movement and exposure time. A stronger ^{252}Cf source (1.1×10^8 n sec^{-1}) has been purchased and a second NaI gamma detector borrowed from CSIRO. The TBN

facility has been set up in Building 53 with existing equipment and, in the short term, will make use of the existing on-line computer facilities in B.53. Linearity, stability, reproducibility and dose depth measurements have been repeated with urea phantoms, simulating patient exposures. Considerable attention has been given to neutron and gamma ray dosimetry. With Health and Safety Division, neutron rem meters have been calibrated with the ^{252}Cf source, and Monte Carlo calculations have been made by Nuclear Technology Division. Single exposure doses are at the lower limits of detection for conventional film badges, but enriched ^{6}Li TLD's may prove to be useful in this regard. H & S D has undertaken responsibility for dosimetry for the TBN project.

(a) In Vivo Determination of Protein for Fibrocystic disease - The National Health and Medical Research Council has approved the Royal Alexandra Hospital for Children research program for the management of children with cystic fibrosis. The major thrust of this program is the testing of parenteral nutritional supplementation using elemental or polymeric formulae via nasogastric or gastrostomy tubes. The measurement of protein in the TBN facility is a central element in determining the efficacy of the protein repletion diets. The Royal Alexandra Hospital for Children is ready to commence neutron exposures (one day per month) as soon as the final testing phase is completed.

(b) Nutritional Indices in Haemodialysis Patients - The Department of Renal Medicine at Royal Prince Alfred Hospital is commencing a study of haemodialysis patients to assess if energy supplementation will improve their nutritional status and to identify the prevalence of other nutritional deficiencies. Measurement of protein with the TBN facility is requested and has been approved by the RPAH Ethics Committee. Subjects are all ambulatory outpatients and would be accompanied by their dietician. About one day per month would be required for neutron exposure.

(c) General Comments - The Safety Review Committee and NHMRC have approved both projects and the NSW Department of Health is to issue the responsible clinicians with a limited licence for this diagnostic procedure. The TBN facility is an

important part of hospital research projects aimed at improving the quality of life of patients with cystic fibrosis or renal disease. If the TBN techniques are adopted as a clinical tool, Department of Health funds should be sought by the hospitals for the establishment of in-house facilities.

1.6 Electron Beam Irradiation of Grain

(J.R. Bird)

At the request of the Australian Wheat Board, Dr J.R. Bird accompanied a technical mission to the USSR to assess the practicality of the use of a 1.5 MeV electron accelerator in the direct irradiation of wheat. An operating facility was inspected at the port of Odessa where wheat is irradiated at up to 400 t/hr for disinfestation of shipments arriving with infested cargo. A visit to the Institute of Physics at Akademgorodok, Novosibirsk allowed discussions with the designers of the accelerator and grain handling system. The mission also visited the Radiation Chemistry Research Institute at Takasaki, Japan and Radiation Dynamics Ltd at Swindon, UK to see alternative accelerator types in operation.

Upon return, a report was prepared for consideration by the Australian Wheat Board including an assessment of accelerator and irradiation technology, effectiveness of electron beam irradiations for disinfestation, possible side effects and the status of public acceptability and legislative measures relating to food irradiation. The technology has been well established through research and applications over the past 20-30 years and the effectiveness of grain irradiation has been fully demonstrated. Much less work has been published on the effects of electron irradiation on the properties of wheat, bread, noodles, etc., although it was claimed that these had been fully investigated in the USSR. The adoption in 1983, of an international codex standard for electron irradiation at energies up to 10 MeV and doses up to 10 kGy has cleared the way for routine use of this technique but considerable effort will be needed in explaining the issues involved to achieve public acceptance.

REFERENCES FOR CHAPTER 1

[1] Hurford, A.J. and Green, P.F., Isotope Geoscience 1, 285-317 (1983).

[2] Ziegler, J.F., Lever, R.F. and Hirvonen, J.K. in "Ion Beam Surface Layer Analysis", Meyer, O., Linker, G. and Kappeler, F. eds. (Plenum Press, N.Y., 1976) p 163.

[3] Dorn, R.I., Quatern. Res. 20, 49 (1983).

[4] Brandt, W. and Lapicki, G., Phys. Rev. A 20, 465 (1979).

[5] Chen, M.H., Craseman, B. and Mark, H., Phys. Rev. A 26, 1243 (1982).

[6] Mukoyama, T. and Sarkadi, L., Phys. Rev. A 28, 1303 (1983).

2. SEMICONDUCTOR AND RADIATION PHYSICS

2.1 Semiconductor Radiation Detectors

2.1.1 Neutron transmutation doping of silicon

(E.M. Lawson, P.J. Lee, A.J. Tavendale)

Controlled, highly uniform doping of crystalline Si by phosphorus, unattainable by conventional crystal growth methods, is effected by neutron transmutation through the reactions

$$^{30}Si + n \rightarrow {}^{31}Si \rightarrow {}^{31}P + \beta^-$$
$$(\tau_{\frac{1}{2}} = 2.6h)$$

giving material which is ideal for application in the manufacture of power thyristors and rectifiers.

As indicated in the previous report, following the decision by the Commission to enter into commercial production of neutron transmutation doped (NTD) silicon using the HIFAR facility, the SRD Group has been required to supply the expertise and effort directed towards accurate measurements of silicon target resistivity versus neutron fluence characteristics of the reactor. Earlier work concentrated on establishment of an appropriate post-irradiation high-temperature annealing cycle including necessary chemical etching and handling procedures together with assurance trials of resistivity measuring equipment (four point probe).

During the present period a high level of effort was provided to the NTD Si project for the main tasks:
(1) Calibration of the neutron fluence - silicon resistivity characteristic of the new interim production rig in HIFAR.
(2) Intercomparison of Japanese (Komatsu) and American (National Bureau of Standards) resistivity standards from silicon.

The second task required careful refinements to our earlier resistivity measuring techniques, particularly in regard to sample temperature stability and ambient humidity conditions for which corrections were found necessary in order to attain best possible accuracy. A systematic error was located in the 4-point resistivity probe instrument (now well-worn) and allowed for. As a result of the precautions we were able to determine resistivities below 120 ohm-cm with an accuracy of better than 0.3% (one standard deviation of the mean).

Further, our measured resistivities of the Japanese supplied 'standards' were within ± 0.5% of their quoted values which was very gratifying, especially in relation to our HIFAR calibrations ((1) above) for customer usage.

A thermal anneal cycle of 800°C for 2 hours combined with phospho-silicate glass gettering was used in the above work, the efficacy of this cycle having been determined previously by deep level transient spectroscopy (DLTS) analysis of annealed NTD Si.

During the period we also commenced study of a simple, rapid thermal anneal technique for removal of radiation defects from neutron irradiated silicon as detected by deep level transient spectroscopy. This technique, using a small tube furnace, involves annealing for times in the range 15-20 sec, at temperatures from 600-900°C. Significant annealing occurs for all combinations of temperature and time. Figure 2.1 shows that traps remaining after 1 min at 600°C are not present if the anneal is 15 sec at 900°C.

2.1.2 Hydrogen in silicon - a study of basic electronic properties

(A.J. Tavendale, A. Williams and D. Alexiev)

Atomic hydrogen may be introduced by diffusion from a low-pressure plasma source into semiconductors. It then has the unique property of being able to neutralise many different chemical and radiation-induced defects which are often deliterious to the operation of semiconductor devices including nuclear detectors. Studies on this topic have been reported extensively by the SRD Group.

Hydrogen is unusual in that it appears to be electrically inactive in semiconductors despite reaction with defects which might imply that it is active (most hydrogen in as-grown crystals is probably in the neutral molecular form, H_2).

However, it has recently been reported that electrically active hydrogen may be the cause of long-life instabilities in MOS (metal - oxide - silicon) memory logic devices, a problem which is of considerable concern to device engineers. Further, it has also been reported that it seems possible to neutralise the commonly used dopant boron in Si using a hydrogen plasma but there is some argument as to whether hydrogen and not some

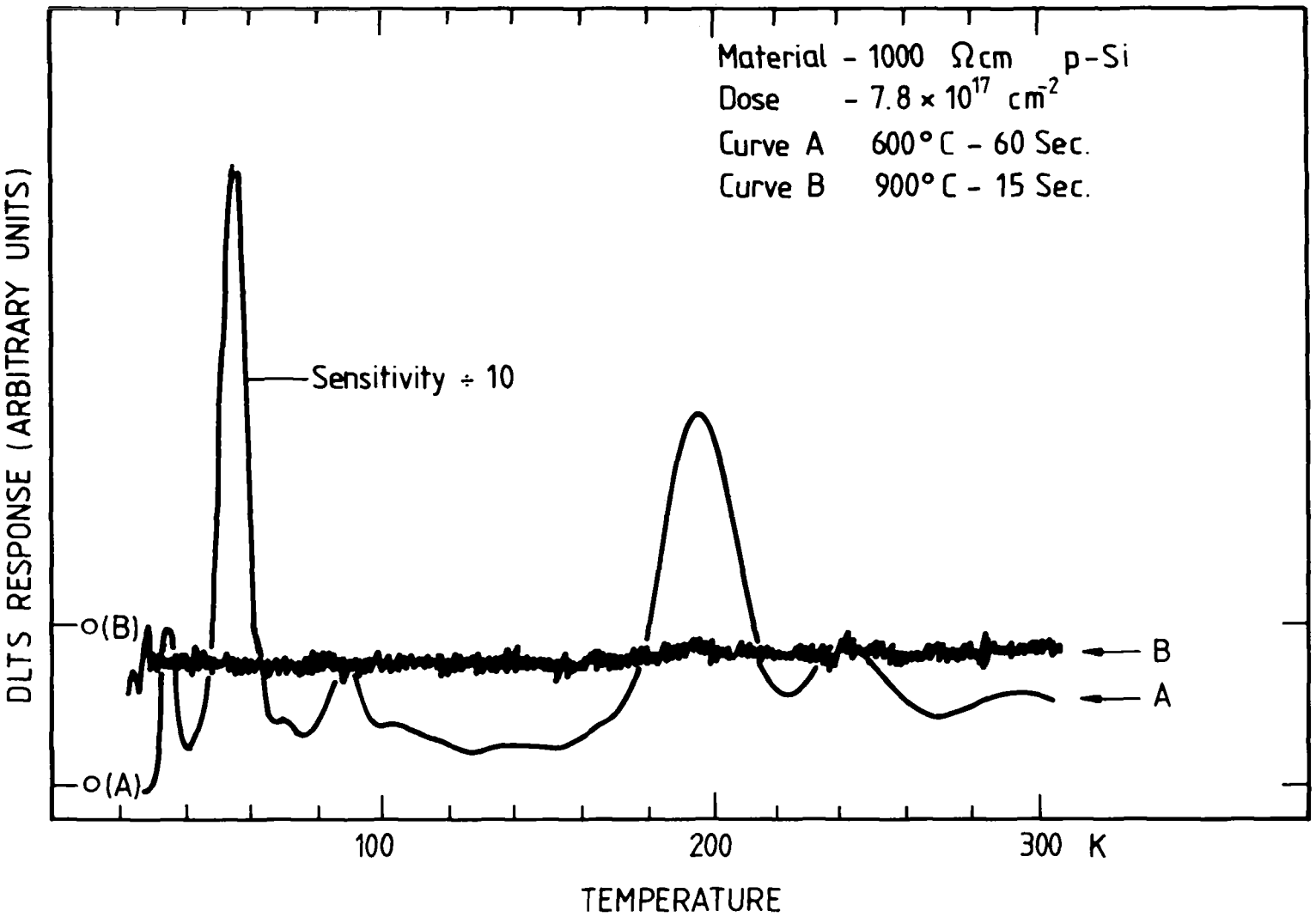

Fig. 2.1 Rapid thermal annealing of NTDSi: demonstration that high temperatures (900°C) and times as short as 15 s can completely anneal NTDSi

other complex of hydrogen (e.g. OH) is the neutralising agent. (It has recently been shown by us (SIMS analysis) and other workers that oxygen is not involved in the neutralisation process.)

Following our earlier interest in the topic, we treated Si with both hydrogen and deuterium plasmas and have demonstrated by isotopic means (diffusion effects) that hydrogen is almost certainly the neutraliser. In addition, and most significantly, we showed that hydrogen appears to drift in Si as a positive ion with a donor level in the upper-half region of the forbidden energy gap, the latter being contrary to general theoretical considerations. Fig. 2.2 illustrates the effect in Schottky diodes from plasma-hydrogen treated silicon.

At present we are conducting secondary ion mass spectrometry (SIMS) analyses of plasma-treated samples in collaboration with staff (Dr S.J. Pearton) of AT and T Bell Laboratories to confirm chemically the results of our electrical measurements.

Hydrogen-ion drift neutralisation of acceptor dopants in p-type Si appears in principle to be similar to the lithium-ion drift process used for deep depletion layer radiation detector fabrication and therefore may be of some practical interest. Studies on the long-term stability of the phenomenon are in progress.

2.1.3 Gallium arsenide for radiation detectors

(D. Alexiev, A.J. Tavendale)

The semiconductor Radiation Detector Group has an active program for introducing new materials for detector construction purposes. One such semiconductor is the compound gallium arsenide which has recently become prominent in the electronics industry for fast logic device applications. GaAs detectors offer room temperature operation because of the wide band gap of the material, and with X- and γ-ray stopping power equivalent to germanium. Small surface barrier detectors were fabricated from liquid phase expitaxial GaAs by the Group in the early 1970's, demonstrating excellent resolution (Eberhardt et al. [7]). However, for higher gamma energies larger depletion volumes are required thereby shifting current interest to bulk Bridgman, zone-refined and Czochralski grown

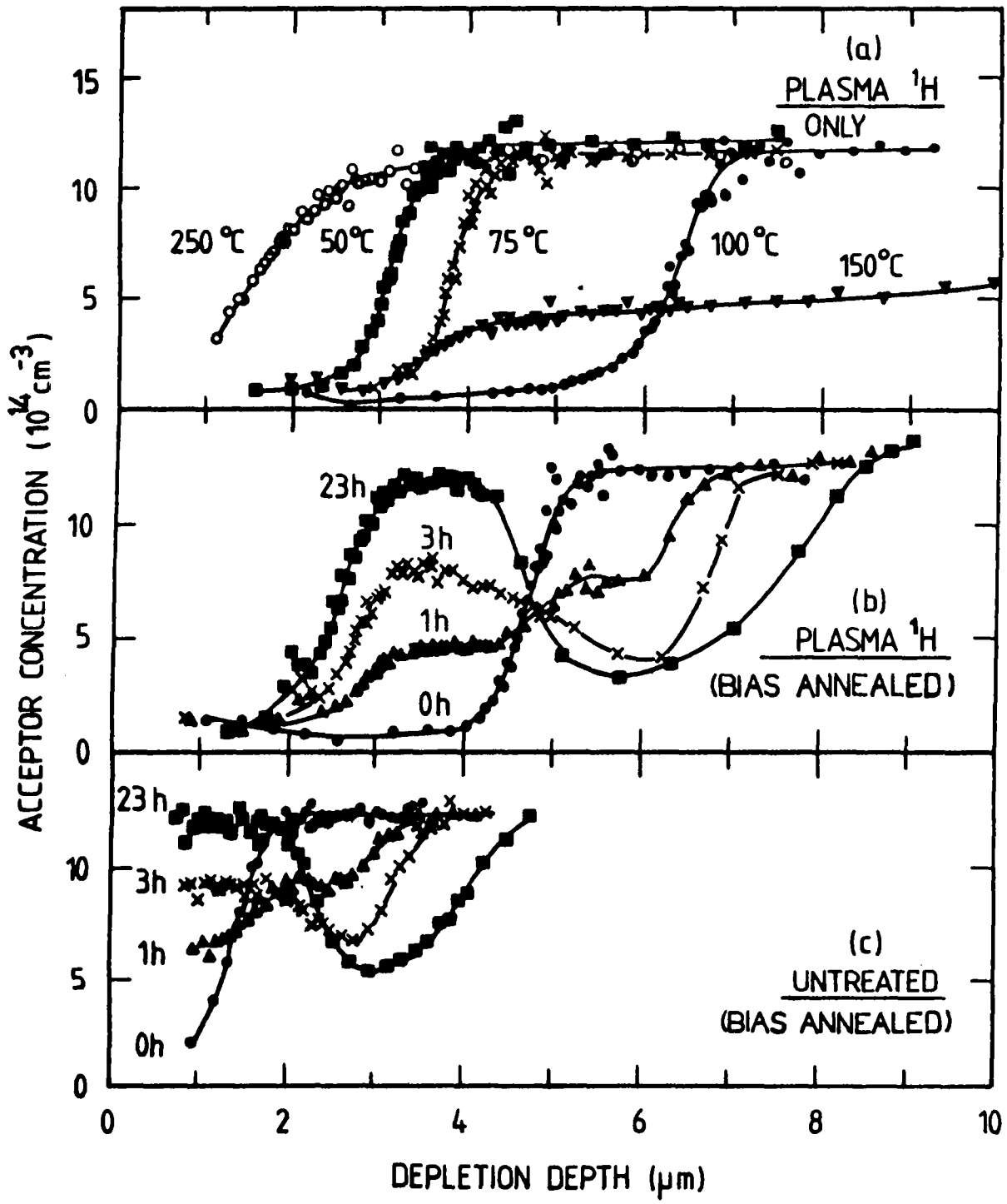

Fig. 2.2 (a) Variation of bulk acceptor compensation with temperature in B-doped, 10 Ω cm p-Si exposed to plasma ^{1}H for 1 h

(b,c) Bulk acceptor compensation variation with time at 80°C in reverse biased Schottky diodes from hydrogenated, B-doped 10 Ω cm p-Si (V_R = 15 V) and untreated Si (V_R = 5 V), respectively.

material. The Czochralski material is generally grown under a liquid encapsulant (B_2O_3) to suppress As vapour loss (LEC material).

As a result of the recent commercial availability of GaAs having claimed improvements in purity and structural quality we decided to assess the potential of this material for detectors. At the same time we investigated the feasibility of using such techniques as thermal annealing and lithium compensation in an attempt to eliminate electrically active defects (traps) present in this material.

A number of undoped n-type, (LEC) semi-insulating wafers and a smaller section of p-type horizontal Bridgman (HB) grown material was obtained from Cambridge Instruments (UK). The material was evaluated using Deep-Level Transient Spectroscopy (DLTS) techniques to examine trapping (recombination) centres. It was found that the semi-insulating GaAs produced a hole trapping spectrum (Fig. 2.3). Compensation was attempted by diffusing lithium and annealing at various temperatures and times. It was found that the Li did not reduce the net residual impurity level but increased the magnitude of hole trap labelled H1 thought to be a native defect and responsible for the high resistivity of the material. Annealing of the material at comparable temperatures and times to that of the Li diffusion did not alter the characteristic hole spectrum. Similarly, no change was noted when the material was subjected to electric-field drift at various temperatures (reverse biased Schottky diodes).

When the semi-insulating GaAs was examined for its crystallinity using the JOEL scanning electron microscope and an infrared transmission microscope, the material appeared to contain significant defect structure. The wafers examined followed a trend from low to high dislocation densities from the core outwards with the outer perimeter containing a fine cellular structure. When examined under higher magnification, these cellular patterns revealed arrays of inclusions. An attempt to analyse these failed, but they are most likely to be contaminants of B_2O_3 or a Si compound of the flux and crucible used during the LEC crystal growth.

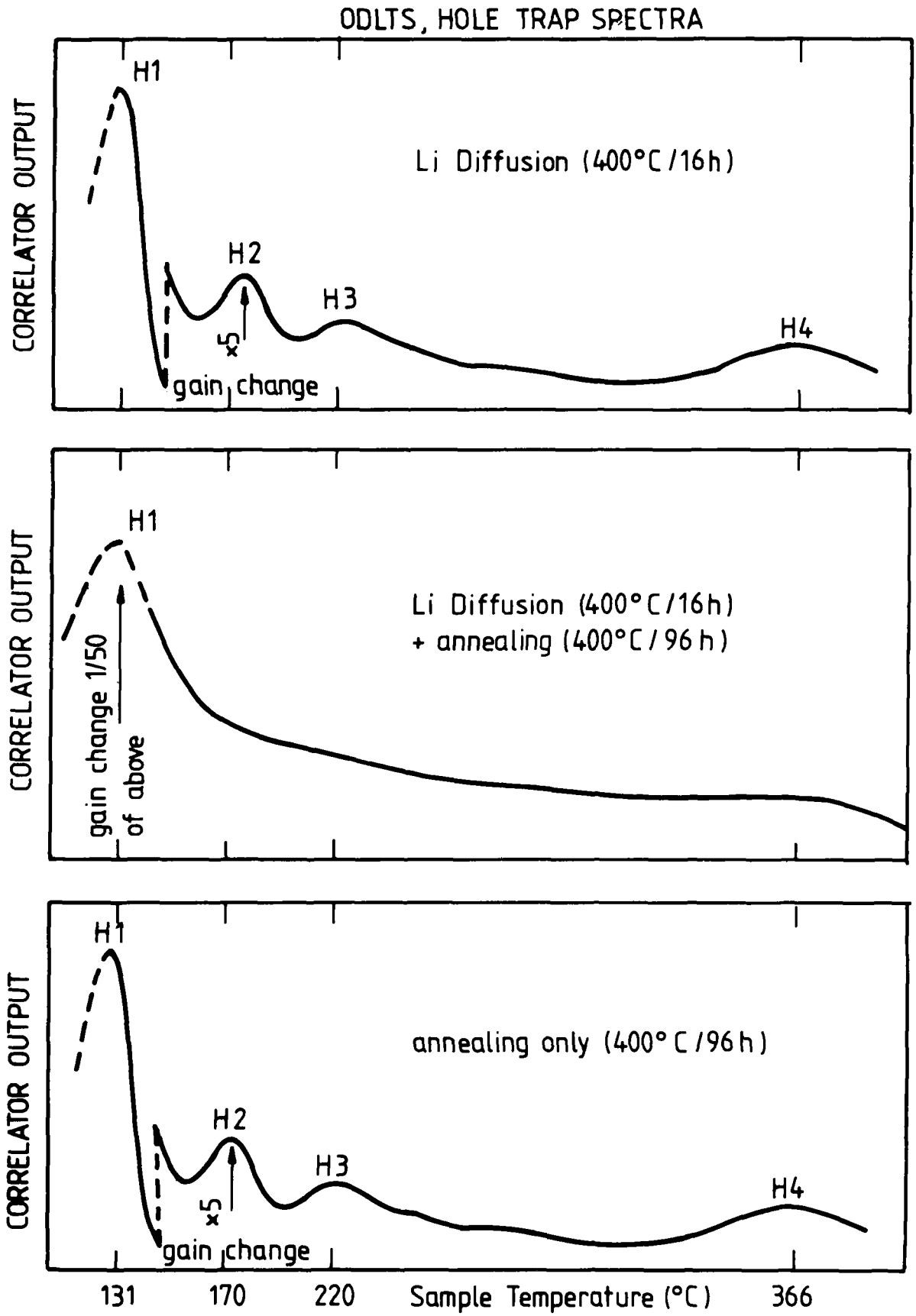

Fig. 2.3 A hole spectrum of four major recombination centres is shown. Top and lower plots show the native defect composition of the p-type GaAs examined, unaltered by either Li diffusion or thermal anneal treatment. Centre plot shows a marked increase in trap H_1 concentration (correlator output) after Li diffusion followed by annealing.

The p-type (HB) GaAs is being used with Neutron-Transmutation Doping (NTD) experiments in mind. These experiments are currently under way and are aimed at counter-doping the p-type GaAs with the transmuted product donors Ge and Se to a 'titrated' n-type GaAs.

Since each NTD run requires annealing at high temperatures to restore damage caused by the irradiation process, some prior characterisation is necessary. DLTS spectra were taken from a number of samples annealed under a Ga-In alloy getter. 'Finger-print' spectra were obtained showing two shallow and two deep acceptors with field dependency of one of the deeper hole traps.

2.1.4 Semiconductor radiation detector services

(P.J. Lee, A.A. Williams)

Provision of maintenance and repair services for large-volume lithium-drifted germanium X-ray spectrometers continued at a significant level covering isotope applications, safety, environmental science and SYNROC projects. Six large-volume detectors were serviced or supplied. Design of a new, horizontal-mounted Si(Li) X-ray spectrometer for PIXE analysis was commenced, a special feature of this instrument being an extended horizontal detector housing. The new type preamplifier hermetically-sealed housings implemented earlier for use with liquid nitrogen-cooled detector systems continue to function very successfully.

2.2 Radiation Standards

2.2.1 Radioactivity standards - documentation of activity metrology

(K.F. Mears)

The Radiation Standards Group is at present involved in the documentation of the procedures that have been developed over the past years and most commonly employed at the AAEC metrology laboratories.

Whilst it was hoped that computerisation of the counting procedures would help relieve the pressures brought about by under staffing, it has also emphasised the need for comprehensive documentation of the present state of the art and acquired knowledge.

In conjunction with the preparation of this documentation, modification, or, in some instances, a complete overhaul of the computer programs previously used for counting and measuring, work is needed. An obvious demand for such a thorough revision became evident when the need arose to eliminate shortcomings in the existing programs. The basic construction made these programs practically uninterpretable or maintainable.

The main areas of documentation at present being looked at are those related to the $\beta\gamma$ coincidence counting equipment, and radioactive measurement by the ion chamber method.

In each case the existing single main programs have been re-written into some twenty or so sub-programs, each relatively independent and readily understandable with the result that data processing and coding have been simplified.

As well as setting down the present level of knowledge such documentation will serve as a basis for future development and possibly indicate new avenues for research.

The establishment of a procedure for processing Neutron Flux monitors is also receiving considerable attention and is being documented. Information about the energy spectrum of the neutron flux in HIFAR can be obtained by irradiation of a number of flux monitor wires or foils and measuring the saturation activity of the irradiation product. The specific saturation activity can be found by observing the gamma-ray spectrum of each monitor, soon after irradiating and measuring the total count under the photo peak produced by one of the gamma rays emitted by the product nuclide. The metrology laboratory receives neutron flux-monitors such as titanium, iron and aluminium alloyed with 0.01% cobalt which have been irradiated along with minerals used in SYNROC manufacture. The radioactivity of these wires is determined from the activity of the product nuclides ^{46}Sc, ^{54}Fe, ^{58}Fe and ^{60}Co in association with an MCA using the Ge(Li) detector.

2.2.2 Ion chamber analysis

(H.A. Wyllie)

The use of the Ion Chamber in the Radioisotope Standards Laboratory of the Radiation Standards Group has been described by Urquhart 1985 [8]. An E Report on Ion Chamber Analysis has been prepared by H.A. Wyllie in which the equations used by

Urquhart are derived rigorously in order to show clearly the advantages of the experimental methods used.

It has been shown from the derivation of the equations that activity determinations are not affected by changes in the ion chamber capacitances or in the selected ranges of potential difference across the integrating capacitors.

2.2.3 Coincidence counting corrections

(H.A. Wyllie)

$4\pi\beta/\gamma$ - coincidence counting provides one of the most important methods for determining the absolute disintegration rate of a suitable radioactive material. However, there are difficulties in making the corrections for dead-time loss and accidental coincidences. Bryant [9] derived a correction formula for the special case of equal non-extending dead-times in the two detector channels. However, there is a deficiency in the derivation presented by Bryant. This omission has been addressed and Bryant's original derivation extended and tested experimentally.

Sources were prepared from a ^{60}Co solution, their activities ranging from 2 to 70 kBq. The corrections for sources of low activity are quite small. Hence the effectiveness of a correction formula can be checked by seeing if the measurements in sources of high activity gives the correct value for the radioactivity concentration of the solution from which the sources were prepared. The modified version of Bryant's formula designated Mk I in Fig. 2.4, was shown to be an improvement over the original formula, but still not completely adequate.

2.3 Absorbed Dose Standards

2.3.1 Graphite microcalorimeter control system

(S.L. Sherlock)

Given the proposed installation of high-energy medical linear accelerators in Australian hospitals during 1986, the urgent need has arisen to extend the Commonwealth Standard for absorbed dose from ^{60}Cobalt energies to 25 MV. The existing Urquhart designed graphite microcalorimeter was intended to meet this need. However, the calorimeter must be transported to the hospital sites to enable direct measurement under high energy beams.

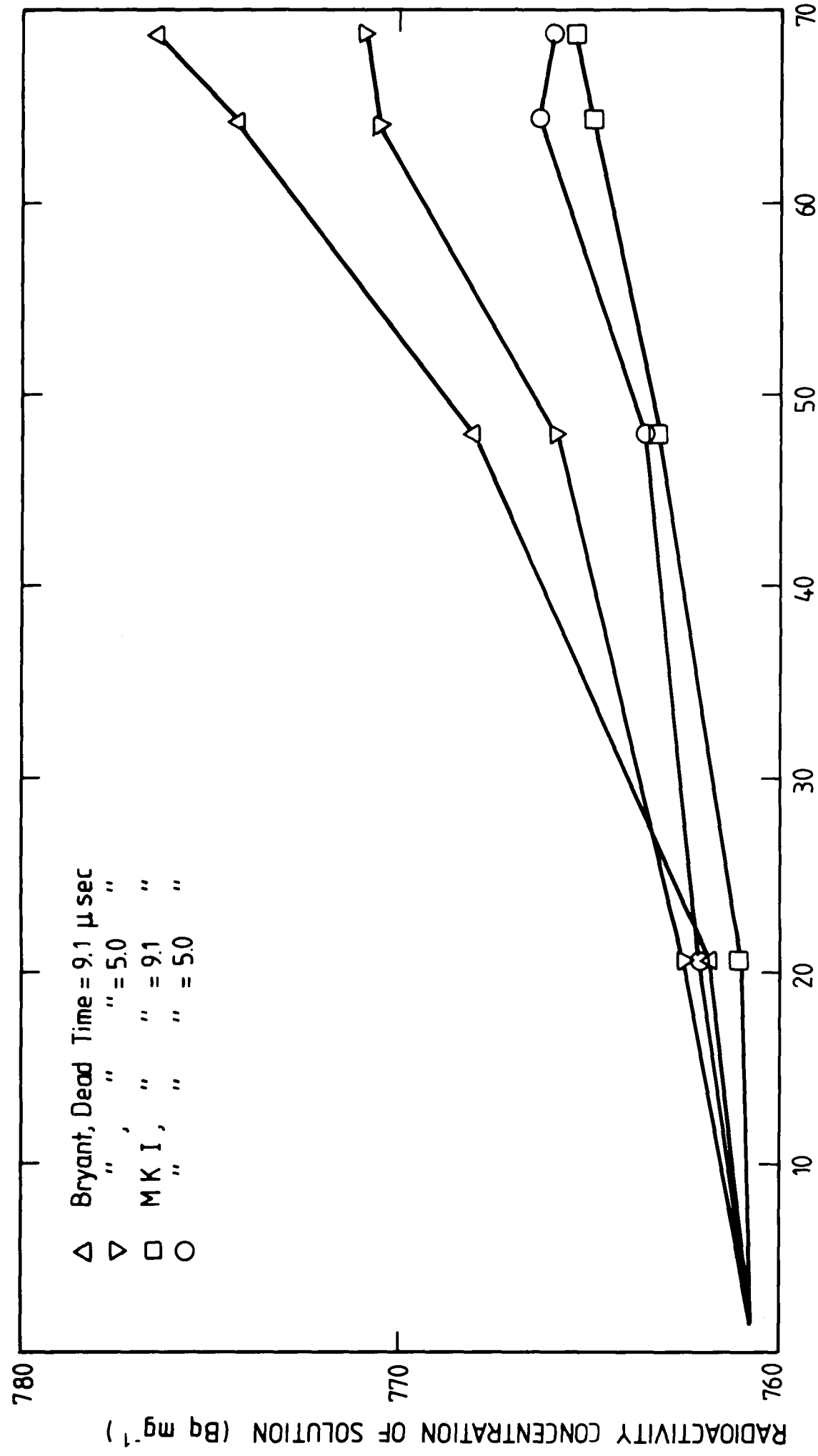

Fig. 2.4 Radioactivity concentrations calculated by Bryant's formula and the modified (Mk I) formula

The requirement to operate the calorimeter out of its home laboratory places stresses on the temperature control system which cannot be alleviated with the existing electronics. Accordingly, the process is in hand to place the calorimeter under full computer control.

This requires the development of suitable algorithms based on a mathematical model of the calorimeter. In particular, control of temperature drifts in the absorber is critical to accurate measurement. It has been suggested that such drifts are induced by the existing dual proportional control system. This effect has been modelled mathematically using Newton's Laws of Cooling and treating the calorimeter as a system with four semi-adiabatic components. With independent proportional controllers acting on mantle and phantom, and with time lags allowing for thermistor delay in sensing temperature, it is found that the fixed duty cycle together with such lags give rise to oscillations in temperature. This is seen for a step input to the phantom (mantle controller only acting) in Figure 2.5.

However, an undesirable feature of the proportional controller is such that a change in the overall operating conditions gives rise to a shift in the temperature control point. Thus while the controller can manage a perturbation dropping to initial conditions in the phantom, it cannot correct a step input.

This latter correction requires a change in algorithm to compensate for increased heat transfer from the phantom. With the new algorithm it is found that the improvement is quite significant. Perturbation at time of the step input is reduced by two orders of magnitude, while long term drift is reduced by a factor of 10.

To summarise, a realistic mathematical model of the calorimeter has been developed. This model indicates that a system using independent proportional controllers will inevitably couple ambient temperature changes into the absorber, albeit with considerable attenuation.

However, since temperatures with a resolution of 10 μK must be measured, an improvement by a factor of 10 remains desirable. This can be achieved by linking the temperature of the phantom into the mantle control algorithm.

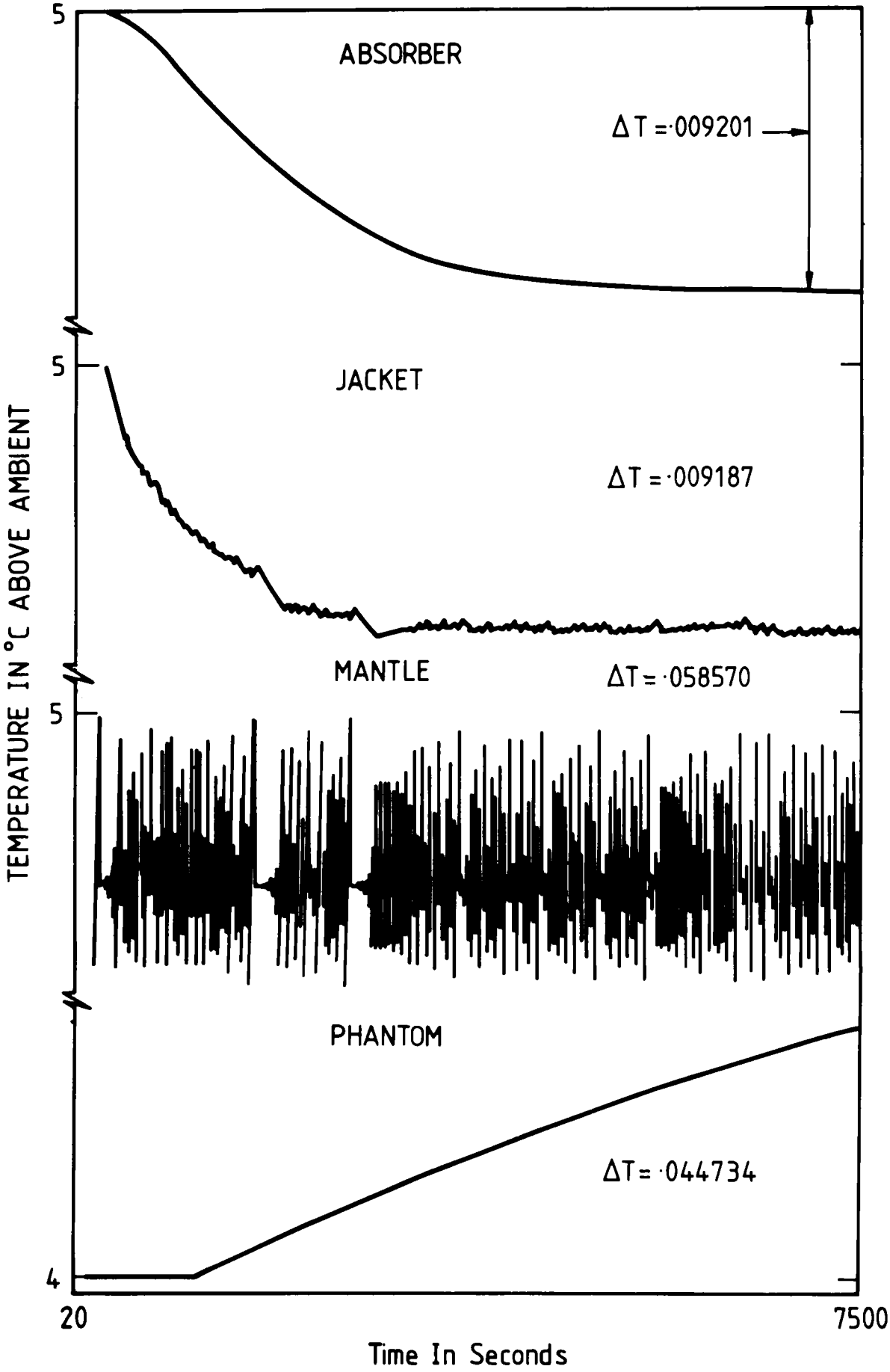

Fig. 2.5 Oscillations in temperature due to excessive gain in mantle proportional controller

The flexibility of a computer implemented controller algorithm promises an improvement over the existing analogue system by a factor of at least ten in temperature stability of the absorber.

2.3.2 Feasibility study for a water calorimeter

(E.P. Johnson)

The Radiation Standards group of the Applied Physics Division maintains three instruments which are regularly used in absorbed dose calibration work.

These are:

(i) The Australian Commonwealth Standard of measurement for absorbed radiation dose to graphite. (The graphite calorimeter).

(ii) A working standard of absorbed dose to graphite.

(iii) A working standard of absorbed dose to water.

The working standard of absorbed dose to graphite is a thimble type ionisation chamber with a graphite build-up cap. It measures exposure in a small volume of air, but its response has been calibrated against the primary standard.

The working standard of absorbed dose to water is a similar ionisation chamber but with a delrin build-up cap. It has been indirectly calibrated against the calorimeter to measure absorbed dose in water by a dose transfer experiment. Much of the accuracy of the primary standard is lost because of uncertainties in the dose transfer experiment. A better instrument would therefore be a valuable asset to the group, and a novel invention - the water calorimeter - seems to have considerable potential for this purpose.

A water calorimeter has the advantages of an absolute standard in the preferred medium combined with transportability. It requires no vacuum pump, is easy to construct, and its internal configuration may be changed for experimental purposes without recourse to workshops. Problems due to conduction and convection of heat away from the measurement point have been shown to be negligible if total dose and irradiation time are kept within certain limits. In a water calorimeter, not all of the absorbed radiation is converted into heat energy. A small percentage is involved in chemical changes to the water molecules. This phenomenon, known as heat defect, is another prob-

lem associated with water calorimetry. It is likely that accurate figures for the heat defect will be available in the near future. Otherwise the water calorimeter could itself be used to investigate the phenomenon. In that case it could be calibrated against the graphite calorimeter and used as a working standard.

A decision has been made to construct a prototype water calorimeter and design details are currently being developed.

2.3.3 IAEA dose intercomparison

(E.P. Johnson)

The IAEA periodically organises dose intercomparisons with about 30 standard laboratories around the world taking part. Each laboratory is sent a number of unirradiated TLD phosphors and asked to irradiate them to a prescribed dose using the correct procedures. The phosphors are then returned to the IAEA and the dose "read". These intercomparisons indicate the extent of variation of dose measurements between laboratories.

The Radiation Standards Group of the Applied Physics Division participated in such an intercomparison in April 1985.

2.3.4 Dose calibration of a Baldwin-Farmer chamber

(E.P. Johnson)

A Baldwin-Farmer chamber and dosimeter from Westmead Centre were calibrated in terms of absorbed dose to water for ^{60}Co gamma radiation. This was done by comparison with the AAEC working standard under identical geometric conditions. Full details of this calibration are given by Johnson [10].

2.3.5 Extension of the Commonwealth standard of absorbed dose from ^{60}Co energy to 25 MV

(Stuart L. Sherlock)

With the imminent installation of high energy linear accelerators in both Sydney and Melbourne hospitals, the need has arisen to provide direct measurement of absorbed dose for energies to 25 MV for photons and 18 MeV for electrons.

The present standard for absorbed dose at ^{60}Co energies is a graphite microcalorimeter, maintained at the AAEC Lucas Heights Research Laboratories on behalf of CSIRO. With improvements to the control and monitoring circuits, this calorimeter is suitable for providing direct measurements of absorbed dose to 25 MV.

A thorough theoretical analysis of calorimeter operation suggests that computer control and monitoring techniques are appropriate. In particular, solution of Newton's Law of Cooling, with variable power for a four-body calorimeter, allows development of a computer simulation model. Different temperature control algorithms may then be run and assessed using this model. In particular, the application of a simple differencer is examined.

Successful implementation of the calorimeter for energies up to 25 MV could lead to the introduction of an Australian Absorbed dose protocol based on calorimetry, thereby reducing the uncertainties associated with exposure-based protocols.

REFERENCES FOR CHAPTER 2

[7] Eberhardt, J.E., Ryan, R.D. and Tavendale, A.J., App. Phys. Lett. 17 427 1970.

[8] Urquhart, D.F., AAEC/E627 (1985).

[9] Bryant, J., Int. J. App. Rad. Isotopes 14 143 (1963).

[10] Johnson, E.P., AP/TN 190 (1985).

3. ELECTRONIC SYSTEMS

3.1 Instrument Design

(G.C. Watt, A.N. Bransgrove, D. Ius and M. Hurry)

Work is nearing completion on an optical-fibre data telemetry system for the 3 MeV Accelerator top terminal which will allow continuous display of 4 of the terminal potentials, 2 of the alternator bearing temperatures and an analogue of the alternator waveform as a means of monitoring the state of the machine. Measurement of these parameters has been made feasible only by the low loss, large longitudinal voltage withstand capabilities and low cost of plastic fibre-optic cables.

Work is proceeding on the development of a high voltage pulser, and interfaces to other instruments, for the automation of Deep Level Transient Spectroscopy measurements on silicon samples under the control of an NEC Personal Computer. The design is complete and construction is about half completed.

Experimental and design work is in progress for a multi-channel, optically-isolated, wideband, analogue telemetry system for obtaining data from Fusion experiments. Good rejection of pulsed RF signals is mandatory in this application and will be achieved by a combination of shielding, balancing and isolation. This system will maintain a calibrated gain by continuously regulating the received amplitude of an added pilot tone, in the same manner used for long distance telephony.

An initial batch of 10 logarithmic-reading survey meters (type 643) have been manufactured by a development contractor and has been placed in service. The group is maintaining liaison with the contractor in refining the case design and in assembling the remaining 40 units of the order.

3.2 Instrument Maintenance

(G.M. Carter, E.J. Mutch, A.E. Godwin, R.A. Philips, K. Butterfield, P.R. Weir)

Approximately 500 maintenance jobs were completed, and 160 inspections of P&E orders were carried out. Problems were encountered during the year as a result of staff shortages, but the situation was relieved with the recruitment of two new officers to the Group. Refurbishment of the site public address system has now been completed.

3.3 Digital Systems

(P.J. Ellis, E.J. Reid, W.O. Hill, C.G. Laman, N.M. Hudson)

The increase in the use of newer video-display units with RS232C communication and the replacement of some older units with the newer models has resulted in the need to adapt SMUT units with a small converter card. This has only occurred on the Supersmut boxes which have suitable signals available at chip level. At the same time, the units have also been modified so that when the power is not switched off the SMUT unit automatically switches the line driver receiver off the line. This enables the unit to remain switched on and be isolated from power surges when the unit has to remain on as in Building 51 or the user has not bothered to switch it off.

The four digit accuracy amp-hour meter for Isotope Division was installed. The unit monitors the electrolysis current passed through a cell and totes the charge in Amp-Hours or in grams of water disassociated. The unit which has a four digit commercial panel meter and which operates using four digit arithmetic does not quite agree with experimental weighings. The operating program is currently being modified to ensure that the unit will operate reliably over the ten day charging period without introducing discrepancies.

The site computer network has needed a series of paths that are independent of each other but which can be used together to service and extend the existing base. The first Alternate Path developed was another computer node which can take over the function of the PDP-9L and run the dataway from the IBM when and if required. The next pathway will be an LSII/23 installed on an IBM channel specifically for use with data dumping and retrieval from the Pyramid computer. This unit will mainly be handled by AM&C once the initial drivers, receivers, etc. are installed.

On-going development for the Fibre Optics Link is mainly in the Node-Nodule communication area. This Link will be added to the Alternate Path processors in roughly the same fashion as the two existing interfaces. Three INTEL 8086 multi-processors are used to control the data paths and to maintain independent control of the IBM channel and the dataway. The dataway inter-

face consists of a parallel input-output card in the multi-processor box and a completely different dataway control unit which was specifically developed to be controlled from a micro-processor. The IBM channel interface consists of a similar input-output module with separate driver-receiver pairs that are capable of handling the IBM bus signals. The processors have permanent read-only memory programs so that the system is easily recoverable when power outages and faults occur. A parallel interface has been installed which is capable of accessing the Fibre Optics Link through one of its Nodules. The interface consists of command and response bytes as well as bi-directional data bytes which are controlled through various interrupts. A Nodule has been connected to the Intel Multi-Bus and suitable test programs have to be developed prior to connecting other nodules to this nodule.

Various systems have been upgraded with improved software caused by updated requirements and/or newer interfaces. These include the Supersmut controllers mainly in the area of key-board character queueing, the Instron LSI11/23 which has been upgraded to operate an IEEE 488 bus from within the existing system software, and several dataway test programs which are used to try to cycle on a fault.

The Dataway has been improved considerably over most of the period. The main problem is that so many units can contribute to a fault, all of them taking some form of error correction, which makes the fault, if any, or the offending software quite tedious to pinpoint.

4. SAFEGUARDS AND NUCLEAR PHYSICS

4.1 Safeguards

4.1.1 Neutron coincidence counting

(M. Hines, J.W. Boldeman, K.J. Thorpe, I. Delaney, J. Fallon)

The accurate assay of the plutonium content in reactor waste products is an important requirement in the application of effective safeguards. Current assaying techniques use neutron coincidence counting (NCC) to detect the neutrons associated with the spontaneous fission of ^{240}Pu. The technique is based on the time correlation of the spontaneous fission neutrons. Existing instrumentation, notably the high level neutron coincidence counter (HLNCC), is capable of obtaining accuracies of up to 1%. The accuracy of this instrument, and of similar instruments, is principally determined by the availability of appropriate standards. Furthermore, standard NCC techniques suffer from neutron multiplication within the sample. Correction procedures for these effects require a large number of standards and are only suitable for samples of well defined composition.

A program has been initiated to assist in the development of NCC techniques. The program includes the following:

1. An investigation of the principles involved.
2. A study of existing instrumentation and possible design variations.
3. The development of methods which are based on high efficiency neutron detection.
4. Evaluation of nuclear data suitable for safeguards applications.

Liquid scintillation neutron coincidence counting (LSNCC)

Initial research in the principles of NCC has been performed using a large, high efficiency (up to 85% for neutrons), liquid scintillation tank. In comparison, the neutron detection efficiency of conventional ^{3}He, polyethylene moderated systems (e.g. HLNCC) is typically 12 to 17%. The higher efficiency of the LSNCC has made it possible to develop a NCC technique that involves the detection of a distribution of neutrons arising from a fission event. Because of this, the amount of information from the measurement is increased, making

it feasible to correct more accurately for neutron multiplication.

(a) Principle of Method

The method that has been developed for the LSNCC involves the following general procedures:

1. Initially a ^{252}Cf fission chamber is used to provide an absolute measurement of the scintillator response to ^{252}Cf prompt fission neutrons. Two 40 μs counting gates are used for this purpose. The first gate is triggered by the fission event and contains ^{252}Cf spontaneous fission neutrons (prompt), while the second gate, initiated 140 μs after the event, contains only background. By comparing the average difference in the foreground and background gates with the known number of neutrons emitted in the fission event $[\bar{\nu}(^{252}Cf) = 3.757]$ the neutron efficiency may be determined without the use of standards.
2. The efficiency for ^{240}Pu spontaneous fission neutrons may be obtained from the ^{252}Cf figure by making a small correction for the difference in the fission neutron spectra. A distribution for ^{240}Pu neutron detection D_i may be obtained for this efficiency using the relation

$$D_i = \varepsilon^i \sum_{j=0}^{i_{max}-i} \frac{(i+j)!}{i!j!} (1-\varepsilon)^j P_{i+j}$$

where P_i is the known neutron emission probability distribution and ε the neutron efficiency.
3. Because the liquid scintillator is gamma sensitive, the actual distribution that is observed contains the detection probability associated with the ^{240}Pu spontaneous fission gamma rays (prompt). This prompt gamma detection probability may be obtained from the neutron efficiency and folded into the neutron distribution to produce a 'total' distribution T_i.
4. A plutonium distribution is counted in a similar manner to the measurement of the neutron efficiency. However, instead of triggering off a fission event, a random scintillator event is used to initiate the foreground gate. The distribution associated with this random trigger may

be obtained from the total distribution T_i by use of the equation

$$M_i = \frac{1}{\bar{T}} \sum_{j=i+1}^{i_{max}} T_j$$

5. The entire distribution of events collected in the foreground gate F_i and the background gate B_i, is then used to provide a number of estimates of the fission rate f. If B represents the average in the background gate and τ the gate length, the fission rate estimates f_i are given by

$$f_i = \frac{\bar{B}}{\tau \bar{T}} \sum_{j=0}^{i} \frac{F_i - B_i}{M_j B_{i-j} - B_i}$$

(b) Results

Because of difficulties encountered in obtaining appropriate samples, our investigations have been limited to several small ^{252}Cf and ^{240}Pu sources. Some typical results of fission rate measurements are contained in Table 4.1. It should be noted that these results were obtained without the use of standards and there was some uncertainty in the isotopic compositions of the plutonium samples.

Table 4.1
Fission rate measurements using large liquid scintillator

Isotope	LSNCC Value (fission s^{-1})	Independent Value (fission s^{-1})
^{252}Cf:		
source 1	19980	19810
2	453	460
3	145	144
4	124	123
^{240}Pu:		
source 1	183	174
2	595	541
3	976	926

(c) Prototype LSNCC

Results obtained using the large liquid scintillator have illustrated the viability of a liquid scintillator based NCC technique. The next step in instrumentation development has been the design of a small, portable LSNCC to be used specifically for safeguards purposes. A cross section of the detector is shown in Figure 4.1.

Computations have been performed in collaboration with G.S. Robinson (Nuclear Technology Division) and the characteristics of the detector fully investigated. The calculated neutron efficiency of the detector, as a function of energy is shown in Figure 4.2. The calculated efficiency of the tank for ^{240}Pu fission neutrons has been calculated as 65%.

HLNCC investigations

The HLNCC developed at Los Alamos National Laboratory, USA, is the basis of the instrumentation presently being used by IAEA safeguards inspectors for Pu assay. To investigate the characteristics of the HLNCC and to attempt to improve neutron multiplication corrections, a HLNCC is being constructed on site. At this stage we have purchased and tested the 18 ^{3}He tubes (50 x 2.5 cm diameter) for the detector and all design details have been finalised. The detector is intended to be a replica of the new HLNCC II which is presently being tested at Los Alamos National Laboratory.

Neutron multiplication in NCC

Neutron multiplication results from neutron induced fission within the fissile component of the sample (mainly ^{239}Pu). In a NCC detector there are three contributions to the net neutron multiplication:

1. fast fission induced by spontaneous fission neutrons;
2. fast fission induced by (α,n) neutrons; and
3. thermal fission produced by neutrons that have been reflected from the detector.

Calculations have shown that although the contribution of thermal neutron fission is significant in polyethylene moderated ^{3}He neutron detector systems (e.g. HLNCC), its contribution to the total multiplication in the LSNCC is less than 2% for plutonium samples up to 2 kg. Thus neutron multiplication in the LSNCC involves a combination of (1) and (2) above.

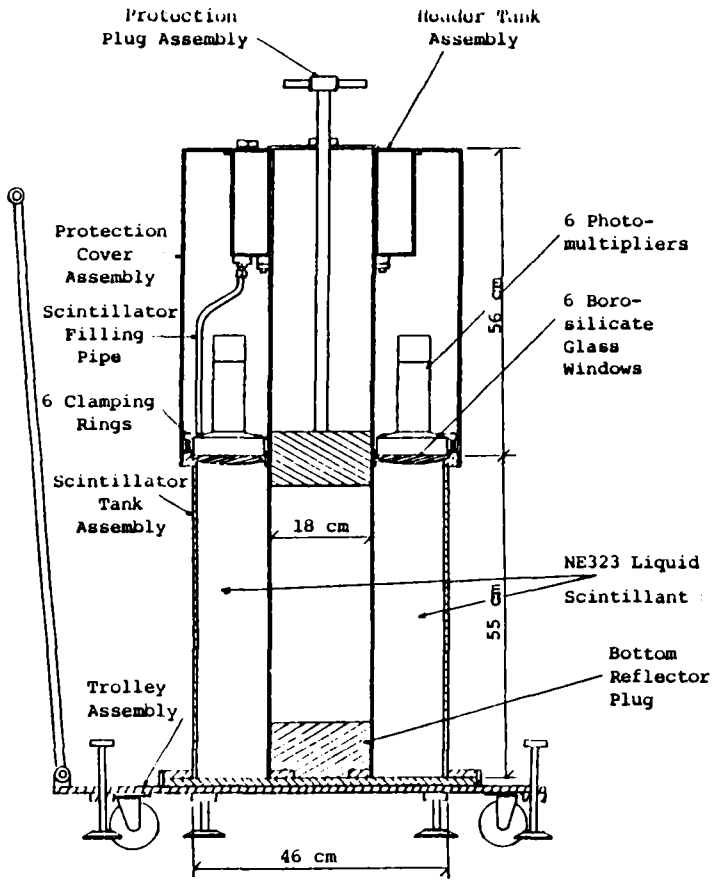

Fig. 4.1 Cross section of portable LSNCC

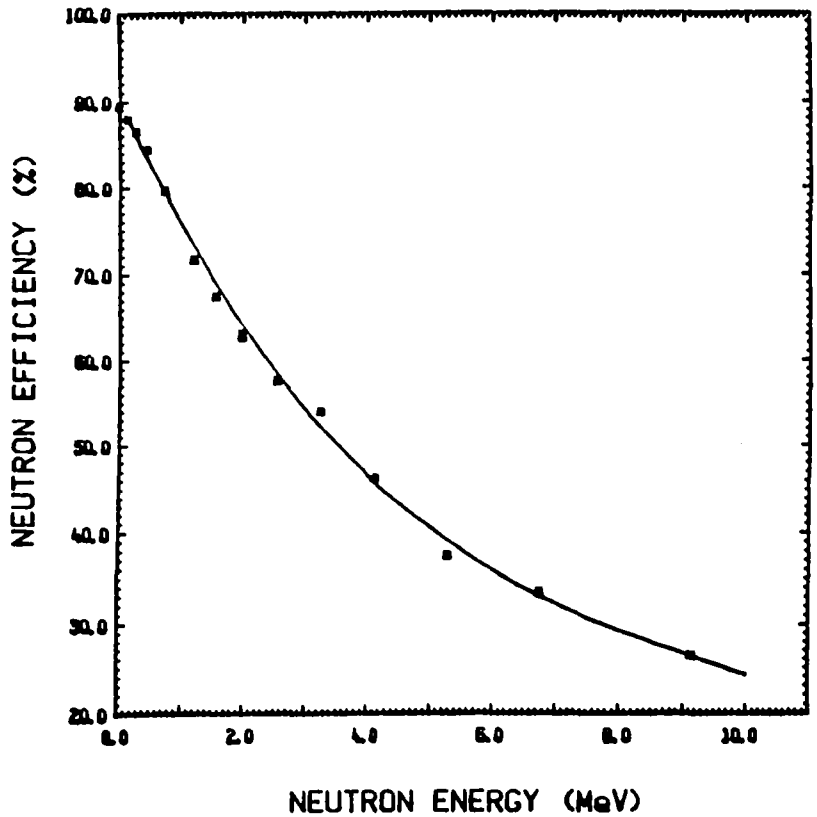

Fig. 4.2 Efficiency of portable LSNCC as a function of energy

(a) Multiplication of Spontaneous Fission Neutrons

Fast fission by spontaneous fission neutrons may be described by a 'super fission' concept. Neutrons produced in the spontaneous fission of ^{240}Pu may induce fast fission, producing neutrons which may induce further fission, etc. Since this 'cascade' of neutrons occurs instantaneously with respect to the electronics, the observed neutron distribution detected in the scintillator is perturbed by this effect. Calculations have been performed to quantify the multiplication effect on the spontaneous fission neutron distribution. Figure 4.3 shows the effect of 5 and 10% multiplication on the neutron probability distribution for the spontaneous fission of ^{240}Pu.

(b) Multiplication of (α,n) Neutrons

Multiplication of (α,n) neutrons is very similar to that described for spontaneous fission neutrons, the difference being that the cascade is initiated by a random (α,n) neutron. Hence multiplication gives rise to a secondary induced fission source of strength R*p, where R is the (α,n) rate and p is the probability of fast fission. A correction for this effect involves the derivation of the appropriate probability distribution and the subtraction of this component of the total correlated count.

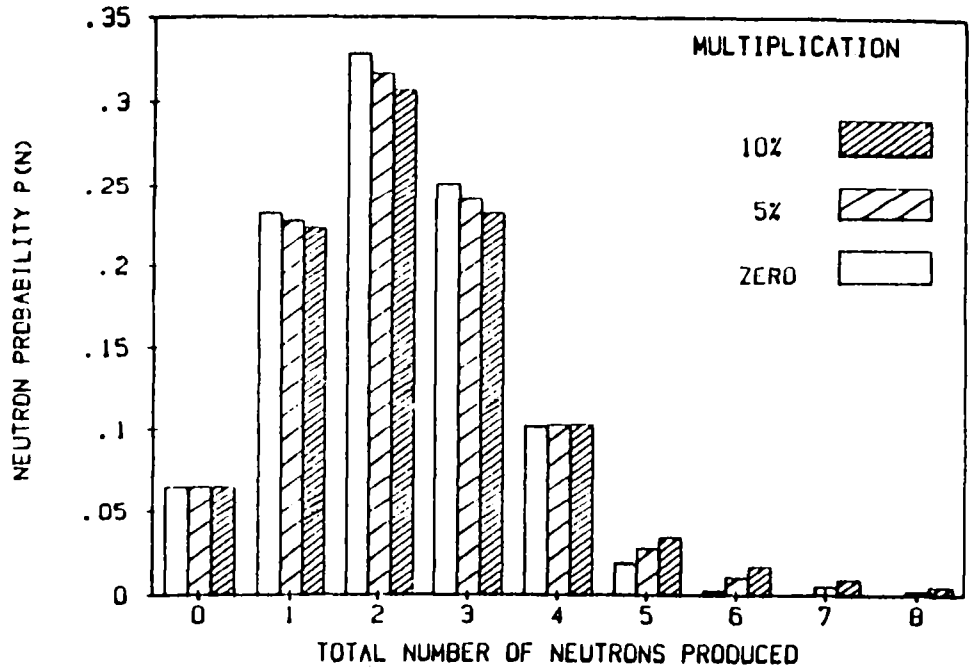

Fig. 4.3 Effect of neutron multiplication on the neutron probability distribution for the spontaneous fission of ^{240}Pu. The approximation was made that the fast fission probability p is the same for spontaneous and neutron-induced fission neutrons (average energy ~2 Mev).

4.1.2 Gas phase enrichment monitor

(J.W. Boldeman, J. Fallon)

As part of the first Australian assistance program to the IAEA in the implementation of international safeguards (BAAP I), a gas phase enrichment monitor was developed to enable an inspector to make accurate measurements of the ^{235}U enrichment of the UF_6 samples taken from the product, feed and tail lines of gas centrifuge enrichment plants. A prototype instrument was demonstrated to IAEA personnel in Almelo in September 1983.

Following the extended field trials of the gas phase enrichment monitor (GPEM) at Ningyo, Japan, the IAEA has made a number of suggestions regarding the detailed operation of the instrument. These include:

(a) Replacement of the Davidson MCA supplied by IAEA standard MCA.

(b) Introducing the option of choosing the counting time.

(c) Some rationalisation of the software.

These modifications were made and a revised system was demonstrated in early August 1985.

At the conclusion of this demonstration, some hardware changes were also suggested. During its extended use in Japan the GPEM was placed in a building which experienced sub zero temperatures at certain times. The instrument supplied was unable to operate under these conditions. The IAEA has requested that a revised instrument be supplied which is heated so that the environment has no effect on its operation.

The necessary equipment to construct a third GPEM is being assembled. This version will be designed to fit in a heated box. The IAEA has been requested to itemise any additional changes.

4.1.3 In-line gas phase enrichment monitor

(J.W. Boldeman, P. Baxter)

A gas phase enrichment monitor has been installed in-line on the experimental gas centrifuge test bank at Lucas Heights. This monitor is a modified version of the instrument developed for the IAEA. The original instrument was completely computer-controlled to ensure foolproof operation by enabling the operator to perform the necessary tasks under instruction

from the computer. This operating system was too restrictive for use on the cascade in an experimental situation so the program was modified to enable operator control of the instrument. Modifications to the original manifold design have enabled the new instrument to be integrated into the product sampling manifold of the cascade. The design is such that enrichment measurements can be carried out in situ without taking samples away for analysis.

4.1.4 Go no-Go monitor

(P. Baxter, J.W. Boldeman)

The limited frequency unannounced access inspection concept of the Hexapartite Agreement requires, for its implementation, a monitor system which will allow an IAEA inspector to verify that the UF_6 gas passing through any pipe in the cascade hall of a centrifuge enrichment plant has an enrichment in ^{235}U of less than 20%. Monitors of this type which are being developed in a number of support programs, have been given the name Go No-Go monitors. To arrive at a reasonably accurate value for the ^{235}U enrichment typical Go No-Go monitors require two separate measurements:

(a) the total uranium pressure within the pipework is measured using gamma-ray induced X-ray fluorescence; and

(b) the ^{235}U content is determined by measuring the emission rate of the 185.7 keV gamma-rays from the decay of ^{235}U.

This second measurement is greatly complicated by deposits of uranium and its daughter products on the walls of the pipework. The gamma rays emitted by the deposit can be up to ten times the number emitted by the gas at normal operating pressure and enrichment.

Two separate methods have been developed to allow the ^{235}U count rate from the wall deposit and the gas itself to be separated. In the US support program a two-geometry system has been investigated in which the relative size of the two sources of the 185.7 keV gamma-rays is varied. In the system developed in the UK, the ratios of the 84 keV and 63 keV gamma-rays from the thorium daughter products of the decay of ^{235}U and ^{238}U respectively are determined as well as the 185.7 keV decay rate.

The equipment being developed at AAEC is designed to be able to use either measurement system. Initial evaluation will be carried out using the two-geometry technique.

A high purity germanium detector is used to measure both the gamma and X-rays emitted from the deposits and the gas. The X-ray fluorescence measurements are carried out using a highly collimated ^{57}Co source (10 mCi) (Figure 4.4) to excite characteristic uranium X-rays.

The two-geometry method of determining the ^{235}U content of the gas requires two separate measurements. One measurement uses a wide angle collimator, the other uses a narrow angle collimator.

The ^{235}U count rate (185.7 keV gamma-rays) U_W in the wide angle measurement can be written

$$U_W = G + D \tag{1}$$

where G is the count rate from the gas and D is the count rate for the walls. The ^{235}U count rate U_N for the narrow angle geometry is given by

$$U_N = aG + bD \tag{2}$$

where the constants a and b specify the reduction in the detector geometry for the gas and wall deposits respectively. These constants depend only on geometry and can therefore be calculated. The ^{235}U count rate from the gas above can be determined from the solution of equations (1) and (2), i.e.

$$G = \frac{bU_W - U_N}{b-a} \tag{3}$$

The total uranium content of the gas is determined by using the X-ray fluorescence count rate. The X-ray fluorescence count rate is proportional to the total uranium content of the gas for a given source strength. This measurement is taken concurrently with the narrow collimation measurement as the same detector geometry is used for both. As can be seen in Figure 4.4 the only U X-rays seen by the detector are those in the shaded area, thus eliminating any counts from the wall.

The equipment is installed on the experimental gas centrifuge cascade in Nuclear Technology Division. An aluminium

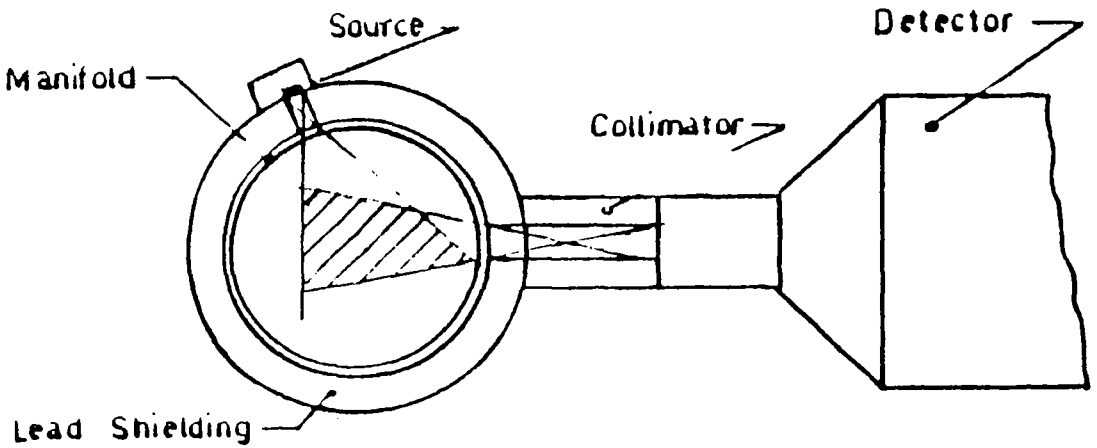

Fig. 4.4 Go No-Go Monitor Detector Geometry

manifold section comparable in size to pipes in overseas cascades was installed in the product line. When the cascade is operating, valuable information on in situ performance will be obtained.

Development work on the Go No-Go detector will continue in a laboratory situation after the cascade is shut down. This work will involve closed loop experiments to investigate the most viable method of detection given the low gas pressures and large deposits that will be encountered.

4.1.5 Nuclear data

Measurements of the prompt fission neutron spectrum from the spontaneous fission of ^{252}Cf

(J.W. Boldeman, B. Clancy*, D. Culley**)
(*Nuclear Tech. Div. **ASNT)

The prompt neutron emission spectrum from the spontaneous fission of ^{252}Cf has been measured for the energy range 0.124 to 15.0 MeV. In the measurement program, seven separate measurements were made of the spectrum between 1.0 and 15.0 MeV using a plastic scintillator as the neutron detector. For the energy range 0.124 to 2.66 MeV, a ^{6}Li glass scintillator was used as the neutron detector. The data are presented with respect to a Maxwellian distribution with T = 1.42 MeV. Some positive and negative deviations with respect to this distribution have been observed. These measurements were presented to the IAEA AGM on Nuclear Standard Reference Data held at Geel in November 1984. These corrections have now been incorporated into the data. The modifications included a correction for the effect of the experimental time resolution and one for the fission fragment loss below the bias on the fission counter. This percentage loss of fission fragments was estimated using the neutron coincidence technique. The combined experimental data for all measurements are shown in Figure 4.5 with respect to the reference Maxwellian with T = 1.42 MeV. The fine details of the deviation of the data from the reference Maxwellian are shown in Figure 4.6.

The LSNCC that is being developed as part of BAAP II depends on basic nuclear data for its calibration. An assessment and, where necessary, a new measurement, is being made of all relevant nuclear data.

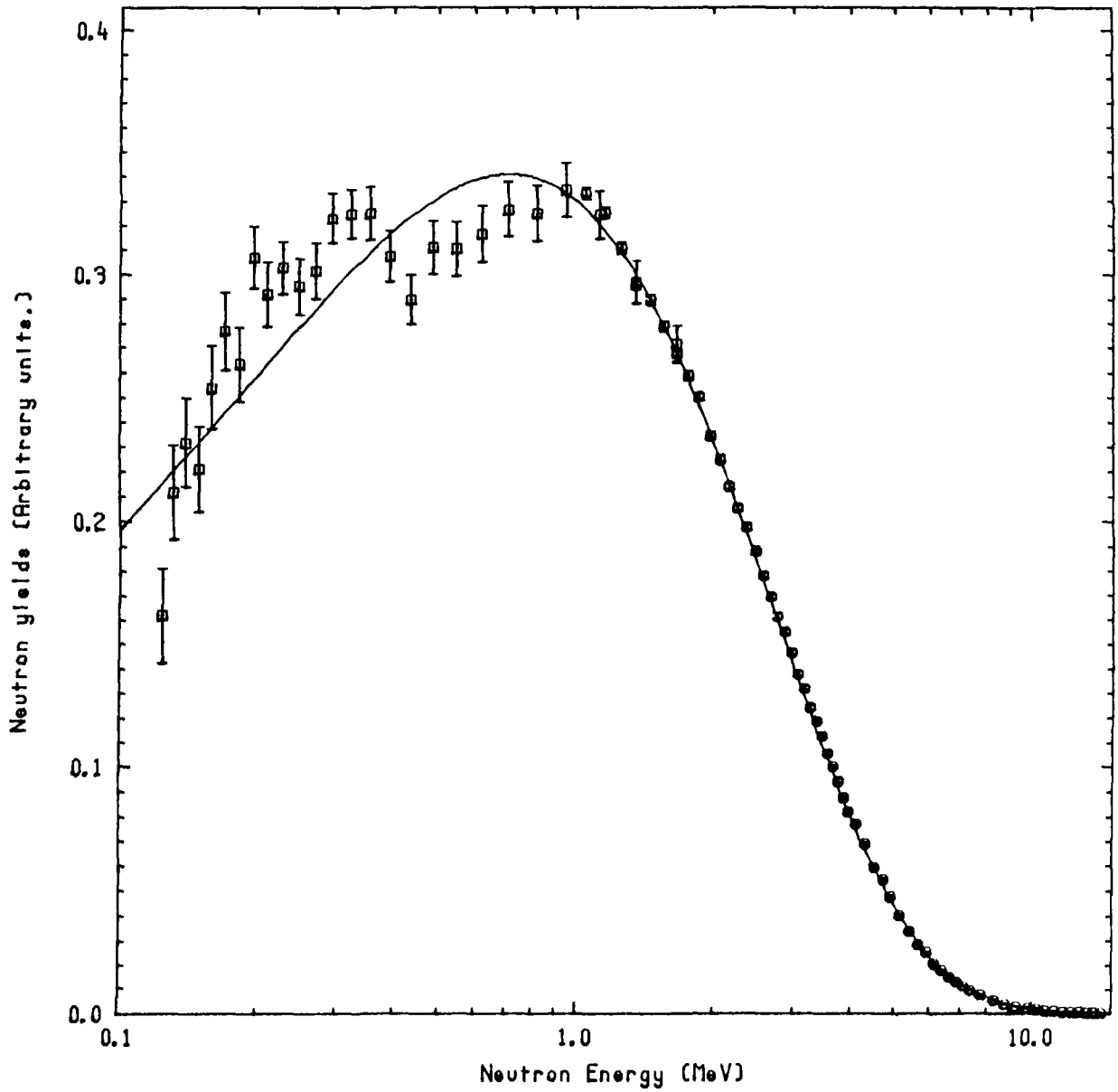

Fig. 4.5 Combined experimental data for all measurements of the prompt fission neutron spectrum of ^{252}Cf. Also shown is a reference Maxwellian with T = 1.42 MeV.

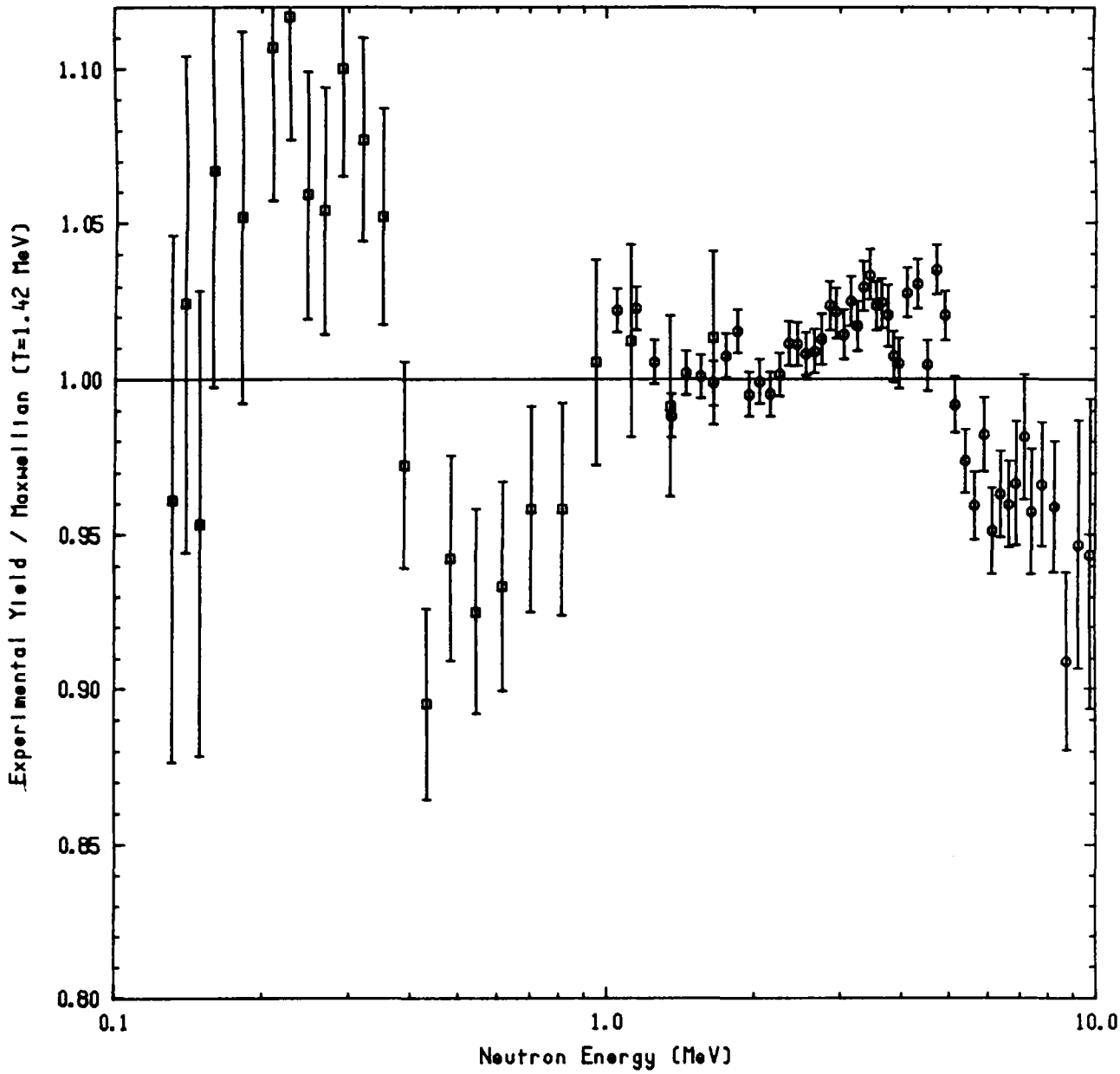

Fig. 4.6 Deviations of the experimental data from the reference Maxwellian with T = 1.42 MeV

Evaluated $\bar{\nu}$ and P_ν data for ^{240}Pu and ^{242}Pu

(M. Hines, J.W. Boldeman)

Prompt Nubar ($\bar{\nu}_p$)

A weighted average of $\bar{\nu}_p$ (^{240}Pu) was obtained from the more accurate experimental values presented in the literature. When consideration was given to both experimental procedures and validity of results, only the experimental results of Frehaut et al. [11], Zhang et al. [12] and Boldeman and Hines [13] were included. The $\bar{\nu}_p$ values were all renormalised with reference to $\bar{\nu}_p$ (^{252}Cf) = 3.757 and the weighting was based on the stated experimental uncertainties of the $\bar{\nu}_p$ measurement. This resulted in the recommended value of $\bar{\nu}_p$ (^{240}Pu) = 2.155±0.009.

The recommended value of $\bar{\nu}_p$ (^{242}Pu) is the value recently published by Boldeman and Hines [13]. This value was $\bar{\nu}_p$ (^{242}Pu) = 2.145±0.009. It should be noted that the errors in $\bar{\nu}_p$ for ^{242}Pu and ^{240}Pu from Boldeman and Hines [13] were obtained from the original publication by Boldeman [14].

Neutron Emission Probability Distribution (P_ν)

The recommended P_ν distribution for ^{240}Pu was obtained from the weighted mean of the renormalised distribution ($\bar{\nu}_p$ = 2.155) obtained from Frehaut et al. [11], Zhang et al. [12] and Boldeman and Hines [13]. Renormalisation was also performed to ensure that each distribution summed to unity and, in the case of Zhang's higher moments (P_6-P_8), a slight adjustment of these moments was performed because of the error in these results. This error would have been associated with the relatively low efficiency (58.6%) of the scintillator tank used by Zhang. The P_ν distribution for ^{240}Pu is shown in Table 4.2

The recommended P_ν distribution for ^{242}Pu is the distribution presented in Boldeman and Hines [13]. This distribution is shown in Table 4.3.

Evaluated $\bar{\nu}$ and P_ν data for ^{252}Cf

(J.W. Boldeman and M. Hines)

The average number of neutrons emitted in the spontaneous fission of ^{252}Cf ($\bar{\nu}$ for total neutron emission, $\bar{\nu}_p$ for prompt neutron emission) has been the reference standard for the majority of $\bar{\nu}$ measurements and has also been applied as a standard in a number of neutron emission rate experiments. A

Table 4.2
Neutron emission parameters for spontaneous fission of ^{240}Pu

$\bar{\nu}$	2.155±0.009
P_0	0.0657
P_1	0.2311
P_2	0.3304
P_3	0.2509
P_4	0.1012
P_5	0.0186
P_6	0.0021
$\langle\nu^2\rangle_{av}$	5.971
$\sigma^2(\nu)$	1.327
R	0.8218

Table 4.3
Neutron emission parameters for spontaneous fission of ^{242}Pu

$\bar{\nu}$	2.145±0.009
P_0	0.0683
P_1	0.2302
P_2	0.3343
P_3	0.2469
P_4	0.0991
P_5	0.0181
P_6	0.0031
$\langle\nu^2\rangle_{av}$	5.939
$\sigma^2(\nu)$	1.338
R	0.8246

$$\langle\nu^2\rangle_{av} = \sum \nu^2 P_\nu \qquad \sigma^2(\nu) = \sum P_\nu(\nu-\bar{\nu})^2 \qquad R = \frac{\langle\nu^2\rangle_{av} - \bar{\nu}}{(\bar{\nu})^2}$$

comprehensive listing of all determinations of this standard is given in Table 4 1. Preliminary data from White and Axton [15], Axton et al. [16] and Aleksandrov et al. [17] have been superceded by subsequent values. The only new measurement in the table is that of Edwards et al. [18]. A recent evaluation of all $\bar{\nu}$ measurements by Axton [19] which included a comprehensive assessment of all common sources of error, arrived at a recommended value of 3.7661±0.0054 for $\bar{\nu}$ for ^{252}Cf.

Recently there has been renewed interest in the neutron emission probability distribution P_ν for ^{252}Cf because of its application in safeguards measurements. Table 4.5 lists a set of recommended values for P_ν. These values have been obtained by incorporating the recent data from Boldeman and Hines [20] into the evaluation of Holden and Zucher [21].

4.2 Nuclear Physics

4.2.1 The triple humped fission barrier for thorium nuclei

(J.W. Boldeman and R.L. Walsh)

The existence of a triple-humped barrier shape for the ground and near ground state fission channels for nuclei near thorium has been a controversial subject since the original prediction by Moller and Nix [36]. Attempts to verify this proposal have been based on simultaneous analyses of high resolution neutron fission cross sections and fission fragment angular distributions for the thorium nuclei, particularly ^{230}Th. Some reservations ([37]-[39]) have been expressed regarding our previous measurements of the fission fragment angular distributions for neutron fission of ^{230}Th and the analysis based on these data (Boldeman et al. [40]) and the cross section measurement of Blons et al. [41]. Consequently, these measurements have been extended.

The experimental method was similar to that previously used by Boldeman et al. [40] with some modifications to improve the energy resolution. Neutrons were produced via the ^{7}Li(p,n)^{7}Be reaction using analysed proton beams from a 3 MeV Van de Graaff accelerator incident on thin targets of lithium. The actual energy resolution was determined by measuring (twice each day) the total cross section of ^{32}S (0.15 atom barn^{-1}) in the vicinity of the narrow resonance at 586.9 keV. A measurement at a particular energy required from 4 to 20 days. The

resolution function was triangular in shape. The absolute reference energy for all measurements was the resonance in ^{32}S at 724.8 keV. The energy precision was therefore better than ±0.5 keV. Fragment detection was achieved with six surface barrier detectors feeding six pulse height analysers.

Table 4.4
$\bar{\nu}$ values for spontaneous fission of ^{252}Cf

Experiment	Value
Liquid Scintillator	
*Asplund-Nilsson et al. (1963) [22]	3.792±0.040
*Hopkins and Diven (1963) [23]	3.777±0.031
*Boldeman (1974) [24]	3.755±0.016
Zhang and Liu (1980) [25]	3.754±0.018
Spencer et al. (1982) [26]	3.782±0.007
Manganese Bath	
White and Axton (1968) [15]	superseded
Axton et al. (1969) [16]	superseded
#De Volpi and Porges (1970) [27]	3.747±0.019
Aleksandrov et al. (1975) [17]	superseded
Bozorgmanesh (1977) [28]	3.744±0.023
Aleksandrov et al. (1980) [29]	3.758±0.015
Smith and Reeder (1984) [30]	3.767±0.011
Axton and Bardell (1984) [31]	3.7509±0.0107
Boron Pile	
+Colvin and Sowerby (1965) [32]	3.739±0.021
Edwards et al. (1982) [18]	3.761±0.029
Evaluation	
Axton (1984) [18]	3.7761±0.0054

*Revised by Boldeman (1977) [33]
#Revised by Smith (1977) [34]
+Revised by Ullo (1977) [35]

The corrected angular distribution data were fitted with Legendre polynomials: $1+a\cos^2\theta+b\cos^4\theta$. The parameters derived for the measurements at each energy and the anisotropy $(\sigma(0°)/\sigma(90°))$ are listed in Table 4.6. The experimental data are consistent with our previous measurements. The fission cross section derived from the angular distribution data is in satisfactory agreement with the data of Blons et al. [41] (Figure 4.7).

Table 4.5
Neutron emission parameters for spontaneous fission of ^{252}Cf

$\bar{\nu}_p$	3.757
P_0	0.00219
P_1	0.02608
P_2	0.12600
P_3	0.27374
P_4	0.30399
P_5	0.18493
P_6	0.06639
P	0.01473
P	0.00188
P	0.00007
$\langle\nu^2\rangle_{av}$	15.719
$\sigma^2(\nu)$	1.6034
R	0.8474

$$\langle\nu^2\rangle_{av} = \sum \nu^2 P_\nu \qquad \sigma^2(\nu) = \sum P_\nu(\nu-\bar{\nu})^2 \qquad R = \frac{\langle\nu^2\rangle_{av}-\bar{\nu}}{(\bar{\nu})^2}$$

Table 4.6
Angular distribution data

Energy (keV)	a	b	$\sigma(0°)/\sigma(90°)$	Energy (keV)	a	b	$\sigma(0°)/(90°)$
681±9*	1.88	-1.02	1.86±0.20	735±3	0.84	0.92	2.76±0.14
697±8*	1.01	-0.24	1.77±0.08	740±4	0.93	1.20	3.13±0.25
700±4	0.90	0.00	1.90±0.15	745±3	-0.49	2.32	2.83±0.14
708±2	0.63	0.59	2.20±0.13	755±5	0.83	0.24	2.07±0.14
709±2	1.04	-0.24	1.80±0.12	764±4	1.51	-0.08	2.43±0.32
710±2.5	0.35	0.65	2.00±0.14	780±8*	0.50	1.90	2.40±0.15
715±3	0.26	1.08	2.34±0.13	- - - -	- - - - - - - - - - - -		
718±2.5	0.98	0.68	2.66±0.14	707±5			1.73±0.14
720±2.5	0.23	1.61	2.84±0.13	713±5			2.38±0.20
724.5±2.5	0.27	1.85	3.12±0.17	721±6			2.81±0.22
728.5±3	0.03	2.02	3.05±0.16	725±4			3.21±0.24
730±3	0.27	1.86	3.13±0.17	727±6			3.12±0.29

*Data from earlier measurement

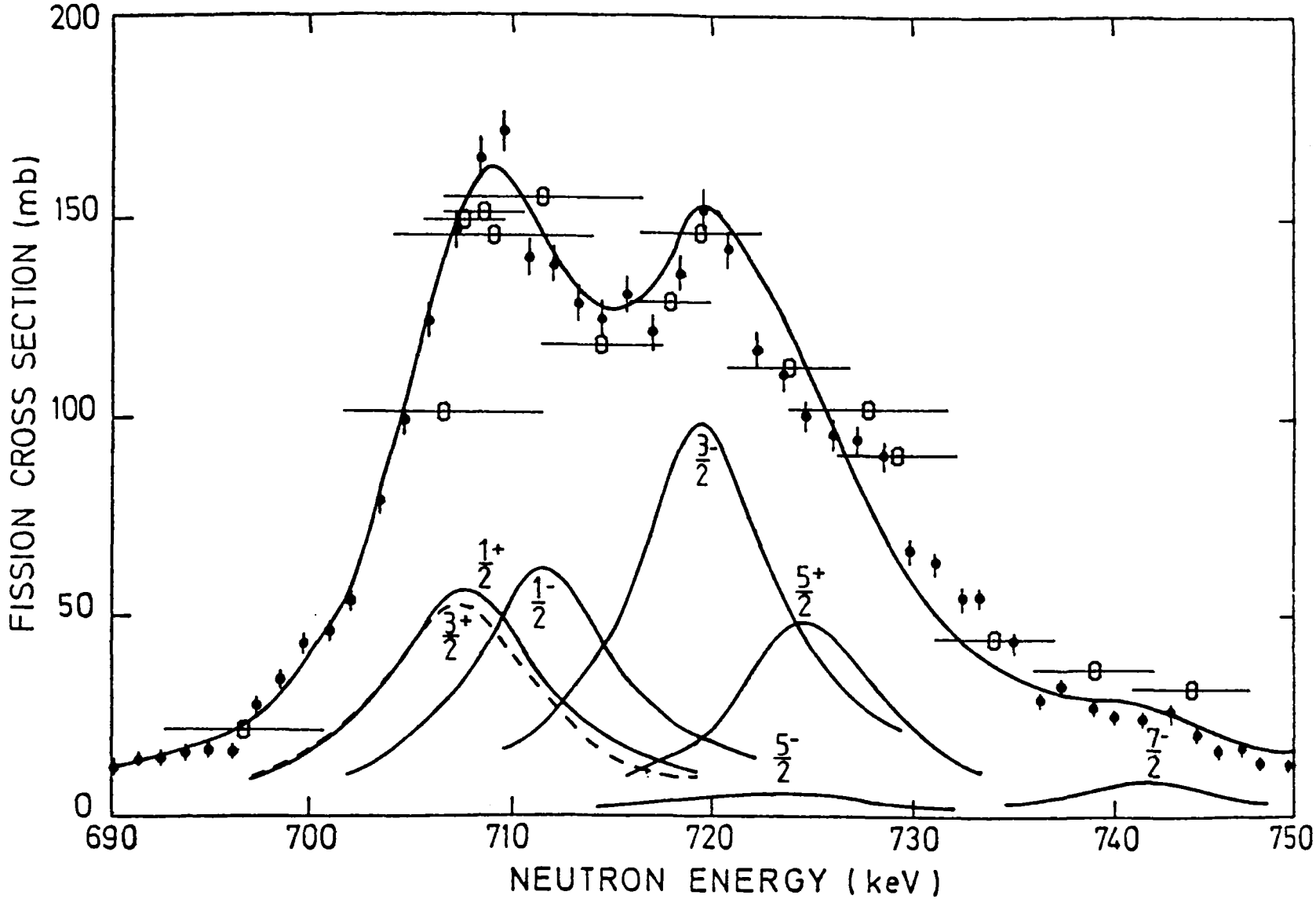

Fig. 4.7 Calculated neutron fission cross section compared with the data of Blons et al. [41]. Also shown are the fission cross section data from the angular distribution measurements.

The third well in the fission barrier for the thorium nuclei results from the consideration of asymmetric deformations in the calculation of the potential energy surfaces. The interpretation of the structure in the ^{230}Th cross section has been based on the concept of a pure vibrational resonance associated with the third well of this triple-humped fission barrier. The fission state consists of the coupling of the single particle state to a rotation of the nucleus as a whole. Since the deformation violates reflection symmetry, the state is degenerate with respect to parity. The resonance clearly has $K = {}^{1}/_{2}$ and therefore the energies of the two rotational bands are given by

$$E(J^{\pi}) = E^{\pi} + \frac{\hbar^2}{2j}\left[J(J+1)-K(K+1) + a^{\pi}(-1)^{J+\frac{1}{2}}(J+\tfrac{1}{2})\right]$$

The parameters that are important from the viewpoint of the present analysis are the moment of inertia constant $\hbar^2/2j$, the decoupling parameters a^+ and a^- and the energy difference E^+-E^- for the two bands. Previous analyses of earlier data have been catalogued by Blons et al. [38] according to which of the $J = {}^{3}/_{2}^{+}$ and $J = {}^{3}/_{2}^{-}$ channels were associated with the two peaks in the fission cross section at 708 and 719.5 keV. In our original analysis, the peak of the $^{3}/_{2}^{+}$ cross section was located at 708 keV and the $^{3}/_{2}^{-}$ at 719.5 keV. In the analysis preferred by Blons et al. [39] the alternative was the case. The fission fragment anisotropies calculated in the two analyses have been compared with the present experimental data in Figure 4.8(a). Neither analysis reproduces the present angular distribution data, particularly on the higher energy side of the resonance where the 0° cross section is overestimated.

Recently Lynn [38] has considered possible modifications of the theory, one of which included some splitting of the $K = {}^{1}/_{2}$ strength associated with the resonance at 715 keV and the $K = {}^{3}/_{2}$ strength at 950 keV. In our previous analysis of the ^{230}Th data it was clear that the energy dependence of the angular distributions required a small $K = {}^{1}/_{2}$ structure at 850 keV. The present data suggest some $K = {}^{3}/_{2}$ strength at 720-750 keV. In accordance with the suggestion of Lynn [38],

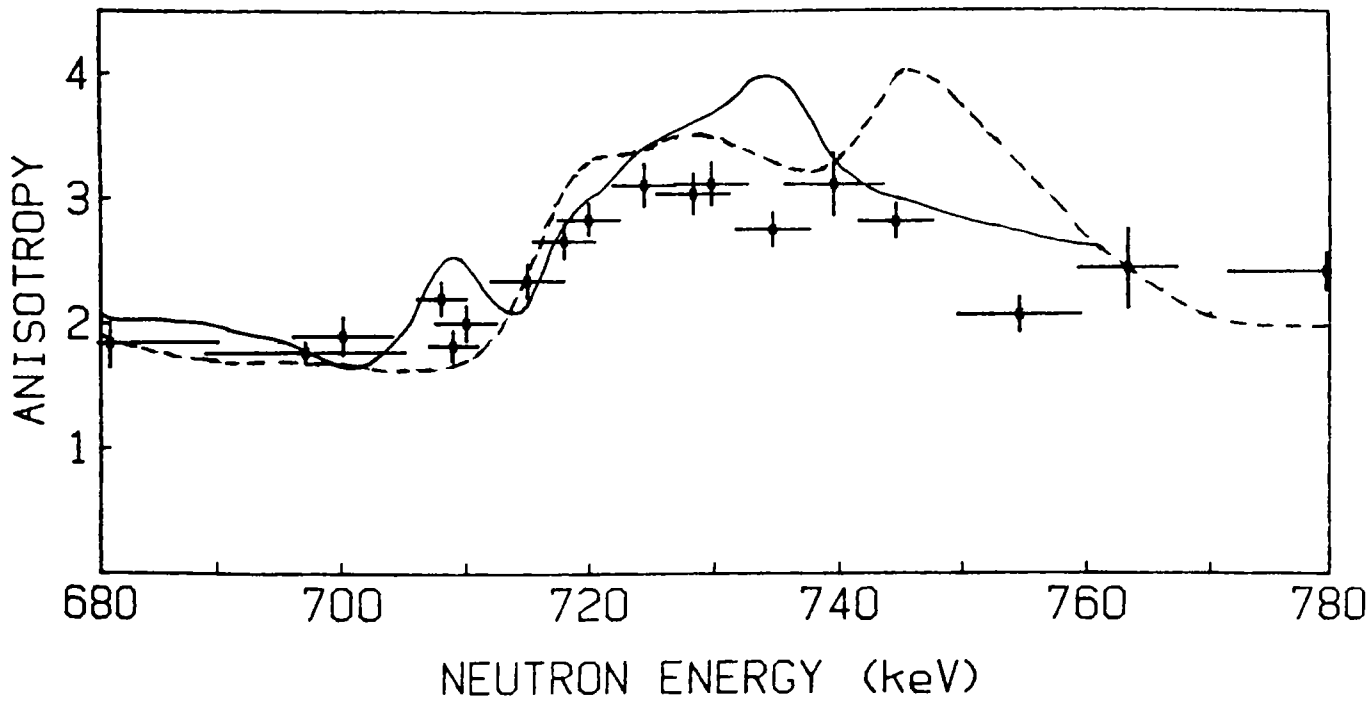

Fig. 4.8(a) Comparison of the present anisotropy data with those calculated in our previous analysis - - - - and in the preferred analysis of Blons et al. [39] ———.

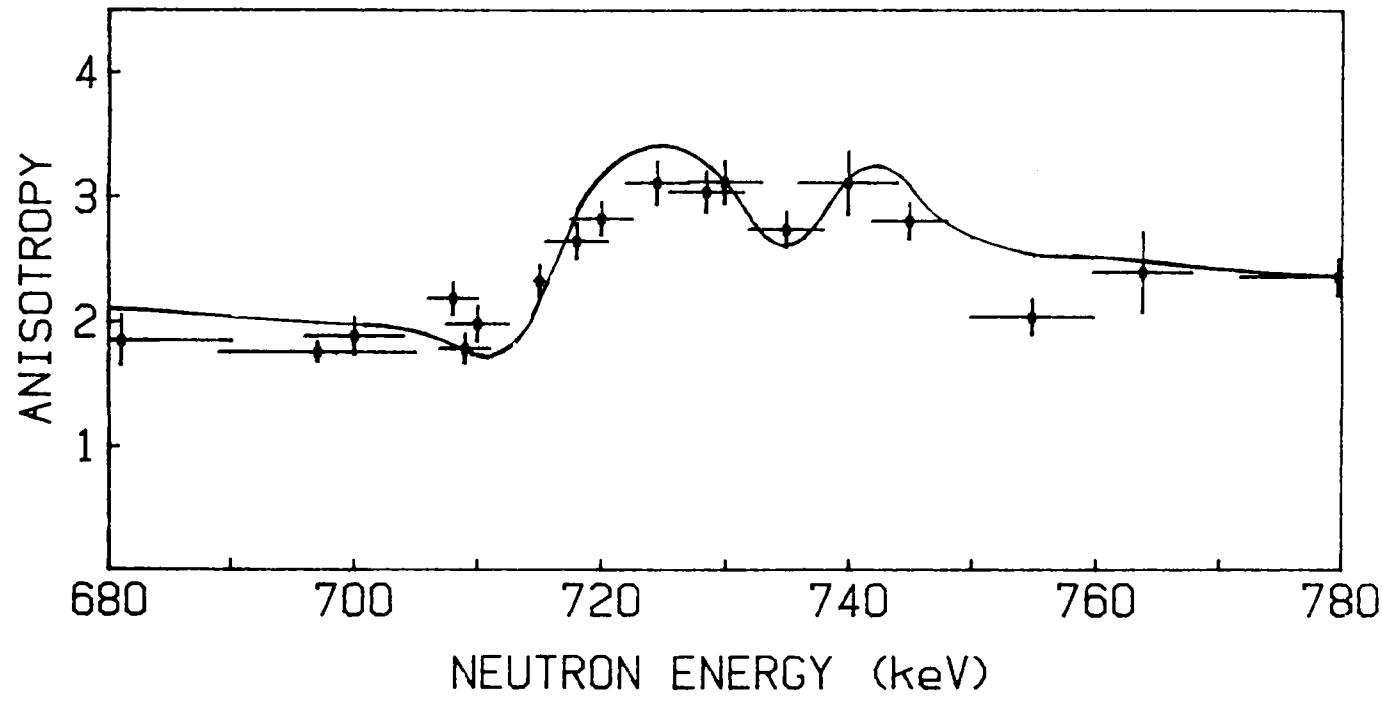

Fig. 4.8(b) Comparison of the anisotropy data with those calculated in the present analysis.

10% of the strength of the $K = {}^{3}/_{2}$ resonance has been shifted to 720-750 keV, while 3% of the strength of the $K = {}^{1}/_{2}$ resonance has been moved to 850 keV. These extensions could have been applied either to our previous analysis or the preferred analysis of Blons et al. [39]. However, our calculation was unable to reproduce the details of the Blons et al. calculation without extensive modification of the transmission coefficients, so we persevered with the principle of our previous analysis. However, the parameters $\hbar^2/2j$, a^+, a^- and E^+-E^- were revised to 1.65, -1.1, 0.6 and -6.7 keV respectively, to reproduce accurately the energies of the structures seen in the ^{230}Th(d,pf) cross section measurement of Blons et al. [42]. The fission cross section calculated under these conditions is shown in Figure 4.7. The calculated anisotropy shown in Figure 4.8(b) is now in much better overall accord with the experimental data.

4.2.2 Spin dependence of $\bar{\nu}_p$ and $\bar{E}_K$ for neutron fission of ^{239}Pu in the resonance region

(R.L. Walsh*, J.W. Boldeman) (*Work performed during attachment to Centre d'Etudes de Bruyères-le-Châtel, France.)

There presently exists a data discrepancy for the spin dependence of $\bar{\nu}_p$ and $\bar{E}_K$ for ^{239}Pu(n,f) between the thermal region (below 1 eV) and the resolved resonance region (1-400 eV). ($\bar{\nu}_p$ is the average number of neutrons emitted per fission; $\bar{E}_K$ is the average total fragment kinetic energy.) For the region below 1 eV, data on ν_p and E_K are in good agreement with one another and imply a spin dependence of 2%. For the region above 1 eV the situation is conflicting, with some measurements supporting the result below 1 eV and other implying little or no spin dependence of $\bar{\nu}_p$ and $\bar{E}_K$.

Therefore, the data above 1 eV were examined to seek to rectify this discrepancy. Features such as resonance spin assignments, comparisons with thermal $\bar{\nu}_p$ values and mass yield curve parameters were evaluated. However, the discrepancy is still apparent.

A paper on this work has been accepted for publication in Nuclear Physics A.

4.2.3 Calculation of energy spectrum of fission neutrons

(R.L. Walsh*) (*Work performed during attachment to Centre d'Etudes de Bruyères-le-Châtel, France.)

A computer code FISNEN (Fission Neutron Energies) was written to calculate the energy spectrum of neutrons emitted in fission. The formalism of Madland and Nix [43] was used. FISNEN calculates this spectrum from 0 to 20 MeV for a range of fissioning nuclei and for a range of incident energies. Spontaneous fission is also treated. The code is applicable to both single and multiple-chance fission. Two versions are available: an 'approximate' calculation, where the compound nucleus formation cross section $\sigma_c(\varepsilon)$ is assumed constant, and the 'exact' calculation where the energy dependence of $\sigma_c(\varepsilon)$ is included.

Figure 4.9 shows the calculated fission neutron spectrum (FNS) for 2 MeV neutron induced fission of ^{239}Pu ('exact' calculation). Because 2 MeV is approximately equal to the mean energy of fission neutrons, Figure 4.9 thus represents an FNS induced by a source which is itself an FNS.

For fission of ^{235}U the calculation agrees very well with experimental data. For fission of ^{239}Pu, discrepancies exist above 8 MeV in the secondary spectrum. Work is continuing to eliminate this discrepancy by refinement of various nuclear parameters used in the calculation and by inclusion of other fission characteristics, e.g. fragment spin.

4.2.4 Variation of even-odd charge effects with excitation energy in ν(A) and mass yield for ^{252}Cf(sf)

(R.L. Walsh)

The computer analysis program (see 1983/84 Annual Report of Applied Physics Division) was further extended to incorporate elliptical windows in the kinetic energy vs mass surface in addition to circular windows. The aim was to match the shape of the contour lines in this surface as closely as possible. It was found, however, that the variation of even-odd charge fine structure in ν(A) (neutrons) and Y(A) (mass yield) with excitation energy E* was most marked for a window given by a combination of two circles.

Figure 4.10(a,b,c) shows the effect on ν(A) of sliding the two-circle data window across the ^{252}Cf mass energy surface

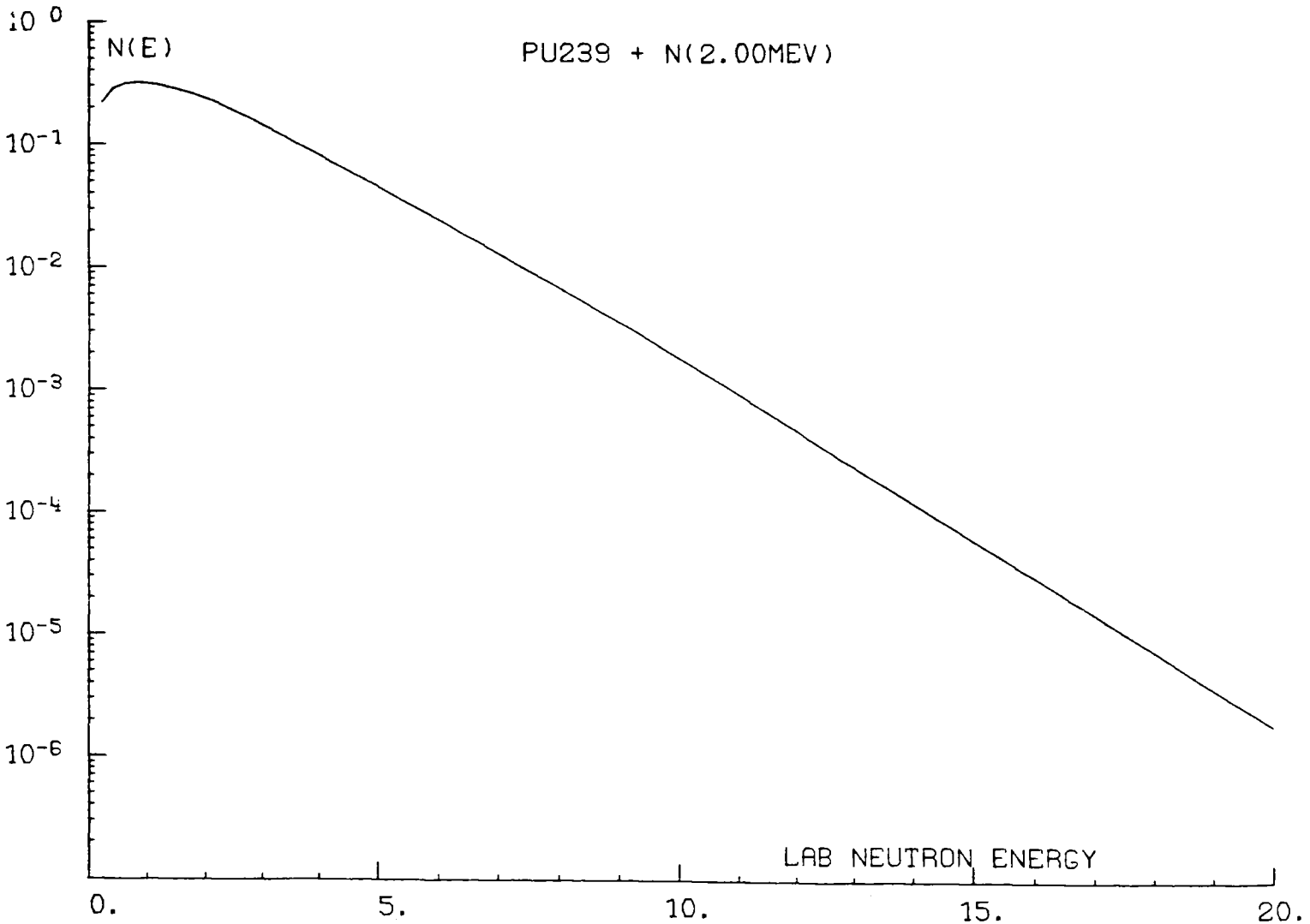

Fig. 4.9 Energy spectrum of fission neutrons for 2 MeV neutron fission of ^{239}Pu calculated by the code FISNEN. Value assumed for nuclear level density parameter is a = A/(11 MeV), where A is a compound nucleus mass number.

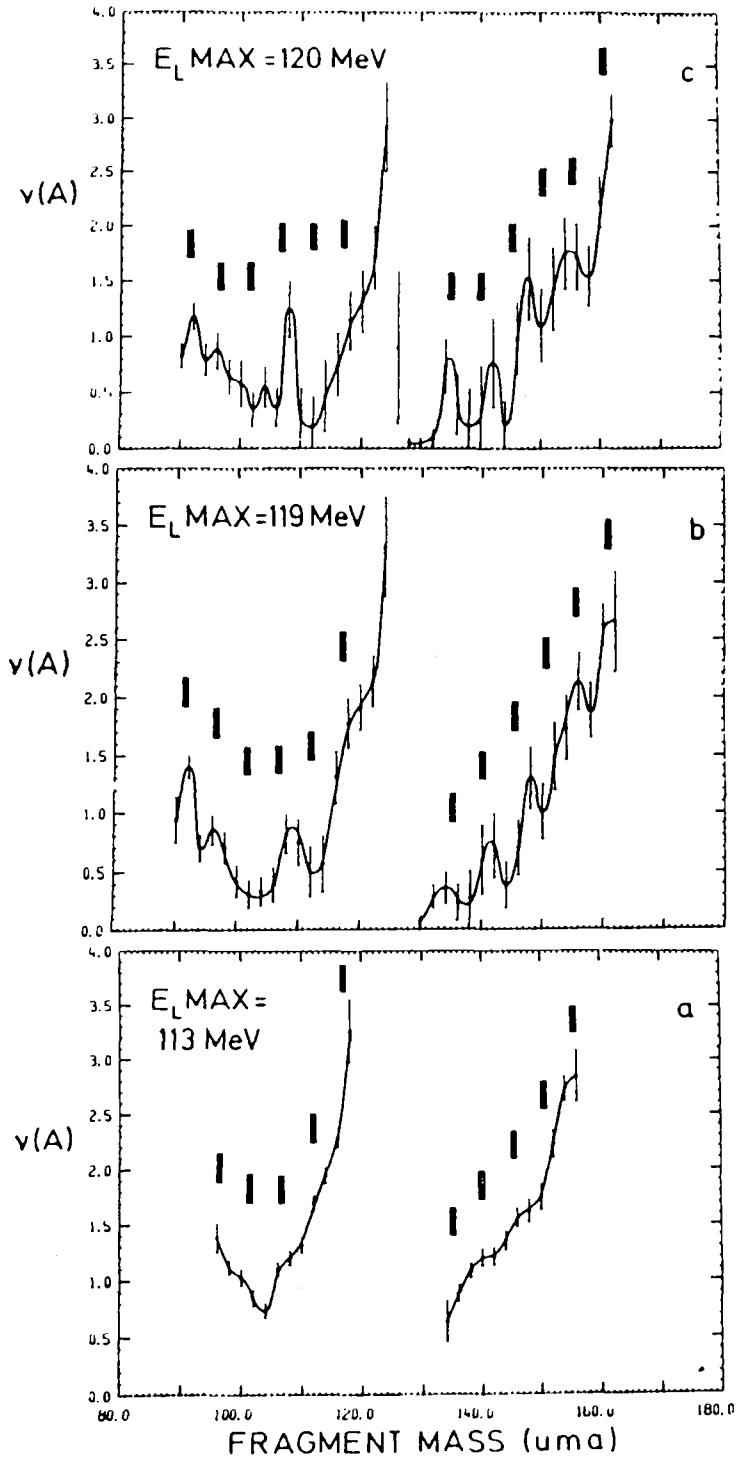

Fig. 4.10(a,b,c) Variation of ν(A) even-odd charge effects with decreasing E* (i.e. increasing E_LMAX). Vertical bars show location of evenly charged fragments in ^{252}Cf(sf).

(A_H-E_L) to regions of low excitation energy E*. The ν(A) curve is smooth for E_LMAX = 113 MeV, but strong even-odd charge effects are seen for E_LMAX = 119 and 120 MeV. (E_LMAX labels the maximum energy of a data window.) Similar behaviour is observed in the mass yield curve.

A poster paper on this work was presented to the International Conference on Nuclear Data for Basic and Applied Science, Santa Fe, USA, 13-17 May 1985.

4.2.5 SNIF - Standard Neutron Irradiation Facility

(D.D. Cohen, J.W. Boldeman, R.L. Walsh, A. Katsaros, M. Lavin*) (*University of Queensland)

Recently we have experienced an increased demand, mainly from radiation biologists, for our neutron irradiation facilities. This has prompted us to set up a standard neutron irradiation facility with its own dedicated leg on the 3 MV Van de Graaff. We will be using the Li(p,n), Be(d,n) and ^{2}D(d,n) reactions in the first instance to produce well characterised neutron beams of known energy, energy spread and intensity. Calibrated plastic scintillators, Li glass scintillators and a Long Counter are used to monitor the neutron intensities.

Furthermore we are currently working on acquiring sufficient expertise to convert these neutron intensity-energy distributions into depth-dose distributions for a variety of both thick and thin tissue type targets.

Currently we can supply up to 3 x 10^8 n cm $^{-2}s^{-1}$ with energies from tens of keV to several MeV. This corresponds to absorbed doses in tissue of up to 4.6 krad h^{-1} for 1-2 MeV neutrons, and of about 0.85 krad h^{-1} for 100 keV neutrons.

4.2.6 3 MV Van de Graaff accelerator

(J.W. Boldeman, I.F. Senior, A.E. Croal, K. Thorpe, J.P. Fallon)

The 3 MeV Van de Graaff accelerator operated for 3564 hours. Neutron Physics used 2489 hours of the total time with applications of nuclear techniques using the remainder. Maintenance time was 1803 hours following a major failure of both the alternator and drive motor (see AP Annual Report 1983/84) and a pressure-dependent leak in the accelerating tube.

Pressure Dependent Leak

The rectification of the alternator/drive motor problems took four weeks of maintenance. On gassing up the accelerator for the first time following this failure, the base pressure rose from 0.1 mPa to 2 mPa at ~2.03 MPa tank pressure. After almost eight weeks of methodically eliminating components, the fault was rectified by replacement of the accelerating tube. A helium leak check of the tube at atmospheric pressure failed to show any leak over a period of hours.

The reason for the fault could have been damage sustained when the alternator seized and caused wild mechanical oscillations of the accelerator terminal which, in turn, bumped the end of the tube, partly springing a glue joint. There was also some pitting of the gasket seat at the base end of the tube. Most of this was removed but resulted in no improvement of the fault.

Poor Beam Focus

Under some beam conditions good focussing of the beam could not be achieved. Beam cross section often resembled a doughnut with a sector removed and the beam was heavily steered when tube focus was adjusted. This fault was eventually traced to the asymmetric position of the tube focus electrode in the accelerating tube. The beam had been hitting the accelerating tube about halfway along its length.

Alternator Problems and Modifications

Following the previous rebuilding of the failed alternator, which had included remetalling and grinding of the bearing journals, it was decided to remove further metal from the journals. It was thought that the stated tolerances did not allow the journal at the free end to slide through the bearing inners when the shaft thermally expanded. The stated tolerances were $50.0^{+0.006}_{-0.005}$ mm while the journals were ground to 50.0 mm + 0.003 mm sliding end and 50.0 mm + 0.005 mm fixed end. A further 0.004 mm was removed from both ends.

A new lubricating grease, Arconol L64, designed specifically for vertically mounted inverted motors was also introduced. The volume of lubricant was increased from ~5 cm^3 to ~20 cm^3 per bearing. Expected lifetime is between 2000 and 3000 hours. This new grease may enable us to overcome a

problem that occurred when the oil content of the grease previously used separated and was centrifically dispersed from the housing onto the carbon earthing brush. This brush would then either stick in its holder or become ineffective due to increased contact resistance. The result was arc discharge between the ball race outers and/or the outers to housing. There was no apparent damage to the balls, but on occasions a pair of bearings were lightly welded together.

Helium/Neon Source Gas

Approximately 25% by volume of Ne gas was added to the He source bottle. When ionised in the standard HVEC nanosecond RF ion source, the following output on target was obtained: Ne^{+}, 3 μA at 2 MV and Ne^{++} 300 nA at 2 MV. Previous ionisation of other gases has worn away the aluminium extraction canal at a faster rate than does hydrogen, with Ne reducing this lifetime to <20%. A nickel canal will be evaluated in the near future.

Other failures that occurred during the year included a fuse and high voltage rectifier in the source focus power supply; "O" ring seals on the corona points drive shaft; several occasions where control rods between base and terminal needed adjustment, and often needed shortening to compensate for growth in the Perspex rod; the loss of refrigerant from the chiller used to extract heat from the tank and several thermionic valve failures in control console equipment.

Bunched Beam Operation

Some preliminary tests were performed to determine the output pulse shape and current density of a bunched d.c. beam as compared with a bunched chopped beam. The aim is to produce a large current density in the bunched d.c. beam. The unwanted d.c. component would then be post-deflected. The best output obtained was 2-3 ns FWHM with ~32% of the measured target current (45 μA) being in the pulse. The repetition rate was 18 MHz. 1 MHz and ~30% modulation was apparent and was possibly introduced in the buncher. More tests are to follow.

Vacuum Evaporation Systems

(A.E. Croal, J.P. Fallon)

There are at present two operational evaporation systems and a third is under development. One is for specialised evaporation of actinides and the other for general purpose evaporations of Li, Au, Al, Ba and others.

The actinide evaporator is basically a home-made UHV system but incorporates a 100 mm butterfly valve between the chamber and pumping system. The "O" rings in this valve have two disadvantages, namely, a poorer ultimate vacuum and starting problems with sublimation and ion pumps. The latter is due to absorbed air in the titanium layers following normal leakage past the "O" rings after extended shutdowns. The general purpose evaporation is based on a Varian FC12 UHV system and incorporates both electron gun and resistive heating. When high vapour pressure sources are used regularly in this chamber, surface contamination results in poor vacuums due to outgassing. Chemical cleaning of both the upper and lower halves of the chamber is necessary using a mix of hydrochloric, sulphuric and nitric acids. Repeated cleaning of the system has resulted in one weld being eroded to the point of vacuum leaking. To accommodate the high vapour pressure materials, a third evaporator is being prepared. It will operate at a worse vacuum than the FC12 and be pumped using an oil diffusion pump. Many targets have been produced throughout the year, the bulk of these being Li with thicknesses of 3-30 keV and natural uranium with thicknesses of 5-20 $\mu g\ cm^{-2}$.

4.2.7 ARGAS (AINSE Residual Gas Analysis System)

(A. Katsaros, D.D. Cohen, AINSE)

Recently the need arose for a versatile, portable vacuum pump system, which would be required to service the many situations in the accelerator group.

The system had to cover three main areas:-

(1) Residual gas analysis

(2) Portable pumping system

(3) Leak detection of clean and dirty systems.

The ARGAS system (AINSE Residual Gas Analysis system) was built over past twelve months with these specifications in mind.

Briefly some of the features are:-

(1) Turbo pump system provides no backstreaming of oil

(2) Ultimate pressure better than 3×10^{-7} mbar (0.03 mPa)

(3) Ability to detect masses from 2 to 40

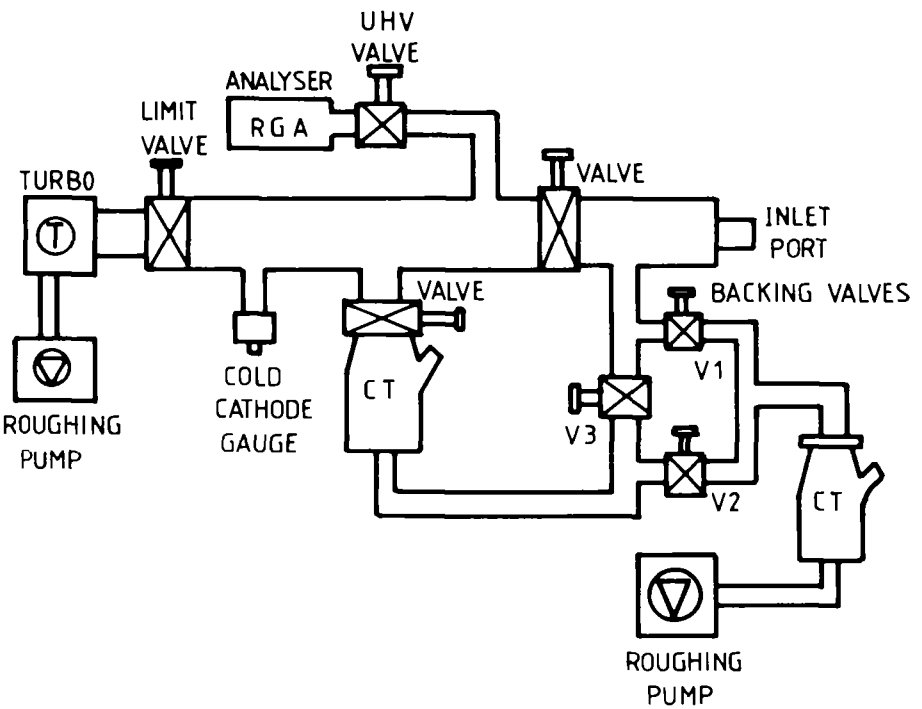

Fig. 4.11 Block diagram of ARGAS

(4) Ability to differentiate between N_2 and CO gases in system which have the same mass

(5) Quick cycle time

(6) Low maintenance

Figure 4.11 illustrates the ARGAS system.

4.2.8 High alpha activity handling suite

(R.L. Walsh)

A high alpha handling suite has been constructed in Room 10, Building 56, by Engineering Services and Operations Section, in accordance with design advice provided by Applied Physics Division. The previous suite in Building 2 is now de-commissioned.

REFERENCES FOR CHAPTER 4

[11] Frehaut, J., Mosinski, G., Bois, R. and Soleilhac, M. (Centre d'Etudes de Bruyères-le-Châtel) CEA-R-462b (1974).

[12] Zhang, H., Zuhua, L., Shengyue, D. and Shaoming, L., Nuc. Sci. Eng. 86, 315-331 (1984).

[13] Boldeman, J.W. and Hines, M., Nuc. Inst. and Method. 91, 114-116 (1985).

[14] Boldeman, J.W., AAEC/TM385 (1967).

[15] White, P.H. and Axton, E.J., J. Nucl. Energy 22, 73 (1968).

[16] Axton, E.J., Bardell, A.G. and Aubric, B.N., J. Nucl. Energy 23, 457 (1969).

[17] Aleksandrov, B.M., Belov, L.M., Drapchinskij, L.V., Kramarovskij, Ya. M., Lozhkomoev, Gr. E., Matyukhanov, V.G., Petrzhak, K.A., Prusakov, A.G., Sorokina, A.V., Shlyamin, Eh. A., Migun'kov, O.A., Stukov, G.M., Schchebolev, V.T. and Yaritsyna, I.A., Proc. 1975 Kiev Conf., Vol. 5, p. 166.

[18] Edwards, G., Findlay, D.J.S. and Lees, E.W., Ann. Nucl. Energy 9, 127 (1982).

[19] Axton, E.J., European Appl. Res. Rept.-Nucl. Sci. Technol. 5, 609 (1984).

[20] Boldeman, J.W. and Hines, M.G., Proc. IAEA AGM on Neutron Standard Reference Data, Geel, Nov. 1984 (to be published).

[21] Holden, N.E. and Zucker, M.S., Proc. IAEA AGM on Neutron Standard Reference Data, Geel, Nov. 1984 (to be published).

[22] Asplund-Nilsson, I., Conde, H. and Starfelt, N., Nucl. Sci. Eng. 16, 124 (1963).

[23] Hopkins, J.C. and Divon, B.C., Nucl. Phys. 48, 433 (1963).

[24] Boldeman, J.W., Nucl. Sci. Eng. 55, 188 (1974).

[25] Zhang, H.Q. and Liu, Z.H., Chin. J. Nucl. Phys. 2, 29 (1980).

[26] Spencer, R.R., Gwin, R. and Ingle, R., Nucl. Sci. Eng. 80, 603 (1982).

[27] De Volpi, A. and Porges, K.G., Phys. Rev. C1, 683 (1970).

[28] Bozorgmanesh, H., Thesis, University of Michigan (1977).

[29] Aleksandrov, B.M., Korolev, E.V., Kramarovskij, Ya. M., Lozhkomoev, G.E., Matyukhanov, V.G., Petrzhak, K.A., Prusakov, A.G., Sorokina, A.V. and Shylamin, Eh. A., Proc. 1980 Kiev Conf., Vol. 4, p. 119.

[30] Smith, J.R. and Reeder, S.D., EPRI-NP-3436 (1984).

[31] Axton, E.J. and Bardell, A.G., paper submitted to Metrologia (1984).

[32] Colvin, D.M. and Sowerby, M.G., Proc. IAEA Symp. Physics and Chemistry of Fission, Salzburg, Vol. 2, p. 25 (1965).

[33] Boldeman, J.W., NBS Special Publication 493, 182 (1977).

[34] Smith, J.R., Proc. ^{252}Cf Workshop, Brookhaven National Laboratory, 6 Dec. 1977.

[35] Ullo, J.J., Proc. ^{252}Cf Workshop, Brookhaven National Laboratory, 6 Dec. 1977.

[36] Moller, P. and Nix, J.R., 3rd IAEA Symp. Physics and Chemistry of Fission, Rochester, Vol. 1, p. 103 (1974).

[37] Bjornholm, S., and Lynn, J.E., Rev. Mod. Phys., 52, 725 (1980).

[38] Lynn, J.E., J. Phys. G. Nucl. Phys., 9, 665 (1983).

[39] Blons, J., Mazur, C., Paya, D., Ribrag, M. and Weigmann, H., Nucl. Phys., A414, 1 (1984).

[40] Boldeman, J.W., Gogny, D., de L. Musgrove, A.R. and Walsh, R.L., Phys. Rev., C22, 627 (1980).

[41] Blons, J., Mazur, C., Paya, D., Ribrag, M. and Weigmann, H., Phys. Rev. Lett., 41, 1282 (1978).

[42] Blons, J. Fabbio, B. Hisleu, J.M. Mazur, C., Patin, Y., Paya, D. and Ribrag, M. (1985), Proc. Int. Conf. Nucl. Data for Basic and Applied Science, Santa Fe, USA, 13-17 May 1985.

[43] Madland, D.G. and Nix, J.R., Nuc. Sci. & Eng. 81, 213 (1982).

5. FUSION PHYSICS

5.1 General

The main research program in Fusion Physics Section involves the experimental and theoretical analysis of rotamak plasmas. Some of this work has been performed in collaboration with Professor I. Jones of Flinders University, and we acknowledge his contributions. The second major area of research, carried out in collaboration with Dr B. Clancy from Nuclear Technology Division and Dr N. Cramer from Sydney University, involves the theory of plasma heating using Alfvén waves. Significant progress, which is detailed below, has been achieved in both of these fields during the year.

One of the year's highlights was the participation of Fusion Section staff in an IAEA sponsored workshop on Advances in Compact Torus Research, held in Sydney on 4-7 March 1985. At this meeting which was hosted by the AAEC, the latest results in spheromak, field-reversed-configuration and rotamak research were reported. This meeting was particularly useful as it showed that these different approaches to plasma confinement have many areas of common interest; for example, transport processes and Larmor radius effects. The meeting also resulted in an increased awareness in the fusion community of the rotamak project.

In June 1985, Peter Watterson joined the Section as a post-doctoral fellow. Peter is at present on a 6 month attachment to the School of Physical Sciences, ANU, to work with Dr R. Dewar on the development of the PEST equilibrium and stability code to allow modelling of the rotamak.

An overview of the rotamak and Alfvén wave research is now presented, followed by a more detailed description of specific topics.

The rotamak is a high β, compact torus, with or without a toroidal magnetic field, in which the toroidal current is driven by an applied rotating magnetic field. Over the past year progress has been made in the experimental analysis of rotamak behaviour as a function of:

(i) the power input via the rotating magnetic field,

(ii) the applied vertical field strength and shape, and

(iii) the vessel filling pressure.

The major conclusion is that, for an appropriate choice of vertical field strength, stable and reproducible discharges can be established at all input power levels examined to date. However, due to energy loss channels which are at this stage, unidentified, the plasma remains cool (<10eV) at presently available power levels. Future work is aimed at overcoming the losses and heating the plasma.

To provide a model of the rotamak energy balance, a semi-analytic solution of the Grad-Shafranov equation is being used to evaluate the dominant energy flows, both for laboratory and reactor size plasmas. Other rotamak theoretical work involves the formulation of equations that describe toroidal equilibrium in the presence of a small amplitude rotating field, and the analysis of toroidally axisymmetric oscillations.

Progress in the theory of Alfvén waves includes a comprehensive comparison of the MHD and kinetic theory predictions of Alfvén wave heating, and analysis of the quasi-electrostatic wave density oscillations and energy deposition profile for the TORTUS tokamak at Sydney University, the wave and instability spectrum of reverse-field pinches, properties of MHD surface waves and the excitation of torsional Alfvén waves by a localised antenna. The kinetic theory code ANTENNA has been improved to allow calculation of the energy deposition profile in the plasma and to treat general density distributions.

It is with great sorrow that we report the death of Professor Ray Grimm in August 1984. Ray had recently taken up his position as Head of Fusion Physics Section, and the loss of his dynamic yet good humoured leadership has been felt by us all.

5.2 Experimental Rotamak Project

(G. Durance, G.R. Hogg, J. Tendys)

Following the commissioning of the high-power RF amplifiers, a systematic study has been undertaken of the effects on the long-duration (~15 ms) rotamak discharges of increasing the amount of RF power transferred to the plasma. The available RF power can be controlled by varying the charging voltage, Vc, on the capacitor bank which acts as a power supply to the final RF amplifiers. (Vc is effectively the plate voltage on the final amplifier tube.) Results for three values of Vc are shown in

Fig. 5.1 a-g, where Vc is used as a label to distinguish the individual curves. The maximum RF power which can be transferred is restricted by the design of the present Helmholtz coils.

The results shown in Fig. 5.1 a-g have been obtained with a hydrogen filling pressure of 150 Pa. The vertical magnetic field needed for plasma equilibrium has been generated by passing current through two coils (31 cm diameter separated by 50 cm) positioned symmetrically about the Pyrex discharge vessel. These coils produce a simple mirror-type magnetic field distribution. In these experiments the magnitude of this externally-applied field has been increased to the maximum value compatible with reliable discharges for each value of Vc. No attempt has been made to match properly the plasma load to the amplifier output for each case; instead, the matching has been performed for the Vc = 8 kV case (at the time of maximum current) and has not been altered for the other Vc values.

The waveforms of the applied vertical field that have finally been used are shown in Fig. 5.1a. The corresponding driven toroidal currents, power inputs and line-averaged electron number densities are shown in Figs. 5.1 b-d. The electron number densities have been estimated using an 8 mm microwave interferometer positioned so that the microwaves pass through a diameter near the equatorial plane. At Vc = 8 kV, the 8 mm microwave transmission is observed to 'cut-off' ~0.5 ms after the start of the discharge, and to remain cut-off until the very end of the discharge. (The critical density for 8 mm microwaves ~1.6×10^{13} cm^{-3}.)

The radial position of the separatrix (R_s) and the axial position of the neutral points (Z_x) have been determined from magnetic probe measurements (Figs. 5.1 e,f). Oblate compact torus configurations are achieved in each case. At Vc = 8 kV the separatrix appears to be touching the vessel wall which implies that an additional energy loss channel is present.

An estimate of the energy confinement time has been obtained as follows. The thermal energy content of the plasma

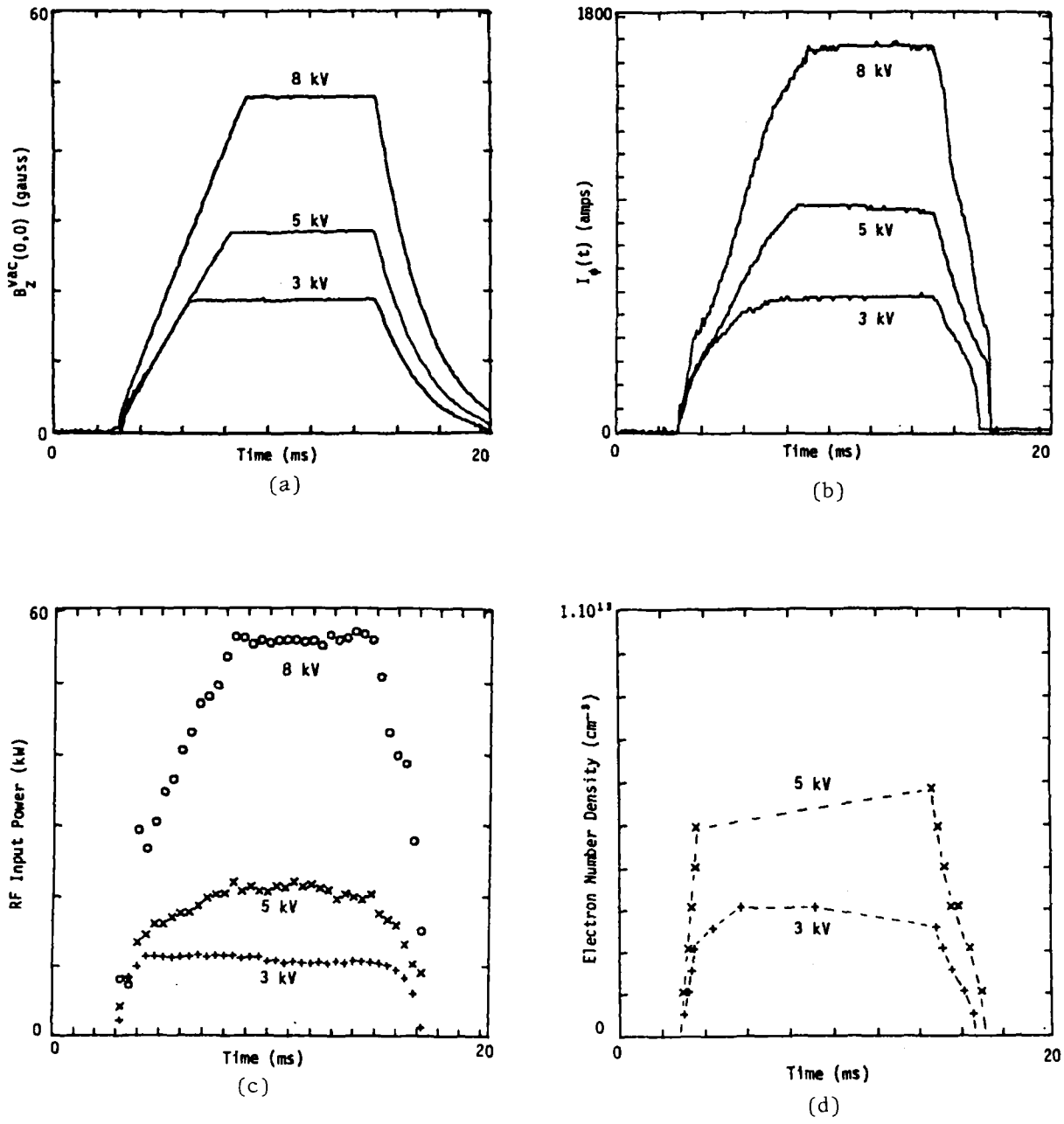

Fig. 5.1 Typical results from medium power, long duration rotamak experiments (p = 150 Pa hydrogen)

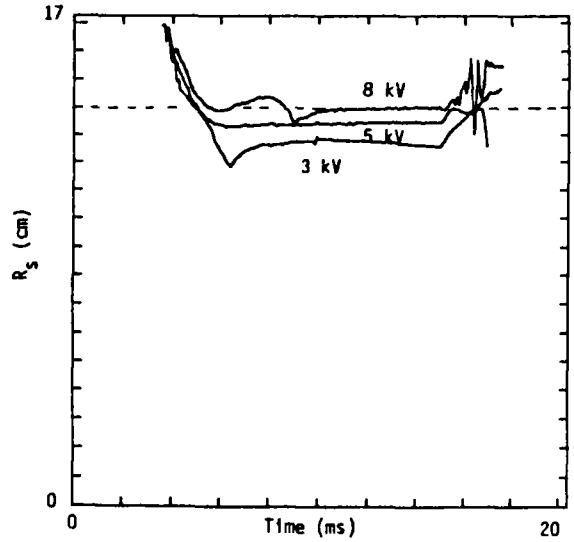

(e)

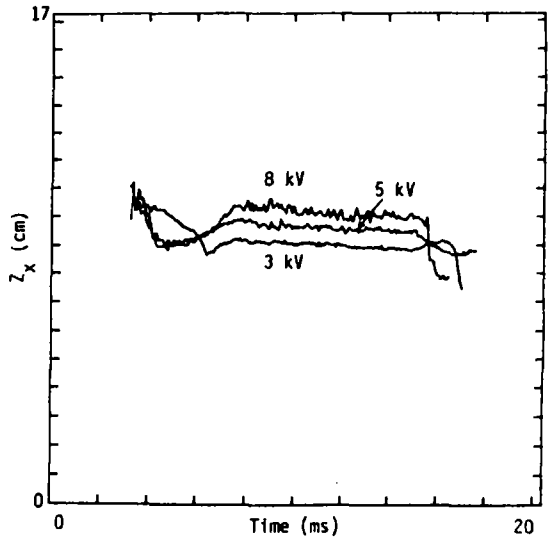

(f)

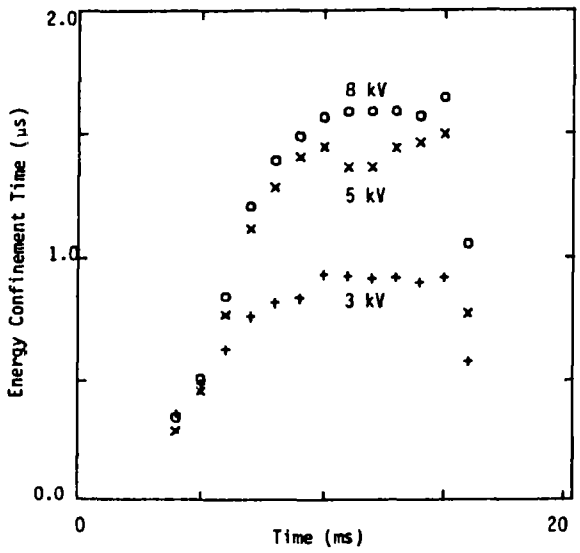

(g)

Fig. 5.1 (continued)

is given by

$$W_p = \frac{3}{2}\int p dV$$

where p is the plasma pressure, and the integral is taken over the volume enclosed by the separatrix surface. A Hills vortex type equilibrium model has been used to evaluate this integral using the measured toroidal current and plasma geometry. The rate-of-change of the plasma thermal energy content is given by

$$\frac{dW_p}{dt} = P_{in} - \frac{W_p}{\tau_E}$$

where P_{in} is the input power and τ_E is the global energy confinement time. Assuming that the plasma is in equilibrium (i.e. $dW_p/dt = 0$), $\tau_E = W_p/P_{in}$. The results using the measured RF input power are given in Fig. 5.1g. The small values of τ_E reflect the presence of large energy loss channels which are, as yet, undefined. The small size of the apparatus presumably contributes to the transport losses.

A large amount of 'slip' between the rotating electron fluid and the rotating magnetic field has been inferred to be present in these experiments by comparing the estimated toroidal current (assuming synchronous rotation) with the measured current. Electron-ion collisions prevent completely synchronous rotation. The high degree of slip presumably arises because the plasmas are relatively cold and hence the resistivities are large. This implies that the screening currents are significant, and, indeed, the rotating magnetic field is observed experimentally to be substantially screened out of the plasma interior. Nevertheless, despite this imperfect penetration, significant toroidal current is driven in every case.

To avoid the energy losses incurred by a plasma/wall interaction, an attempt has been made to control the position of the separatrix by appropriately shaping the externally-applied equilibrium magnetic field. This has been achieved by the installation of two new vertical field coils (50 cm diameter). By varying the separation of these coils, compact torus configurations ranging from oblate to slightly

prolate have been achieved. Moreover the separatrix is observed to be well inside the vessel wall. These configurations have all been sustained for the full duration of the RF pulse with no evidence of any gross instabilities.

It is observed experimentally (see Fig. 5.2) that the RF input power can be empirically related to the driven toroidal current by an expression of the following form

$$P_{in} = I_{tor}^2 R + \text{CONSTANT}$$

Interpreting R as the plasma resistance, it is observed that the plasma resistance decreases from ~18 milli-ohm with the original vertical field configuration to ~6.5-7.5 milli-ohm with the more recent vertical field configurations. This interpretation implies that, for a given vertical field configuration, the plasma temperature does not increase as the input power is increased. The plasma temperature is believed to be low ($\lesssim$ 10 eV) in all these experiments. Techniques to measure the temperature more accurately are presently under development.

In some discharges the toroidal current density distribution has been deduced from magnetic probe measurements. The radial distribution of the current density exhibits a 'double-humped' structure as indicated in Fig. 5.3

Probe measurements have also indicated the presence of a spontaneously-generated bi-directional toroidal magnetic field. This is most pronounced during the 'ramp-up' stage of the driven toroidal current. During the quasi-steady phase of the discharge, the toroidal field is small ($\lesssim$3 gauss) and its distribution is less clear.

A second discharge vessel with the Helmholtz coils encapsulated in a high dielectric strength silicone (Sylgard) is nearing completion. This should overcome the limitations imposed by the present coils, and permit the input power to be increased.

The main thrust of the rotamak research program will now be directed towards achieving higher plasma temperatures.

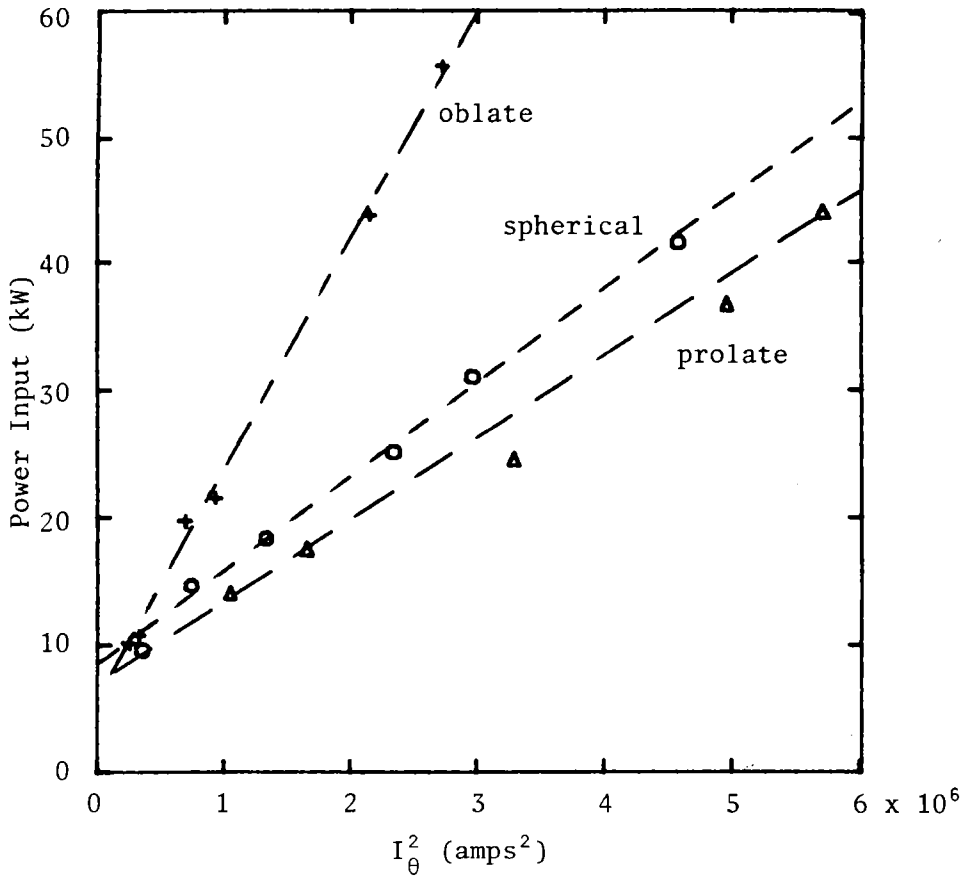

Fig. 5.2 RF input power vs the square of the driven toroidal current. (+ prolate plasma configuration formed with original vertical field coils; 0 near-spherical and Δ slightly prolate cases with new vertical field coils.)

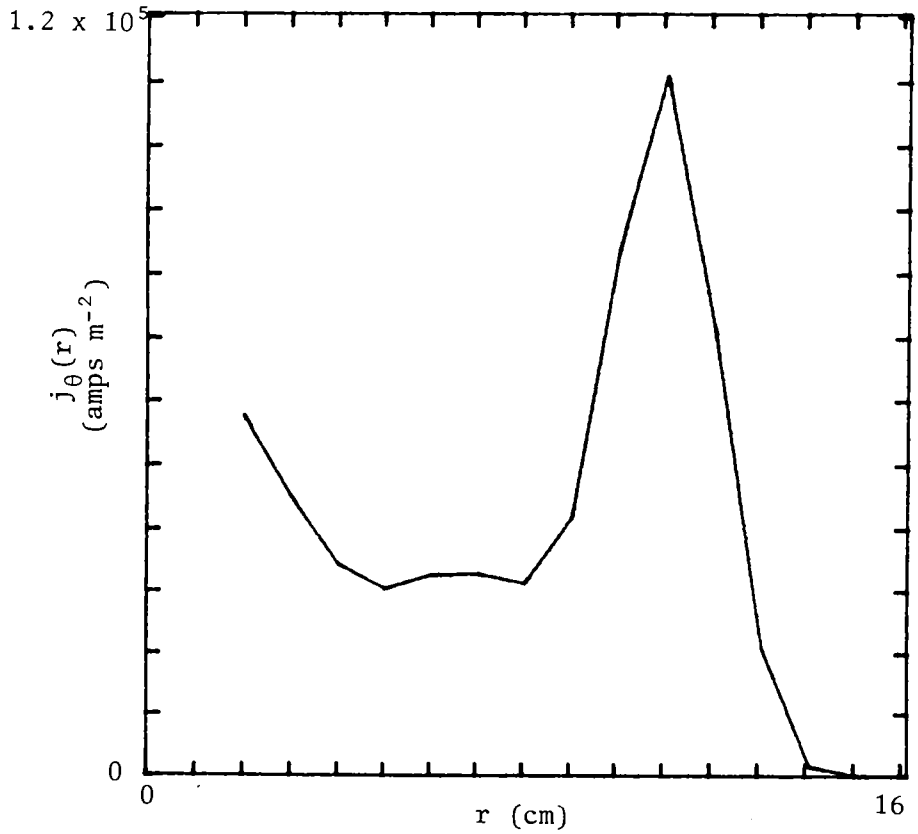

Fig. 5.3 Radial distribution of toroidal current density in z = 0 plane.

5.3 Theoretical Studies

5.3.1 Rotamak equilibrium and power balance

(J.L. Cook, E.K. Rose)

An analytic solution of the Grad-Shafranov equation has been derived for a compact torus with zero toroidal magnetic field and with a plasma pressure which is proportional to the magnetic flux squared. This equilibrium configuration serves as a basis for a transport code which calculates the power balance for typical rotamak conditions. Provided that an anomalous electron thermal conductivity comparable with that observed in tokamaks is used, then reasonable agreement is obtained with measured rotamak plasma parameters. Fig. 5.4 shows, for conditions representative of AAEC rotamak experiments, the time evaluation of electron and ion temperatures assuming that a constant toroidal current commences flowing in a partially ionised hydrogen plasma at t = 0.

5.3.2 MHD equilibria with rotating fields

(W.K. Bertram)

The ideal MHD equations have been used to investigate the equilibrium configurations of a plasma when it is subjected to an external rotating field. It was found that the rigid rotor model is an exact solution of the equations provided there were no internal oscillating currents, and there is no toroidal component of the steady magnetic field. The rigid rotor model was generalised to take into account configurations where these conditions are not satisfied.

5.3.3 Rotamak oscillations

(W. Bertram)

The observed frequency of oscillation (~40 kHz) of a plasma in a rotamak was thought to be due to a fundamental mode of vibration which is axially symmetric. In order to verify this hypothesis, a study was undertaken to investigate the axially symmetric modes of oscillation of field-reversed configurations, of which the rotamak is one example.

Numerical calculations for an infinite cylindrical plasma column yield results of 15-20 kHz for the fundamental mode. It was therefore decided to attempt a similar calculation for the much more complicated spherical configuration. The results we obtained were most encouraging, yielding 47 kHz for the fundamental mode as compared with the experimentally observed value of ~40 kHz.

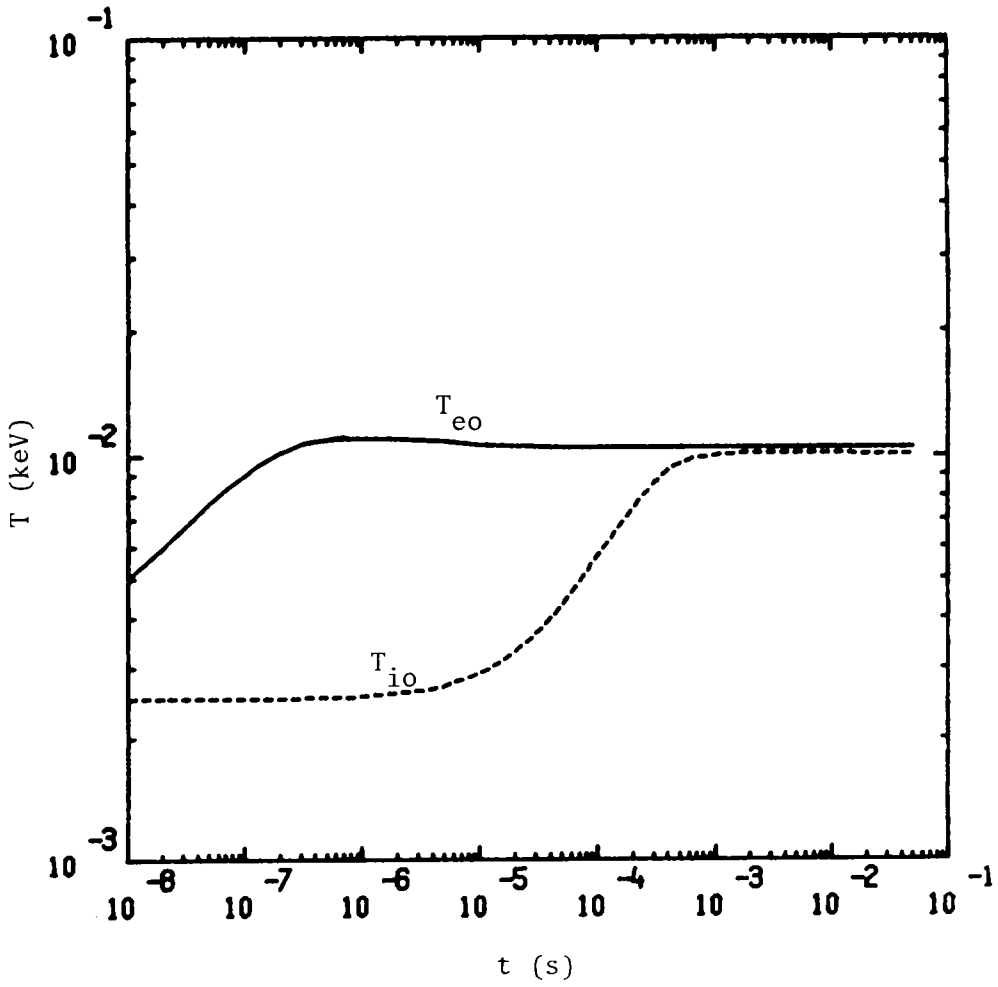

Fig. 5.4 Temperature vs time for low energy experiment

5.3.4 Alfvén wave heating

(B.E. Clancy*, N.F. Cramer**, I.J. Donnelly)
(*Nuclear Technology Division - **Sydney University)

MHD theory with the Hall term has been used to analyse the Alfvén resonance heating of cylindrical plasmas using axisymmetric waves excited by an antenna. An analytic expression for the antenna impedance derived for a simple plasma model has been used to help interpret the computational results for small, medium and large plasmas. We have found that compressional wave eigenmodes give large antenna resistances, however the energy is deposited near the plasma surface. At a frequency just above each eigenfrequency the Alfvén resonance damping is zero. Below the first eigenfrequency the energy can be deposited near the plasma centre, however the antenna resistance is fairly low except for medium size plasmas with a nearly constant central density.

The MHD theory calculations incorporate an artificial damping to dissipate the energy absorbed at the Alfvén resonance position. The correct description of the energy absorption process is given by kinetic theory. We have used this theory to show that, at the Alfvén resonance, the compressional wave is mode converted to a quasi-electrostatic wave (QEW) which propagates towards the plasma centre or edge depending on whether the plasma is hot or warm. The energy absorbed by the plasma agrees with the MHD theory predictions provided the QEW is heavily damped before reaching the plasma centre or edge; if it is not then QEW resonances may occur with a consequent increase in antenna resistance. Also, the relation between ion cyclotron wave resonances and QEW resonances in a hot plasma has been shown. The behaviour described above was demonstrated by numerical solution of the wave equations for small and large tokamak-like plasmas. WKB theory has also been used to derive useful expressions which quantify the QEW behaviour.

5.3.5 Quasi-electrostatic wave density oscillations in TORTUS

(B.E. Clancy*, N.F. Crammer** and I.J. Donnelly)
(*Nuclear Technology Division - **University of Sydney)

Alfvén resonance heating involves the mode conversion of the compressional Alfvén wave to a quasi-electrostatic wave (QEW) at the Alfvén resonance position (at some minor radius r_0). The QEW, which has a short radial wavelength, and which is heavily damped, determines the spatial profile of the plasma heating. Measurements of the QEW dispersion relation for comparison with theory is therefore of importance. This can be done using laser scattering from the electron density oscillations associated with the wave, and such experiments are planned for TORTUS.

Kinetic theory has been used to calculate these density perturbations in TORTUS for a range of plasma temperatures. At high temperatures the QEW is termed the kinetic Alfvén wave; it propagates towards the plasma centre. At low temperatures the QEW carries energy towards the plasma surface and it is called the surface electrostatic wave. The QEW field profiles are usually those of a damped wave propagating away from a source. However, when r_0 is near the centre of a hot plasma, or when r_0

is near the edge of a warm plasma, standing waves with enhanced amplitude can be established.

In the calculation of these waves, TORTUS is modelled by a cylindrical plasma surrounded by an antenna current sheet with space and time dependence $\delta(r-r_a)\cos(m\theta + n\phi - \omega t)$; see Donnelly and Cramer [44] for details. The current sheet generates plasma density oscillations of the form

$$n_{el}(r,t) = n_{el}^{r}(r)\cos(m\theta+n\phi-\omega t) - n_{el}^{i}(r)\sin(m\theta+n\phi-\omega t).$$

Typical results for propagating waves in both hot and warm plasmas are shown in Fig. 5.5 for wave numbers m = -1, n = 1. The density fields are given as a function of $\psi=(\omega t - m\theta - n\phi)$ and r. Fig. 5.5a, in which the central temperature T_{eo} = 200 eV, shows the kinetic Alfvén wave propagating away from $r_0(= 0.6r_p)$ towards the plasma centre. Fig. 5.5b, in which T_{eo} = 50 eV, illustrates the excitation of the QEW at $r_0(\cong 0.7r_p)$. It is interesting to note that this wave is backward propagating, so it carries energy towards the plasma surface but its phase velocity is directed towards r_0. In both cases the wave amplitude is about 10^{-5} of the central plasma density for a half-turn poloidal antenna carrying a current of 1 amp.

5.3.6 Energy deposition by the kinetic Alfvén wave

(B.E. Clancy*, N.F. Carmer** and I.J. Donnelly)
(*Nuclear Technology Division - ** University of Sydney)

In hot plasma the Alfvén resonance damping of the compressional Alfven wave proceeds by its mode conversion to the kinetic Alfvén wave which undergoes electron Landau damping, and thereby heats the plasma, as it propagates away from the resonance position. This wave experiences spatial dispersion due to ion Larmor radius effects, so its radial energy flux can be expressed as $F_r = S_r + T_r$ where $\underset{\sim}{S}$ is the Poynting flux and $\underset{\sim}{T}$ is the thermal energy flux. In a plasma cylinder the period-averaged radial component of the thermal flux associated with the kinetic Alfvén wave can be written as

$$T_r \cong -0.75 \frac{v_i^2}{v_A^2} \frac{\alpha^2 k}{\mu_0 \omega} \mathrm{Re}\left[(1+\alpha Z(\alpha))E_r^* E_z\right],$$

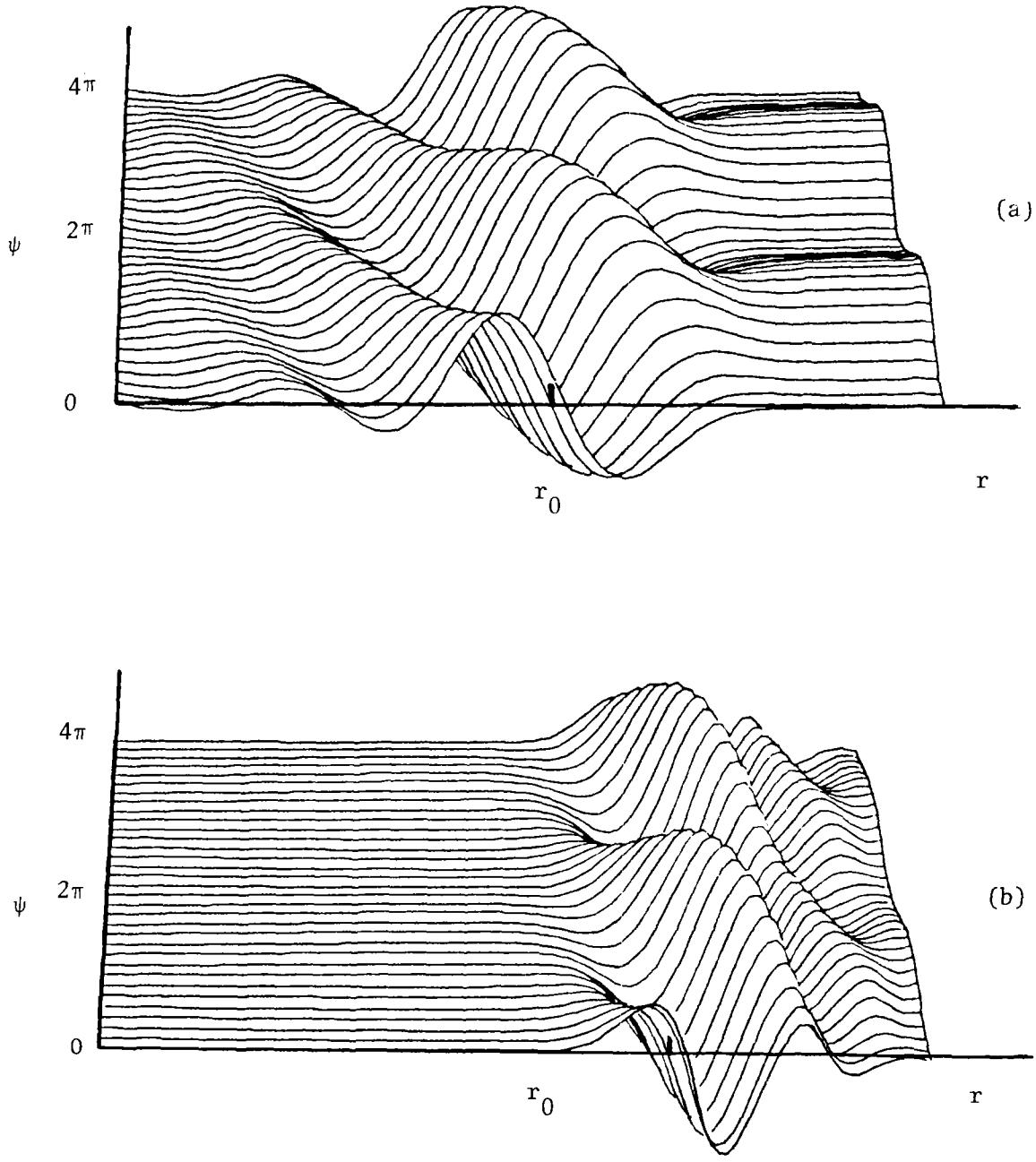

Fig. 5.5 The QEW density field as a function of time and radius for (a) a 200 eV plasma and (b) a 50 eV plasma. Each curve represents constant ψ (or t). The plotted fields extend over two wave periods.

where $\alpha = \omega/2^{\frac{1}{2}}v_e k$, k is the axial wavenumber, $v_{e,i}$ are thermal velocities and $Z(\alpha)$ is the plasma dispersion function. The energy deposition is given by $P = P_S + P_T$ where

$$P_S = -r^{-1}(d/dr)\ r\ S_r \text{ and } P_T = r^{-1}(d/dr) r\ T_r.$$

Fig. 5.6 shows the radial profiles of P, P_S and P_T for a wave with m = -1, n = 1 in a TORTUS plasma with T_{eo} = 200 eV. The frequency is such that $r_0 \cong 0.3r_p$ and a standing kinetic Alfvén wave is established. We see that P_S is negative near r = 0, so it is obviously necessary to include P_T in order to obtain the correct energy deposition profile which is everywhere positive.

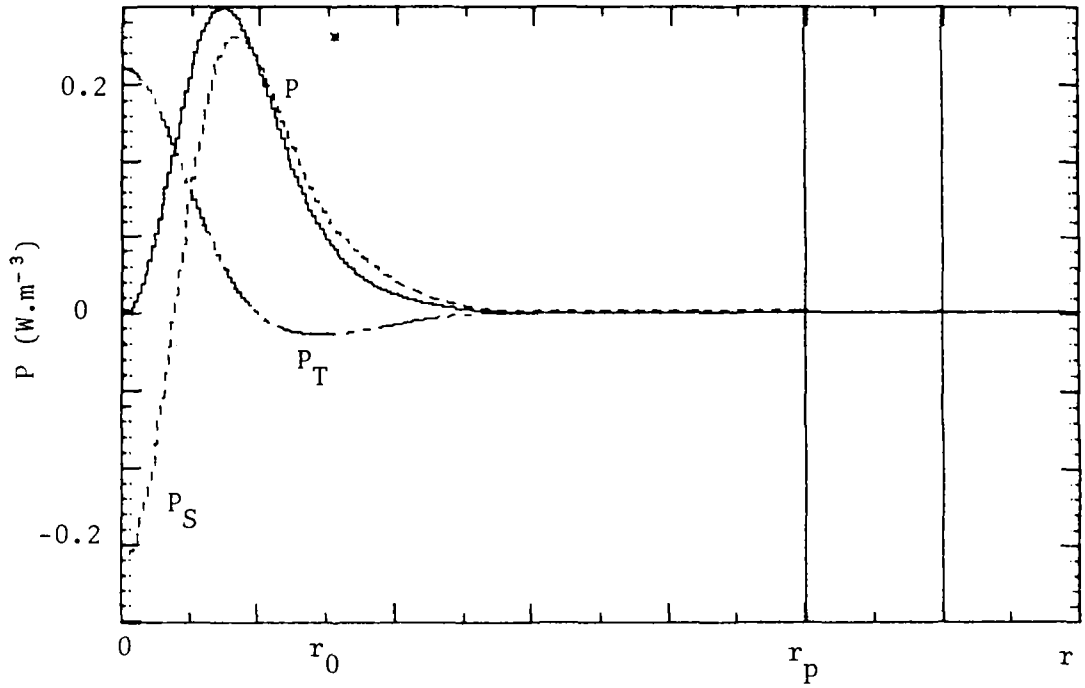

Fig. 5.6 The total energy deposition (P) and its Poynting flux (P_S) and thermal energy flux (P_T) components

5.3.7 The spectrum of a diffuse linear pinch

(N.F. Cramer* and I.J. Donnelly) (*University of Sydney)

As an extension of earlier work on the wave and instability spectrum of a current-carrying plasma, we have calculated the spectrum of a plasma with a strongly twisted magnetic field. Such a (forcefree) field is modelled by the Bessel function model (BFM). The frequency is assumed much less than the ion-cyclotron frequency.

With vacuum boundary conditions, the BFM is found to yield similar modes to the uniform-current case: a surface wave connecting to an unstable mode (the external kink mode), as well as a dense spectrum of discrete (shear) Alfvén waves. For the BFM the surface wave is often located in the Alfvén continuum, so that an impedance calculation with small damping is made to determine the frequency and resonance damping of the mode.

New features of the BFM are:

(1) an extra branch of unstable modes appears when the current is increased past a critical value, and

(2) when the axial field undergoes a reversal in direction (as in the reversed field pinch), a new propagating mode appears which we identify with the fast Alfvén wave propagating primarily along the azimuthal magnetic field.

5.3.8 MHD surface waves

(Y. Amagishi*, I.J. Donnelly)

(*Shizuoka University, Japan)

Surface waves with poloidal wave numbers m = ±1 are being studied as they propagate along a plasma column in the TPH device at Shizuoka University. The measured dependence of phase velocity on frequency is in good agreement with the predictions of the ANTENNA code.

The possibility of exciting and observing kinetic Alfvén waves in TPH has also been predicted, and experiments are planned.

5.3.9 Excitation of Alfvén waves by a localised antenna

(I.J. Donnelly)

A Green's function analysis has been used to study the excitation of low frequency Alfvén waves by localised current elements surrounded by plasma. This showed that currents perpendicular to the ambient magnetic field $\underset{\sim}{B}$ launch compressional waves which propagate almost isotropically away from the source. In contrast, currents parallel to $\underset{\sim}{B}$ launch torsional waves which propagate predominantly along those magnetic field lines which pass close by the source. In particular, for collisional plasmas the torsional wave launched

by the current element $J\hat{z}\delta(r)\delta(z)e^{-i\omega t}$ has a magnetic field component given, for $z >> r/\delta$, by

$$b_\theta = \frac{i\mu_o k_A}{4\pi r}\left[1 - \exp\left(-\frac{k_A r^2}{2\delta z}\right)\right]\exp\left(i(k_A z-\omega t)\right)$$

where $k_A = \omega/v_A$ and $\delta = \omega\nu_{ei}/\Omega_e\Omega_i$.

Experiments carried out using low temperature plasmas in TORTUS have shown excellent agreement with this theory.

5.3.10 Sputtering calculations

(J.L. Cook, E.K. Rose)

Recent experimental evidence shows that the sputtering coefficient, as a function of incident ion energy and angle, has a peak at an angle of about 70°. This affects the Maxwellian average value. A new theory taking this behaviour into account has been developed, and a library of sputtering rates (SPUTLIBII) has been prepared for international circulation.

REFERENCES FOR CHAPTER 5

[44] Donnelly, E.J. and Cramer, N.F., Plasma Physics and Controlled Fusion 26 769 (1984).

6. PUBLICATIONS

6.1 Reports - AAEC/E Series

Alexiev, D. and Tavendale, A.J. [1984] - A deep level transient spectrometer for high resistivity semiconductors using a marginal oscillator detector. AAEC/E598.

Cook, J.L. and Rose, E.K., SPUTLIBII - A revised version of the Maxwellian-averaged rates of sputtering. AAEC/E-report (in press).

Durance, G., Hogg, G.R. and Tendys, J. [1984] - The AAEC rotamak experiment: description and preliminary results at low input power. AAEC/E602.

Durance, G., Hogg, G.R. and Tendys, J. [1984] - The effects of rotating field frequency on the rotamak configuration. AAEC/E603.

Trowse, J., Durance, G., Hogg, G.R., Jones, I.R.* and Tendys, J. [1984] - The effect of an applied toroidal magnetic field on rotamak discharges. AAEC/E617. (*Flinders University of South Australia.)

Urquhart, D.F. [1985] - Calibration and operation of the AAEC working standard of measurement of activity of radionuclides. AAEC/E627.

6.2 Reports - AAEC Internal

Johnson, E.P. [1984] - "Preliminary assessment of TLD procedures - study visit to Westmead Centre", AP/TN185.

Johnson, E.P. [1985] - "Dose Calibration of a Baldwin-Farmer chamber", AP/TN190,

Johnson, E.P. [1985] - "Procedure for use of secondary standard ionisation chambers in absorbed dose measurements", AP/TN191.

Lawson, E.M. and Lee, P.J. [1985] - "Evaluation of Komatsu standards for silicon resistivity", AP/TN194.

Lawson, E.M., Lee, P.J. and Tavendale, A.J. [1984] - "Neutron transmutation doped silicon", AP/TN189.

Williams, A.H. and Tavendale, A.J. [1985] - "Measurement of semiconductor diode capacitance using a lock-in amplifier capacitance meter, AP/TN192.

6.3 Reports - Non-AAEC Series

Boldeman, J.W. (compiler) [1984] - Progress report on nuclear data activities in Australia for 1983-1984. INDC-P14.

6.4 Journal Papers

Bertram, W.K. - Magnetohydrodynamic equilibrium conditions for a plasma in the presence of a rapidly rotating magnetic field. Plasma Physics and Controlled Fusion (in press).

Bird, J.R. [1985] - Ion beam applications in the 1980s: from materials to heritage research. Nucl. Spectrum, 1(1): 19-26.

Boldeman, J.W. and Hines, M.G. [1985] - Prompt neutron emission probabilities following spontaneous and thermal neutron fission. Nucl. Sci. Eng. 91:114-116.

Boldeman, J.W. and Hines, M.G. [1985] - $\bar{\nu}$ for the spontaneous fission of ^{252}Cf. Nucl. Sci. Eng. (in press).

Borg, G.G.*, Brennan, M.H.*, Cross, R.C.*, Giannone, L.* and Donnelly, I.J. - Observations of magnetically guided Alfvén waves in a toroidal plasma. Plasma Physics and Controlled Fusion (in press). (*University of Sydney).

Clayton, E. and Dale, L.S.* [1985] - Determination of fluorine in NBS coal and coal fly ash by proton-induced gamma ray emission and spark source mass spectrometry. Anal. Lett. (in press). (*CSIRO Div. of Chemical Physics, Lucas Heights)

Clayton, E. and Wooller, K.K.* [1985] - Sample preparation and system calibration for proton-induced X-ray emission analysis of hair from occupationally exposed workers. Anal. Chem., 57(6):1075-1079. (*NSW Dept of Industrial Relations)

Cohen, D.D. [1984] - L subshell X-ray production by 1-3 MeV protons and He ions. Nucl. Instrum. Meth., B3, 47.

Cook, J.L. and Rose, E.K. - The effect of the angular dependence of sputtering in fusion reactors. Aust. J. of Physics (in press).

Cramer, N.F.* and Donnelly, I.J. [1984] - "Alfvén waves in current-carrying solar flux tubes", Proc. ASA 5 (4), 481. (*University of Sydney)

Cramer, N.F.* and Donnelly, I.J. [1984] - "Surface and discrete Alfvén waves in a current carrying plasma", Plasma Phys. and Controlled Fusion 26, 1285.

Cramer, N.F.* and Donnelly, I.J. - Modes of perturbation of a diffuse linear pinch: the Bessel function model. Plasma Physics and Controlled Fusion (accepted for publication). (*University of Sydney)

Donnelly, I.J., Clancy, B.E. and Cramer, N.F.* - Alfvén wave heating of a cylindric axisymmetric waves, Part 1, MHD Theory. J. Plasma Physics (in press). (*University of Sydney)

Green, B.E.**, Kennard, C.H.L.**, Smith, G.**, Elcombe, M., Moore, F.H.*, James, B.D.+ and White, A.H.++ [1984] - "The crystal structure of alpha and beta (1,10-phenanthroline) tetrahydroborato (triphenyl-phosphinato) copper (I) and the 2,9-dimethyl-4,7-diphenyl-1, 10-phenanthroline-tetraboratocopper (I)", Inorg. Chim. Acta, 83, 177-189. (*AINSE, **University of Queensland, +LaTrobe University, ++University of Western Australia)

Harrison, M.P., Spicer, B.M. and Cohen, D.D. [1984] - "L sub-shell X-ray production by 100-250 keV/amu ions. Aust. J. Phys. 37 475.

Hill, R.J.*, and Howard, C.J. [1985] - Peak shape variation in fixed-wavelength neutron powder diffraction and its effect on structural parameters obtained by Rietveld analysis. J. Appl. Crystallogr., 18(e):173-180.

Howard, C.J. [1984], A comment on "The peak in neutron powder diffraction" by B. van Laar and W.B. Yelon. J. Appl. Crystallogr., 17(6):482-483.

Irving, M.A.*, Elcombe, M.M. and Smith, T.F.* [1985] - Neutron diffraction studies of CsSCN above room temperature. Aust. J. Phys., 38(1):85-95. (*Monash University)

Lang, D.W. [1984] - The magnetohydrodynamic turbine. Energy Convers. Manage., 24(3):215-222.

Nelmes, R.J.*, Howard, C.J., Ryan, T.W.*, David, W.I.F.**, Schultz, A.J.+ and Leung, P.C.W.+ [1985] - A neutron and X-ray diffraction study of the phase transitions in proustite (Ag_3AsS_3) between 34K and room temperature. J. Phys. C (London): Solid State Phys., 17:L861-L865. (*University of Edinburgh, UK; **Rutherford Appleton Lab., UK; +Argonne Nat. Lab.)

Parsons, P.G. and Allen, B.J. - Accumulation of chlorpromazine and thiouracil by human melanoma cells in culture. Cancer Research (in press).

Pearton, S.J.* and Tavendale, A.J. [1984] - Electrical properties of deep silver- and iron-related centres in silicon. J. Phys. C (London). Solid State Phys., 17(36): 6701-6710. (*Now at A T & T Bell Labs.)

Tavendale, A.J., Alexiev, D. and Williams, A.A. [1985] - Field drift of the hydrogen-related, acceptor-neutralising defect in diodes from hydrogenated silicon. Appl. Phys. Lett. (in press).

Walsh, R.L. and Boldeman, J.W. [1985] - Spin dependence of $\bar{\nu}_p$ and $\bar{E}_K$ for ^{239}Pu(n,f) in the resonance region: the discrepancy between results above and below 1 eV. To be published in Nucl. Phys. A.

Wilson, D.J. and Bentley, K.W.* [1985] - The quantitative determination of uranium in human hair by fission track measurements. Radiat. Eff. (in press). (*Aust. Nat. Univ.)

Wyllie, H.A. and Lowenthal, G.C. [1984] - Ultra-thin radioactive sources. Intl. J. Appl. Radiat. Isot., Vol. 35, No. 4, p 257.

6.5 Conference Papers

Allen, B.J., Blagojevic, N., Gaskin, K.*, Soutter, V.* and Howman-Giles, R.* [1984] - In vivo determination of protein by prompt neutron capture in fibrocystic disease. Proc. Fifth Int. Symp. on Capture Gamma-Ray Spectroscopy and Related Topics, Knoxville, Tennessee, USA, 10-14 September. (*Royal Alexandra Hospital for Children, Camperdown, NSW)

Allen, B.J. and Company, F.Z. [1984] - Evidence for valence transitions in neutron capture gamma-ray spectra in ^{88}Sr. Proc. Fifth Int. Symp. on Capture Gamma-Ray Spectroscopy and Related Topics, Knoxville, Tennessee, USA, 10-14 September. (*Univ. of Wollongong, NSW)

Allen, B.J. and Company, F.Z.* [1984] - Gamma-ray strength function in ^{139}La and ^{141}Pr. Proc. Fifth Int. Symp. on Capture Gamma-Ray Spectroscopy and Related Topics, Knoxville, Tennessee, USA, 10-14 September. (*Univ. of Wollongong, NSW)

Allen, B.J. and Company, F.Z. [1984] - Valence neutron capture in s- and p-wave resonances in ^{32}S. Proc. Fifth Int. Symp. on Capture Gamma-Ray Spectroscopy and Related Topics, Knoxville, Tennessee, USA, 10-14 September. (*Univ. of Wollongong, NSW)

Amagishi, Y.* and Donnelly, I.J. - The Alfvén Wave Resonance. Proc. 1984 Sendai Symposium on Plasma Nonlinear Phenomena, March 8-9, Tohoku University, p 65. (*Faculty of Liberal Arts, Shizuoka University)

Bird, J.R. [1984] - Dating mass spectrometry and nuclear science. Proc. ANZAAS Isotopic Studies Symp., Canberra, 15 May.

Bird, J.R. [1985] - Analytical problems in art and archaeology. Proc. Int. Workshop on Ion Beam Analysis Techniques in Art and Archaeology. Pont-á-Mousson, France, 17-20 February.

Bird, J.R. [1985] - The potential of MeV ion beam techniques in museum science. Proc. Int. Workshop on Ion Beam Analysis Techniques in Art and Archaeology, Pont-á-Mousson, France, 17-20 February.

Bird, J.R. [1985] - X-ray spectrum processing, interpretation and computerisation. Proc. Int. Workshop on Ion Beam Analysis Techniques in Art and Archaeology, Pont-á-Mousson, France, 17-20 February.

Bird, J.R., Clayton, E. and Duerden, P. [1985] - The problems and potential of ion beam techniques in archaeology and art. Nuclear reaction analysis. Proc. Int. Workshop on Ion Beam Analysis Techniques in Art and Archaeology, Pont-á-Mousson, France, 17-20 February.

Bird, J.R., Duerden, P., Wall, T., Clayton, E and McBryde, I.* [1985] - Characterisation of Seelands artefacts. Proc. Second Aust. Archaeometry Conf., Canberra, 11-15 February. (*Aust. Nat. Univ.)

Boldeman, J.W. [1984] - Some aspects of the nuclear physics program at Lucas Heights. Proc. Ann. Meeting of the Japanese Neutron Data Committee, Tokyo, Japan, 13-15 November.

Boldeman, J.W., Clancy, B.E. and Culley, D. [1984] - Measurements of the prompt neutron emission spectrum from the spontaneous fission of ^{252}Cf. Proc. IAEA Ann. General Meeting on Neutron Standard Reference Data, Geel, Belgium, 12-16 November.

Boldeman, J.W. and Hines, M.G. [1984] - Nubar for the spontaneous fission of ^{252}Cf. Proc. IAEA Ann. General Meeting on Neutron Standard Reference Data, Geel, Belgium, 12-16 November.

Boldeman, J.W. and Hines, M.G. [1984] - Prompt neutron emission probabilities following spontaneous and thermal fission. Proc. IAEA Ann. General Meeting on Neutron Standards Reference Data, Geel, Belgium, 12-16 November.

Boldeman, J.W., Hines, M.G., Thorpe, K.J., Delaney, I., Baxter, P. and Fallon, J.P. [1985] - Development of a liquid scintillator neutron coincidence counter*. Proc. 7th ESARDA Symp. Safeguards and Nuclear Materials Management, Liege, Belgium, 21-23 May. (*Work performed under contract with the Aust. Dept. of Foreign Affairs.)

Boldeman, J.W. and Walsh, R.L. [1985] - Neutron fission of thorium-230 revisited. Proc. Int. Conf. on Nuclear Data for Basic and Applied Science, Santa Fe, USA, 13-17 May.

Clayton, E. and Wooller, K.K.* [1984] - PIXE monitoring of heavy metal exposure through hair and blood analysis. Proc. IAEA Meeting on the Coordinated Research Program on Applications of Nuclear-related Techniques in Occupational Health ISPRA, Vareze, Italy, 9-12 October. (*NSW Dept. of Industrial Relations)

Cohen, D.D.*, Bradshaw, S.D., Katsaros, A., Tom, J.* and Garton, D. [1984] - The $^{18}O(p,a)\ ^{15}N$ reaction for enriched water in small biological samples. 3rd Appl. Phys. Conf. of Aust. Inst. Physics, Melbourne. (*AINSE)

Duerden, P., Clayton, E., Bird, J.R., Ambrose, W.* and Leach, F.** [1985] - Obsidian composition catalogue. Proc. Second Aust. Archaeometry Conf., Canberra, 11-15 February. (*Aust. Nat. Univ.; **Univ. of Otago, Dunedin, NZ)

Duerden, P., Clayton, E., Bird, J.R. and Cohen, D.D.* [1985] - Recent work at Lucas Heights on archaeology and art. Proc. Int. Workshop on Ion Beam Analysis Techniques in Art and Archaeology, Pont-á-Mousson, France, 17-20 February.

Durance, G. [1985] - A review of rotamak experiments. Proc. IAEA Technical Committee Meeting on Advances in Compact Torus Research, Sydney, 4-7 March.

Durance, G., Hogg, G.R. and Tendys, J. [1984] - Low power, long duration experiments on the AAEC rotamak. Int. Conf. on Plasma Physics, Lausanne, Switzerland.

Hines, M.G., Boldeman, J.W. and Robinson, G.S. [1984] - The effect of multiplication on the neutron probability distribution in neutron coincidence counting. Proc. IAEA Annual General Meeting on the Evaluation of the Quality of Safeguards Non Destructive Analysis Data, Vienna, Austria, 19-23 November.

Lang, D.W. [1985] - The magnetohydrodynamic turbine concept. Proc. 23rd Symposium on Engineering Aspects of Magnetohydrodynamics, Somerset, PA, USA, 25-28 June.

Walsh, R.L. [1985] - Variation of even-odd charge effects with excitation energy in (A) and mass yield for $^{252}Cf(sf)$. Proc. Int. Conf. on Nuclear data for Basic and Applied Science, Santa Fe, USA, 13-17 May.

Williams, J.S., Chivers, D.J., Elliman, R.G., Johnson, S.T., Mitchell, I.V., Rossitter, K.G., Pogany, A.P., Short, K.T. and Lawson, E.M.* [1984] - The production of porous structures on Si, Ge and GaAs by high dose ion

implantation. Ion Implantation and Ion Beam Processing of Materials Mat. Res. Soc. Symp. Proc. Vol. 27, p 205. (*Applied Physics Div., AAEC; all other authors, RMIT, Melbourne.)

Wilson, D.J. [1984] - The effect of various soil parameters on the interpretation of neutron moisture meter measurements. Proc. Hydrology and Water Resources Symp. Sydney, 14-16 May.

6.6 Monographs

Allen, B.J., Berggvist, I., Chrien, R.E., Gardner, D. and Poenitz, W.P., Neutron Radioactive Capture, Vol. 3 OECD/NEA series on Neutron Physics and Nuclear Data in Pergamon Press 1984. Science and Technology.

Knott, R.B. and Schoenborn, B.P. [1985] - Quantitation of water in membranes by neutron diffraction and X-ray techniques in "Methods in Enzymology", Biomembranes, Protons and Water: Structure and Translocation, Academic Press.

6.7 Non-Commission Work Done at the Research Establishment

Cohen, D.D.* [1985] - Theoretical calculations of the Datz Technique for the $2s_{\frac{1}{2}}$ subshell ionisation cross section from the $L\gamma_1$, $L\gamma_{236}$ and $L\gamma_{44}$ X-ray lines. J. Phys. B. At. Mol. Phys. 18 (in press). (*AINSE)

Cohen, D.D.* [1984] - Comments on several analytical techniques for L-subshell ionisation calculations. J. Phys. B. (London). At. Mol. Phys., B17:3913. (*AINSE)

Davis, R.L., Day, R.K.* and Dunlop, J.B.*, 'Spin Reorientation in $Tm_2Fe_{14}B$' Sol. Stat. Comm. (in press). (*App. Phys., CSIRO).

Davis, R.L. and Kennard, C.H.L.* [1985] - 'Structure of Sodium Tetradenteroborate, Na BD_4', J. Sol. State Chem. (Brief Comm.) 59. (*Univ. of Qld)

James, B.D.* and Davis, R.L. [1985] - 'The Bifurcated Hydrogen Bond in 4-Chloropyridinium Hexachlorostannate (IV). Confirmation via Neutron Powder Diffraction'. Inorganica Chimica Acta 100, L31. (*La Trobe University)

DISTRIBUTION LIST - AAEC/AP PR 84 - 1 JULY 1984-30 JUNE 1985

1.	Professor M. Brennan
2.	Deputy Chairman
3.	Commissioner Dr J.G. Morris
4.	Director
5.	Deputy Director
6.	Deputy Director, Research
7.	Chief, Applied Mathematics and Computing Division
8.	Chief, Environmental Science Division
9.	Chief, Isotope Division
10.	Chief, Materials Division
11.	Chief, Nuclear Technology Division
12.	Chief, Applied Physics Division
13.	Chief, Health and Safety Division
14.	Chief, Technical and Commercial Services Division
15.	Head, Technical Secretariat
16.	Secretary
17.	Director, Public Relations
18.	Director, Regulatory Bureau
19.	Head, Media Relations Office
20.	Executive Officer, AINSE
21-23	Library
24.	Vienna Office
25-65	J.W. Boldeman (for INDC and Bilateral Agreement correspondents)
66-106	J.R. Bird (for special distribution)
107-140	APD Internal Distribution
141-166	Bilateral Agreements (UKAEA 5; US Dept of Energy 16; AECL 5)
167-200	Spares